ABSOLUTE PHASE IN MOBILE CHANNELS

by

Jinyun Ren

B.A.Sc., Tianjin University, Tianjin, China, 1996

M.A.Sc., Tianjin University, Tianjin, China, 1999

Thesis submitted in partial fulfillment
of the requirements for the degree of

Doctor of Philosophy

In the School
of
Engineering Science

SIMON FRASER UNIVERSITY
Spring 2010

APPROVAL

Name: Jinyun Ren

Degree: Doctor of Philosophy

Title of Thesis: Absolute Phase in Mobile Channels

Examining Committee: Dr. Sami Muhaidat, Chair

Dr. Rodney G. Vaughan, Senior Supervisor

Dr. James K. Cavers, Supervisor

Dr. Paul K. M. Ho, Supervisor

Dr. Jie Liang, Internal Examiner

Dr. Gordon L. Stüber, External Examiner
Professor of Electrical & Computer Engineering
Georgia Institute of Technology

Date Approved: March 26, 2010

Declaration of
Partial Copyright Licence

Abstract

Mobile channels are often modeled using a well-defined Rice process. The statistics of its wrapped phase (i.e., phase values in $[-\pi, \pi)$), such as the mean, variance, and probability density function (pdf), are known. The absolute phase is the accumulated phase change over an observation interval. It can be calculated from the wrapped phase but contains more information. Its applications include channel characterization and cognitively tracking mobile users. However, there is little knowledge about the statistics of the absolute phase.

In this thesis, the theory of the absolute phase is developed. The absolute phase is defined formally, and various formulations, based on unwrapping and on other methods from FM receiver analysis, are presented. These formulations lay a basis for analyzing the statistics of the absolute phase for a well-defined Rice process.

The statistics of the absolute phase is affected by scattering directionality of the channel. New theoretical results are developed for the mean, variance and pdf of the absolute phase in isotropic scattering. The mean of the absolute phase is then derived for directional scenarios with scattering modeled by the von Mises distribution. The smooth transition of the von Mises distribution to the uniform distribution enables this mean to include isotropic scattering as a special case.

Development of the absolute phase will foster new techniques in mobile communications. An example in isotropic scattering is a new Rice factor estimator which uses only the absolute phase. Since no amplitude is involved, the receiver structure can be simplified. This estimator achieves comparable performance, when the Rice factor is small, to existing estimators which require amplitude or both amplitude and phase.

To demonstrate and confirm the new theoretical results, a channel simulation technique, based on the inverse discrete Fourier transform, is extended to include both isotropic and directional scattering. The simulation and theoretical results are in good agreement.

Keywords: Absolute phase; Rice phase; phase statistics; Rice factor; mobile channel; directional channel; modeling and estimation; mobile communications; cognitive radio

In loving memory of Tiantian (Emma)

Acknowledgments

I am sincerely thankful to my current senior supervisor at SFU, Dr. Rodney G. Vaughan, who took me as his student at the lowest time of my graduate studies. This thesis would not have been possible without him. His heart-warming encouragements help me recover my self-confidence in achieving the doctoral degree; his expert and broad knowledge in communications guide me in the right track towards my goal; his financial and spiritual supports enable me to accomplish the thesis quickly.

I wish to thank my first senior supervisor at SFU, Dr. Jacques Vaisey, who believed in my ability of being a Ph.D. from the very beginning. Even for only 14 months working with him, I was inspired by his passion to life, his love to teaching, his knowledge to research.

I would like to express my special thanks to my second senior supervisor at SFU, Dr. John S. Bird. His guidance and expert knowledge in sonar helped me build a solid theoretical background on statistical signal processing in three years, and made my transition to other research areas possible.

It is my honor to thank my examining committee, Dr. Gordon L. Stüber and Dr. Jie Liang; my supervisory committee, Dr. James K. Cavers and Dr. Paul K. M. Ho; and the defence chair, Dr. Sami Muhaidat, for their valuable contributions.

I am indebted to many of my past and present lab colleagues for their encouragement and advice during these years. Special thanks to Alireza Banani, Qi Yang, and Maryam Dehghani Estarki for their discussions and helps during my research.

Thanks to my parents and family for encouraging me to pursue the doctoral degree. I owe my deepest gratitude to my husband, Yifeng Huang, for walking me anytime with his love, patience, encouragement and support.

Finally, I would like to thank the brothers and sisters in SFU Christian Fellowship for their company towards the true treasure of life.

Contents

List of Tables

List of Figures

Nomenclature

List of Abbreviations

AOA	Angle-of-Arrival
APK	Absolute Phase based K estimator
BER	Bit Error Rate
BS	Base Station
CAG	Complex Amplitude Gain
CLT	Central Limit Theorem
CRB	Cramer-Rao Bound
FFT	Fast Fourier Transform
FIR	Finite Impulse Response
GSM	Global System for Mobile communications, originally *Group Speciale Mobile*
HPBW	Half-Power BeamWidth
IDFT	Inverse Discrete Fourier Transform
IIR	Infinite Impulse Response
LCR	Level Crossing Rate
LOS	Line-of-Sight
MIMO	Multiple Input Multiple Output
MLE	Maximum-Likelihood Estimator
NLOS	Non-Line-Of-Sight
OFDM	Orthogonal Frequency Division Multiplexing
pdf	probability density function
PLL	Phase-Locked Loop
PMF	Probability Mass Function

PSD	Power Spectral Density
RF	Radio Frequency
RMSE	Root Mean Square Error
RSS	Received Signal Strength
SER	Symbol Error Rate
SNR	Signal-to-Noise Ratio
TDOA	Time Difference Of Arrival
TOA	Time Of Arrival
w.r.t.	with respect to
WSSUS	Wide Sense Stationarity and Uncorrelated Scattering
ZCR	Zero-Crossing Rate

List of Symbols

α_i	Initial phase of the ith diffuse component
$\bar{\phi}_A(T)$	Mean of the absolute phase at time T
β_0	AOA of the dominant component w.r.t. the mobile velocity
$\ddot{\rho}(\tau)$	Second derivative of $\rho(\tau)$
ΔL	Antenna spacing in terms of wavelengths, $\Delta L = \Delta z/\lambda$
ΔR_N	Average number of the difference between the positive and negative 2π crossings
Δz	Distance between two antennas
$\dot{\phi}_C(t)$	Derivative of $\phi(t)$
$\dot{\rho}(\tau)$	Derivative of $\rho(\tau)$
$\dot{y}(t)$	Derivative of $y(t)$
ϵ_ϕ	Estimated error of the mean of the absolute phase
η	Total efficiency factor from propagation, $\eta = \eta_{pol}\eta_{imp}\eta_{ant}$
η_{ant}	Antenna efficiency
η_{imp}	Impedance match efficiency
η_{pol}	Polarization efficiency
$\hat{\mu}_p$	Estimated pth moment of the signal envelope
$\hat{\sigma}^2$	Estimate of σ^2
$\hat{A}$	Estimate of A
$\hat{K}_{24}$	Estimated K obtained using the (2,4) moment-based estimator
$\hat{K}_{AP}$	Estimated K obtained using APK
$\hat{K}_{ML}$	Estimated K obtained using MLE
κ	Directionality parameter of a directional scenario
λ	Wavelength at the carrier frequency
$\langle G_{path}(d)\rangle$	Path gain at distance d in multipath environment
$\langle G_R(\theta_R, \phi_R)\rangle$	Mean effective gain for the receive antenna
$\langle G_T(\theta_T, \phi_T)\rangle$	Mean effective gain for the transmit antenna
μ_1	Mean of the Poisson process that models the number of negative 2π crossings
μ_2	Mean of the Poisson process that models the number of positive 2π crossings
ν^2	Variance of $\dot{y}(t)$

ω_c	Carrier angular frequency, $\omega_c = 2\pi f_c$
ω_o	Radial frequency of an oscillator
$\phi(t)$	Time-varying phase of a Rayleigh or Rice process
ϕ_1	Short notation for $\phi_W(0)$
ϕ_2	Short notation for $\phi_W(T)$
$\phi_A(T)$	Absolute phase at time T
$\phi_A^d(T)$	Unwrapped channel phase including both the absolute phase and the distance-dependent phase
$\phi_A^{(c)}(T)$	Absolute phase obtained by click analysis
$\phi_A^{(i)}(T)$	Absolute phase obtained by phase derivative integration
$\phi_A^{(u)}(T)$	Absolute phase obtained by unwrapping
$\phi_A^{(z)}(T)$	Absolute phase obtained by the zero-crossing technique
$\phi_C(t)$	Continuous phase at time t
$\phi_W(t)$	Same as $\phi(t)$, but W here to emphasize "Wrapped
ϕ_{rand}	Random phase owing to propagation in multipath environments
$\phi_{W2}(t)$	Same as $\phi_W(t)$, but 2 here is to emphasize the phase is in two quadrants only
$\phi_{W4}(t)$	Same as $\phi_W(t)$, but 4 here is to emphasize the phase is in four quadrants
ρ	Short notation for $J_0(2\pi f_D T)$
$\rho(\Delta L)$	Spatial correlation coefficient function of two antennas in terms of ΔL
$\rho(\Delta z)$	Spatial correlation coefficient function of two antennas separated by Δz
$\rho(\tau)$	Correlation coefficient function of the component (i.e., either real or imaginary part) for a Rayleigh channel
$\rho_{\phi\phi}(\tau)$	Phase correlation coefficient function for a Rayleigh channel
$\rho_{a^2a^2}(\tau)$	Power correlation coefficient function for a Rayleigh channel
$\rho_{aa}(\tau)$	Envelope correlation coefficient function for a Rayleigh channel
$\rho_{ss}(\tau)$	Channel CAG correlation coefficient function for a Rayleigh channel
$\rho_{xx}(\tau)$	Correlation coefficient function for the real part of a Rayleigh channel
$\rho_{yy}(\tau)$	Correlation coefficient function for the imaginary part of a Rayleigh channel
σ^2	Variance of the real or imaginary part of a Rayleigh process
σ_ϵ^2	Variance of estimate error, ϵ_ϕ
σ_g^2	Total power of the designed Doppler filter

$\sigma^2_{\phi_A^{(c)}}(T)$	Variance of the absolute phase obtained by Rice click analysis
$\sigma^2_{\phi_A^{(r)}}(T)$	Variance of the absolute phase obtained by correlation technique
$\sigma^2_{\phi_A^{(z)}}(T)$	Variance of the absolute phase obtained by zero-crossing technique
σ_θ	Angular spread (standard deviation) of a directional scenario in radians
$\sigma^2_{N_{r2\pi}}$	Variance of the number of 2π crossings
τ	Time difference in autocorrelation functions
τ_i	Average delay between the scatterers at Position i and the BS
τ_d	Delay spread
τ_m	Normalized delay spread, $\tau_m = \tau_d W_{system}$
θ_0	Mean direction of a direction scenario
θ_i	AOA of the ith diffuse component
φ_0	Initial phase of the dominant component
ϱ	Normalized envelope level by the average power of the channel
$\zeta(T)$	Phase difference, $\zeta(T) = \phi_W(T) - \phi_W(0)$
A	Magnitude of the dominant component
$a(t)$	Magnitude of a Rayleigh process
$A[k]$	Gaussian random variable in discrete frequency domain
a_i	Complex amplitude of the ith diffuse component
$B[k]$	Gaussian random variable in discrete frequency domain
c	Speed of light
$C_h(0)$	Autocovariance of $Z(t)$
$C_{aa}(\tau)$	Autocovariance of the envelope of a Rayleigh process
d	Nominal distance between the transmit and the receive antenna
f	Frequency in general
$F_G[k]$	Filter coefficients in Digital frequency domain
f_n	Maximum Doppler frequency normalized by the sampling frequency, $f_n = f_D/f_s$
f_s	Sampling frequency of the mobile channel
f_D	Maximum Doppler frequency
f_m	Normalized Doppler spread or fading rate, $f_m = f_D T_{symbol}$
$G_{path}(d)$	Path gain at distance d in a LOS link
$G_R(\theta_R, \phi_R)$	Directional gain for the receive antenna
$G_T(\theta_T, \phi_T)$	Directional gain for the transmit antenna

$h(n)$	Channel samples for a Rice process in discrete time domain
$h(t)$	Well-defined Rice channel CAG
$I(t)$	In-phase (real part) of a Rician channel CAG
I_D	Index of dispersion of a Poisson process
K	The Rice factor
k	Sample index in the digital frequency domain
k_c	Wavenumber at the carrier frequency, $k_c = 2\pi/\lambda$
k_m	Digital frequency index corresponding to the Maximum Doppler frequency
K_{bias}	Estimator bias for K
L	Observation interval as distance in wavelengths, $L = f_D T$
M	Number of uncorrelated receive channels
M_{rx}	Number of uncorrelated receive antennas
M_{tx}	Number of uncorrelated transmit antennas
N	Number of samples used for IDFT
n	Sample index in discrete time domain
$N(\varrho)$	Normalized level crossing rate given the level ϱ
N_d	Number of diffuse components
N_s	Number of available samples for K estimation
$N_{2\pi+}(0,T)$	Number of 2π positive crossings during $(0,T)$
$N_{2\pi-}(0,T)$	Number of 2π negative crossings during $(0,T)$
$N_{2\pi}(0,T)$	Cumulative number of 2π crossings during $(0,T)$
$N_{\pi}(0,T)$	Cumulative number of $I(t)$ crossing zero during $(0,T)$
$N_{r2\pi}(0,T)$	Cumulative number of Rice clicks during $(0,T)$
$p(\phi_A)$	pdf of the absolute phase
$p(\theta)$	Angular distribution of the effective scattering in mobile channels
$p(\zeta)$	pdf of the difference of two phases
$p(K_b)$	pdf of K_{bias}
$p(n)$	PMF for the number of counts
$p(u)$	Doppler power profile
$p_a(a)$	pdf for the magnitude of a Rayleigh process
$P_R(d)$	Received power by the receive antenna at distance d
$p_r(r)$	pdf for the envelope of a Rice process

P_T	Transmitted power by the transmit antenna
$p_v(\theta)$	pdf of the von Mises distribution for directional scenarios
$p_v(u)$	$p_v(\theta)$ in the u domain
$p_{Rice}(\phi)$	pdf for the phase of a Rice process
$p_{uni}(\phi)$	pdf for the phase of a Rayleigh process
$Q(t)$	Quadrature (imaginary part) of a Rician channel CAG
$r(t)$	Envelope of a Rice process
R_+^c	Positive 2π crossing rate
R_-^c	Negative 2π crossing rate
r_c	Correlation coefficient between the positive and negative 2π crossing events
r_g	Radius of gyration of the Doppler spectrum, $r_g = f_D/\sqrt{2}$
$R_{\dot{\phi}_C}(\tau)$	Autocorrelation function of phase derivative
$R_{\phi\phi}(\tau)$	Autocorrelation of the phase of a Rayleigh process
$R_{aa}(\tau)$	Autocorrelation of the envelope of a Rayleigh process
$R_{ss}(\tau)$	Autocorrelation of a Rayleigh process
$R_{xx}(\tau)$	Autocorrelation of the real part of a Rayleigh process
$R_{xy}(\tau)$	Cross-correlation of the real part and imaginary parts of a Rayleigh process
$R_{yx}(\tau)$	Cross-correlation of the imaginary and real parts of a Rayleigh process
$R_{yy}(\tau)$	Autocorrelation of the imaginary part of a Rayleigh process
$s(n)$	Channel samples for a Rayleigh process in discrete time domain
$s(t)$	Time-varying channel CAG for a Rayleigh process, $s(t) = x(t) + jy(t)$
$S[k]$	Discrete spectrum
$S_{\phi\phi}(f)$	PSD of the phase of a Rayleigh process
$S_{aa}(f)$	PSD of the envelope of a Rayleigh process
$S_{ss}(f)$	PSD of a Rayleigh process
$S_{xx}(f)$	PSD of the real part of a Rayleigh process
$S_{yy}(f)$	PSD of the imaginary part of a Rayleigh process
T	Observation interval
t_0	Reference time instant
T_{signal}	Signal duration
T_{sp}	Sampling period of the channel phase

T_{symbol}	Symbol duration
T_s	Repetition time of a sounding signal or of a pilot symbol, a.k.a. channel sampling period
u	u domain, $u = k_c \cos(\theta)$
u_0	θ_0 in the u domain
v	Mobile velocity
W_{system}	System bandwidth
$x(t)$	Real part of a Rayleigh process
$X[k]$	Random variable in discrete frequency domain
$x[n]$	Gaussian random variable in discrete time domain
$y(t)$	Imaginary part of a Rayleigh process
$y[k]$	Gaussian random variable in discrete time domain
$Z(t)$	Vector $Z^T(t) = [\ x(t) \quad y(t) \quad \dot{y}(t)\ ]$

Chapter 1

Introduction

1.1 Background and Motivation

Mobile communication channels experience time-domain and/or frequency-domain fading caused by multipath propagation and the movement of the mobile. The fading results in significant variation of the received signal within even a short time or distance. The received signal, given the transmitted signal as an unmodulated carrier, can be used to describe the channel. Many statistical models are available to synthesize the complex received signal at baseband. One such model is the Rice distribution, which assumes the received signal is the sum of a single, dominant component plus diffuse components [1, 2, 3, 4]. The Rice distribution is a well-accepted, physics-based, experimentally-verified model for the mobile channel in indoor or outdoor propagation environments [5, 6, 7].

Modeling the channel signal using a Rice distribution means that the modeled channel envelope follows the Rice envelope distribution and its wrapped phase follows the Rice phase distribution [2, 4]. The Rice envelope distribution is governed by the K factor, the ratio of the power of the dominant component to the power of the diffuse components of the channel. The Rice phase distribution depends not only on the K factor, but also the angle-of-arrival (AOA) of the dominant component and the mobile velocity [2]. When the dominant component has zero Doppler frequency, the Rice phase distribution is stationary and governed only by the K factor [8]. In this case, and with large K, the Rice phase distribution alone can be used to estimate the K factor [9]. When the dominant component has constant magnitude but fixed, non-zero Doppler frequency, the Rice phase distribution becomes time-variant. In this case, the Rice phase distribution can still be used - but jointly

with the Rice envelope distribution (which is stationary) - to estimate the K factor [10, 11].

In this thesis, the interest is the accumulated Rice phase change over an observation interval, which is defined here as the *absolute phase*[1] in the mobile channel. The absolute phase has not been formally treated in the mobile communication literature, although Rice was aware of it in the context of the FM receiver [15]. Analog communications did not motivate research into the absolute phase because analog receivers could not directly calculate it. The computing power of digital receivers enables on-the-fly phase sampling and frequency tracking, so it is now feasible to acquire the absolute phase and estimate its statistics, such as mean, variance, and probability density function (pdf).

An idealized mobile channel following the Rice distribution is referred to as the *well-defined Rice channel* or the *well-defined Rice process* in this thesis (its definition is given in Section 2.2). For a well-defined Rice channel, the statistics of the absolute phase include more information about the channel than the wrapped Rice phase. For example, neither the Doppler frequency of the dominant component nor the K factor is available from the mean of the wrapped phase, but they are available from the mean of the absolute phase. These extra information can be useful in many mobile applications, including channel characterization and mobile user localization, etc. Information about the phase trajectory of a mobile user, which contains the absolute phase, is useful in location-aware situations. In terms of communications, the trajectory information could be used by algorithms managing handoff or dynamic allocation of bandwidth in a cognitive radio system. These potential applications further motivate research on the absolute phase.

This thesis develops the theory of the absolute phase in mobile communications, including its formal definition and related statistics such as mean, variance and pdf. Development of the absolute phase will foster new techniques in mobile communications. An example presented in this thesis is a new Rice factor estimator which uses only the absolute phase. With no amplitude information required, the receiver structure can be simple, and yet the estimator performs well.

[1]The absolute phase also appears in other research areas, but conveys different meanings. For example, for interferometric synthetic aperture radar, the absolute phase is an unwrapped phase shift between the signals received by two co-located antennas, and is used to estimate the height of the scatterer relative to the reference plane [12, 13]. For few-cycle lasers, the absolute phase represents the phase of the carrier w.r.t. the envelope of the short laser pulse [14].

1.2 Related Work

The term *absolute phase* for the mobile channel was used by Vaughan in 1986 [16], but no formal definition or statistical treatment was provided. Intuitively, the distribution of the absolute phase may be expected to resemble a Gaussian distribution. The Gaussian form has been used previously for the phase distribution, but with the phase wrapped [17], or truncated [18], into the 2π domain. It is shown in this thesis that for a well-defined Rice channel, the distribution of the absolute phase is not Gaussian.

The absolute phase in mobile channels has similarities to the output phase of FM receivers, which was a research topic for several decades from the 1940s. The input to an FM receiver is a sinusoidal signal plus a narrowband Gaussian noise, and therefore it can be modeled as a Rice process [19, 20, 21]. The sinusoid, the Gaussian noise and the signal-to-noise ratio (SNR) are analogous to the dominant component, the diffuse component, and the K factor respectively, of the mobile channel signal. The output of an FM receiver (e.g. limiter-discriminator-integrator) is the accumulated phase change over an observation interval, and is analogous to the absolute phase in the mobile channel.

The statistics of the output phase of an FM receiver are scattered in the literature. For example, the mean of the output phase was derived intuitively by Blachman [22, 23]. The variance of the output phase was analyzed, *viz.*, the correlation technique by Rice [20] and Middleton [24], the zero-crossing technique by Blachman [22], and the click analysis technique by Rice [15]. The pdf of the output phase was developed through: rigorous derivation by partial differential equations [25]; approximations using the central limit theorem [23]; and approximations under high SNR [26, 27, 28]. A more detailed literature review for the mean, variance and pdf of the output phase of an FM receiver can be found in Chapter 4.

The analysis of the output phase of an FM receiver sheds much light on the statistics of the absolute phase in the mobile channel. Some of the results can be applied directly to the absolute phase in mobile channel, but some of them demand scrutiny before making connections. In this thesis, these existing theories are examined in detail and are reinterpreted in the context of mobile channels, supported by simulation results. As an extension, particularly for the mobile channel, the mean of the absolute phase is derived in the presence of directional scattering.

In analog FM receivers, when the FM SNR falls below a threshold, the receiver starts producing "clicks" owing to the sudden phase changes of 2π (in the wrapped phase). This

phenomenon is defined as the click by Rice [15]. There are also other click phenomena defined in FM receivers, *viz.*, the false click and the doublet. Another type of click in mobile channels, recognized as the π jump [4, 16, 29], contributes to the error floor in digital communications. The phase and its associated effects, such as various clicks, are not consistently interpreted in the literature. Therefore, these clicks, as well as the π jump are reviewed. The click treatments from the FM receiver and the mobile channel are brought together in this thesis, and are applied to the mobile channel including their effects on the mean and variance of the absolute phase.

1.3 Thesis Organization

This thesis is organized as seven chapters and four appendices. **Chapter 1** introduces the background, motivation and related work for the absolute phase in mobile channels, and summarizes the contributions.

The channel model, including the scattering directionality, governs the statistics of the absolute phase. Therefore, **Chapter 2** overviews the mobile channel and its modeling in the presence of isotropic and directional scattering. The channel models and corresponding statistics described in this chapter lay the foundation for the rest of the thesis. It is helpful to confirm the theoretical results by simulation. Therefore, different techniques for simulating the mobile channel are overviewed. In particular, a mobile channel simulation technique for directional scenarios is developed based on the inverse discrete Fourier transform technique.

Chapter 3 defines the absolute phase formally, and presents four techniques to formulate the absolute phase, including unwrapping, zero-crossing, phase derivative integration, and Rice click analysis. The background for each formulation is provided, and similarities and connections among these formulations are identified. Since the analysis of the absolute phase is new to the mobile communications, this chapter also offers suggestions for obtaining the absolute phase by simulation and for acquiring the absolute phase in practice.

Chapter 4 provides the theoretical results for statistics (including mean, variance and pdf) of the absolute phase in the mobile channel with isotropic scattering. The related work in the area of the FM receivers is reviewed in detail before each statistic is derived with an emphasis on the differences of the mobile channel from the FM receiver. The theoretical results for the mean and variance of the absolute phase can be transferred from the existing results for the FM receiver by reinterpreting the signal, noise, SNR, and correlation of

signals. However, modeling pdfs of the absolute phase is treated differently from modeling pdfs of the output phase of an FM receiver. A new, approximate model to derive pdfs of the absolute phase is proposed. It decomposes the absolute phase into discrete and continuous events which are independent. The pdf of the absolute phase is so complicated that currently it cannot be obtained, even after approximations, for some scenarios. Thus, the conditions are identified using statistical tests for approximate pdf models to hold. Simulation results in mobile channels are used in this chapter to support the analysis and discussion.

Chapter 5 proposes a new K estimator for MIMO systems, which is based on the mean of the absolute phase with isotropic scattering. The proposed estimator uses only the channel phase, and therefore is robust against the effects of distance-dependent propagation gain and multiplicative shadowing. It requires the mean of the absolute phase, i.e., no amplitude involved, and therefore allows a simple receiver structure. It provides a comparable performance, for small K factor, when compared to other real-time estimators. This chapter also reviews K estimators in detail, analyzes the performance of the proposed estimator and compares it with other real-time K estimators. Simulation results are provided to support the discussion.

Chapter 6 discusses the effects of the scattering directionality on the mobile channel. The directionality of scattering of the mobile channel alters the second-order statistics of the channel, such as correlation, level crossing rate and statistics of the absolute phase, and therefore changes some of results which were based on isotropic scattering. This chapter presents two new research works related to scattering directionality. The first work derives a close-form result for the mean of the absolute phase with directional scattering. The second work presents results that show how the scattering directionality affects the antenna spacings in MIMO systems.

Chapter 7 summarizes the thesis, and suggests future work associated to the absolute phase.

In the **appendices**: (A) compares the absolute phase by unwrapping to the output phase of an FM receiver; (B) reviews the various click definitions and their effects on the absolute phase; (C) summarizes the notations for the different phases; and (D) proves that the absolute phase and the distance-dependent phase are additive after unwrapping.

1.4 Thesis Contribution

The formal treatment of the absolute phase is new. The important contributions of this thesis include, in order of significance:

- mathematically defining the absolute phase as a new variable for the mobile channel (reported in Chapter 3, and published in the special issue on Emerging Wireless Technologies, *Wireless Communications and Mobile Computing*, in 2009 [30]);
- analyzing the statistics (including mean, variance and pdf) of the absolute phase in the presence of isotropic scattering (reported in Chapter 4, and published in [30]);
- deriving the mean of absolute phase in the presence of directional scattering (reported in Chapter 6, and submitted to the *Vehicular Technology Conference* in Fall 2010 [31]);
- deriving the pdf of two correlated Rice phase differences without the modulo $[-\pi, \pi)$ condition[2] (reported in Chapter 4, and published in [30]);
- developing a new Rice factor estimator based on the absolute phase (reported in Chapter 5, and submitted to *IEEE Transactions on Wireless Communications*, currently in revision [32]);
- developing a channel simulation technique for the directional mobile channel using the inverse discrete Fourier transform (reported in Chapter 2, and accepted for the *Vehicular Technology Conference* in Spring 2010 [33]);
- developing an improved framework and model for antenna spacing design in directional scenarios (reported in Chapter 6, and published at the *Vehicular Technology Conference* in Fall 2009 [34]).
- reviewing and comparing various clicks (*viz.*, the Rice click, the false click, the doublet, and the π jump) related to the absolute phase in the mobile channel (reported in Appendix B, and published in [30]).

[2] "Modulo" represents "with respect to a modulus of". The modulo $[-\pi, \pi)$ condition means that the phase values beyond $[-\pi, \pi)$ are wrapped onto $[-\pi, \pi)$.

Chapter 2

Mobile Channel Modeling and Simulation

2.1 Overview of Mobile Channels

2.1.1 Definition of the Mobile Channel

There are many different definitions regarding the mobile channel in the literature [4]. For example, the channel is discussed in terms of fields and waves in the propagation literature, and in terms of bit error statistics in the communication networks literature. A summary of the information flow and terminologies for the mobile channel are depicted in Figure 2.1 [3, 4].

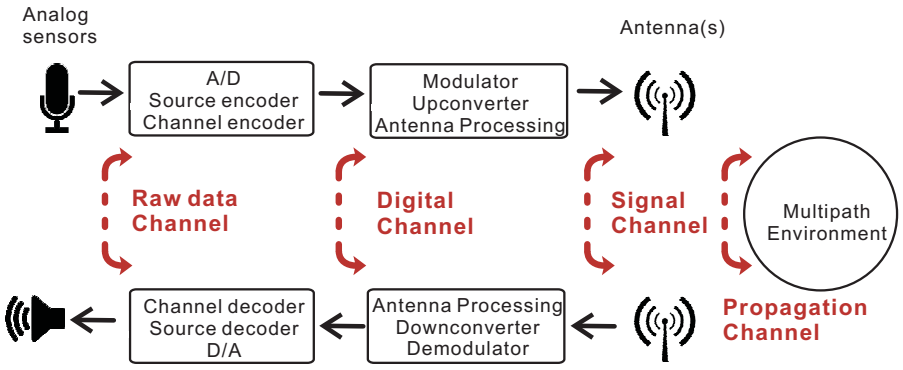

Figure 2.1: Information flow and different definitions for a mobile channel.

The original signal (e.g., voice) is captured by the analog sensors (e.g., microphone), and is received and played back by the analog device (e.g., speaker) at the other end of the radio link. This channel is referred to as the *raw data channel*. The electrical raw information is usually converted to digital bits, compressed by a source encoder, and protected by a channel encoder. The encoded digital bits are sent to a modulator for communication. In a receiver, all these processes are repeated but in a reversed order.

At the transmit side, the modulator assigns the digital bits to complex symbols in the digital baseband. In order to transmit the modulated symbols via an antenna, the digital baseband signal is converted to its analog form, and then upconverted by a mixer to the radio frequency (RF). The antenna-related signal processing, such as beamforming, is implemented either at RF, or within the digital baseband, or both.

At the receive side, the signals are preamplified to establish the SNR. The antenna related algorithms, such as a combiner for diversity, can be implemented with either the analog signals or digitally. If the combining is analog, the combined signal is first downconverted to its analog baseband equivalent, followed by digitization, and then passed through a demodulator (e.g., consisting of a matched filter and an equalizer) to be ready for detection.

The channel from before the modulator to after the demodulator is referred to as the *digital channel*. The performance of the digital channel is classically evaluated by the Bit Error Rate (BER) or the Symbol Error Rate (SER) against the SNR. The channel from before the transmit antenna to after the receive antenna is referred to as the *signal channel*. The channel from after the transmit antenna to before the receive antenna is referred to as the *propagation channel*.

The signal channel is often referred to as the propagation channel in the communications signal processing literature. This may be because the effects of antennas, such as beam patterns, polarization etc., are hard to separate from the propagation channel when sounding a channel. However, it is emphasized here that these two types of channels are different. For example, for the same physical location or locus of the transmitter and receiver (i.e., the same propagation channel), using different antennas will result in signal channels with different properties.

Unless otherwise stated, the *mobile channel* in this thesis means the signal channel, i.e., the propagation channel plus antenna effects. In channel modeling and estimation, it is assumed that the transmitted signal is an unmodulated carrier, so the received signal by the receive antenna becomes proportional to the channel transfer function at the carrier

frequency. The received signal is bandlimited but is often represented by its baseband equivalent in a complex form. The mobile channel in this thesis is modeled by this complex signal which is referred to as the channel *Complex Amplitude Gain (CAG)*.

2.1.2 Propagation Modeling in the Mobile Channel

For a perfect line-of-sight (LOS) environment, the instantaneous received power at the receive antenna can be related to the transmitted power at the transmit antenna using the Friis transmission equation [4],

$$P(d) = \frac{P_R(d)}{P_T} = \eta G_T(\theta_T, \phi_T) G_R(\theta_R, \phi_R) G_{path}(d) \tag{2.1}$$

where d is the nominal distance between two antenna phase centers; $P_R(d)$ and P_T are the received power at distance d and the transmitted power, respectively; η is a total efficiency factor including polarization efficiency (η_{pol}), impedance match efficiency (η_{imp}), and antenna efficiency (η_{ant}); $G_T(\theta_T, \phi_T)$ and $G_R(\theta_R, \phi_R)$ are the directional gains for the transmit antenna and the receive antenna, respectively; (θ_T, ϕ_T) and (θ_R, ϕ_R) are the angles of the signal in the coordinates of the transmit and receive antennas, respectively; $G_{path}(d)$ is the *path gain* at distance d determined by propagation environment, and it is inverse of the *path loss*. In general, the Friis transmission equation defines the path gain. For channel sounding, the transmitted power, the antenna gains, their impedance matches, and the polarization efficiency are taken as known, and the received power is measured, allowing the path gain to be calculated.

The Friis transmission equation can also be used for environments other than the usual application of a perfect LOS. In mobile communications, the transmitted signal usually experiences a multipath environment. Then the received power can be averaged over all the angles [35],

$$\langle P(d) \rangle = \eta \langle G_T(\theta_T, \phi_T) \rangle \langle G_R(\theta_R, \phi_R) \rangle \langle G_{path}(d) \rangle \tag{2.2}$$

where $\langle \cdot \rangle$ is a short notation for $\langle \cdot \rangle_{(\theta,\phi)}$, representing the average over all angles; $\langle G_T(\theta_T, \phi_T) \rangle$ and $\langle G_R(\theta_R, \phi_R) \rangle$ are the averaged gains for the transmit and receive antenna (also called mean effective gains), respectively; $\langle G_{path}(d) \rangle$ is the path gain resulting from the angular averaging of the antenna gains. Equation (2.2) assumes that the transmit antenna gain, the

receive antenna gain, their efficiency factors, and the path gain are mutually independent.

For matched (i.e, $\eta_{imp} = 1$), lossless (i.e., $\eta_{ant} = 1$) antennas, the received signal can be represented by the complex amplitude form of the Friis transmission equation [35],

$$F(d) = \sqrt{\eta_{pol}\langle G_T(\theta_T, \phi_T)\rangle\langle G_R(\theta_R, \phi_R)\rangle\langle G_{path}(d)\rangle}\exp[-j(2\pi d/\lambda + \phi_{rand})] \tag{2.3}$$

where $F(d)$ is the received complex signal relative to the transmitted signal; λ is the wavelength at the carrier frequency; $2\pi d/\lambda$ is the deterministic, distance-dependent phase change due to signal propagation; ϕ_{rand} is random phase variation owing to propagation in multipath environments. For co-polarized antennas and a LOS link, $\eta_{pol} = 1$, but for dense multipath, $\eta_{pol} = 0.5$, and the mean effective gains become $\eta_{ant}/2$, independent of antenna polarization [35].

In this thesis, the antenna terms in (2.3), i.e., η_{pol}, $\langle G_T(\theta_T, \phi_T)\rangle$, and $\langle G_R(\theta_R, \phi_R)\rangle$, are assigned to be constants - following the definition of the classical Friis transmission equation given by (2.1). The propagation terms, i.e., $\langle G_{path}(d)\rangle$ and ϕ_{rand} are treated as random variables owing to the multipath environment.

The path gain $\langle G_{path}(d)\rangle$ is a combined effect of three propagation phenomena, as depicted in Figure 2.2. These phenomena are [1, 3, 36, 37]:

- *propagation gain.* The propagation gain describes the monotonic decrease in received power with increasing distance, d, between the two antennas. The propagation gain can be obtained by averaging the received signal power over a large scale, for example, a few kilometers in radius (i.e., constant d) for macrocells [36]. The model of propagation gain varies greatly with environments. For example, it follows the d^{-2} power law for propagation in the free space, and the d^{-4} power law for propagation involving a direct path plus a ground-reflected path. For multipath environments, the exponent of the distance needs to be estimated from measured data, and can vary from -5.5 to -1.5 [1, 3, 38].

- *shadowing (long-term fading).* When there are obstacles (e.g., buildings or hills) between the transmit and receive antenna, the received signal at a particular distance experiences considerable variation about the mean power predicted by the propagation gain models [37]. This variation is referred to as shadowing or the long-term fading [1]. Its scale depends on the size of the shadowing obstacle. The shadowing can be viewed by averaging the received signal over some tens of wavelengths along

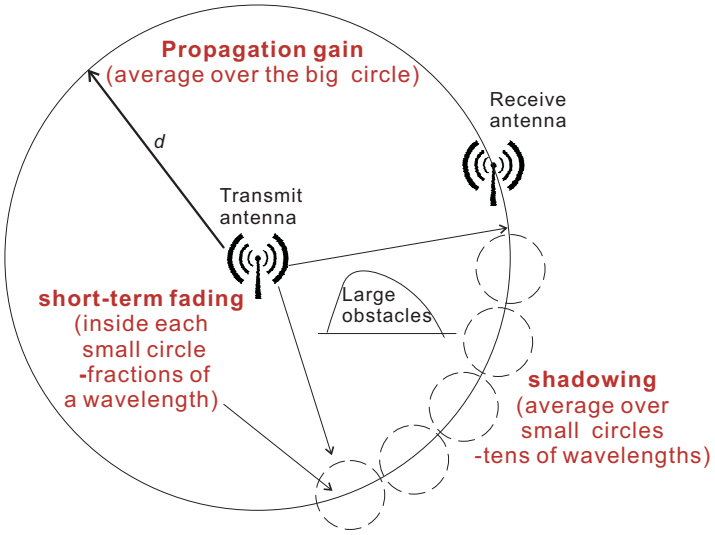

Figure 2.2: Propagation phenomena depicted in a 2D multipath environment. They are propagation gain, shadowing and short-term fading.

a particular radial distance [3]. Shadowing is often modeled, for mathematical convenience, as a slow-varying, log-normal random variable multiplied to the short-term fading [1, 39, 40], and this type of shadowing is referred to as the *multiplicative shadowing* [41]. The log-normal distribution becomes a Gaussian distribution when the shadowing is represented in decibel scale [1]. Other types of shadowing models are available and they are discussed in Section 5.1.1.

- *short-term fading*. When observed within a much smaller scale, say fractions of a wavelength, the received signal exhibits random fluctuation about the mean power predicted by the propagation gain and shadowing models. This variation is referred to as the short-term fading. It is a result of multipath propagation and the movement of the mobile. Depending on whether a LOS or dominant component appears in the received signal, the short-term fading can be modeled as Rician or Rayleigh. The physical scenarios and modeling for the Rician channel are detailed in Section 2.2.1.

The three phenomena are often assumed to be independent, so the path gain, i.e., $\langle G_{path} \rangle$, is their product. Figure 2.3 illustrates a path gain against the distance of two antennas, averaged over a radial distance 30λ (i.e., 10m at the carrier frequency of 900MHz).

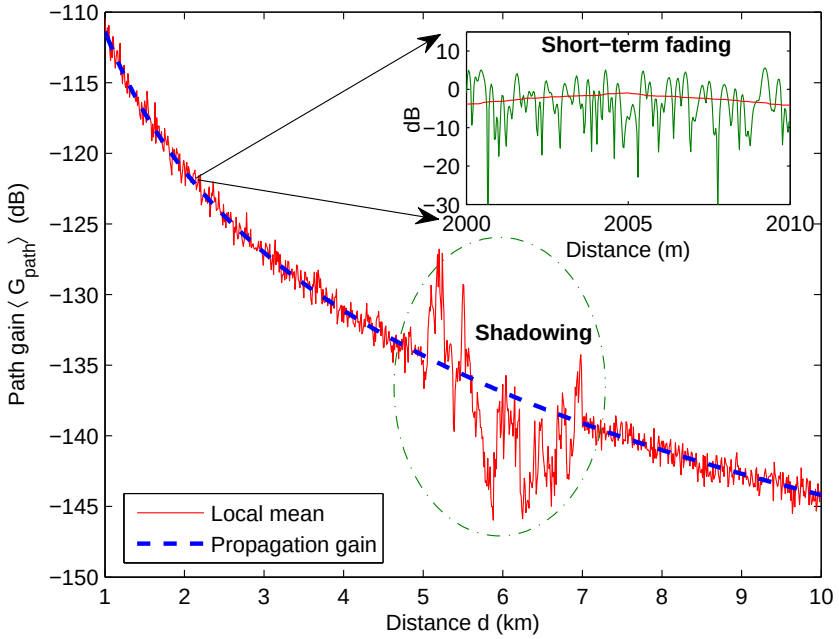

Figure 2.3: A depiction of path gain (averaged over 30λ) at the carrier frequency of 900MHz (i.e., $\lambda = 1/3$m) in a multipath environment with isotropic scattering. The propagation gain is simulated for a suburban area in a medium city using the Okumura-Hata model [38], with the base station (BS) antenna height of 70m, the mobile antenna height of 1.5m. The shadowing (only between 5 and 7 km) is simulated using a log-normal model. The shadowing in dB is Gaussian distributed with zero mean and a standard deviation of 7.5dB, and has a spatial correlation of 0.82 at a distance of 100 m [1, 42]. The short-term fading is Rayleigh distributed, and its power has the standard deviation of 5.57dB and a mean of -2.5dB [43]. The mobile velocity is 120km/h and the sampling period is 1ms.

The propagation gain is simulated for a suburban area in a medium city using the Okumura-Hata model [38], and it decreases from $d = 1$km to $d = 10$km by about 35dB. On top of the propagation gain, the variation due to shadowing (in the indicated shadowing zone of $d = 5$ to 7km) is up to 20dB. The short-term fading is averaged out in this scale, but the magnified version (not averaged, and with the propagation gain removed) in the subfigure shows that the variation of signal power is well above 25dB within a very short distance. These variations are well known and bring great challenges in designing communication systems.

The channel phase, as modeled in (2.3), includes a distance-dependent phase, $2\pi d/\lambda$,

and a random phase, ϕ_{rand}. The distance-dependent phase is from signal propagation and can be removed from the received signal, for example, using synchronization techniques. The random phase is a result of short-term fading. The wrapped version of the random phase is uniformly distributed for a Rayleigh fading channel and does not contain much information about the channel. However, the unwrapped version of the random phase has many interesting properties, and is the theme of this thesis.

2.1.3 Categorization of the Mobile Channel by Short-Term Fading

The effects of short-term fading play significant roles in performance of communication systems. Thus, the mobile channel has been categorized based on short-term fading [1, 3, 36, 37].

In a multipath environment, the received signal at any time instant is a summation of replicas of the transmitted signal, but each replica might have different excess delay (owing to different propagation path lengths) and Doppler frequency shift (owing to the relativistic effect - the movement of the mobile). Consequently, the received signal is spread out in the delay domain (i.e., *delay dispersion*), and/or has a wider spectral width, proportional to the mobile velocity, in the frequency domain (i.e., *frequency dispersion*). Either or both dispersions can be present in typical mobile channels, and are determined only by the environment and the velocity of the mobile.

The delay dispersion affects the *coherence bandwidth* of the channel, while the frequency dispersion affects the *coherence time* of the channel. The coherence bandwidth and the coherence time are two important parameters for the mobile channel. The coherence bandwidth and coherence time can be evaluated by the delay spread (τ_d) and the maximum Doppler frequency (f_D) of the signal channel, respectively[1].

For a communication system, there are two related parameters: the symbol duration (T_{symbol}) in the time domain, and the system bandwidth (W_{system}) in the frequency domain. Approximately, $T_{symbol} = \frac{1}{W_{system}}$.

When the maximum Doppler frequency, f_D, is normalized by the symbol duration[2], T_{symbol}, a useful metric for communication through fading channels is obtained. This normalized parameter, $f_D T_{symbol}$, often called the *fading rate* and denoted here by f_m, describes

[1]For formal definitions of the coherence bandwidth and the coherence time, see, e.g., [1, 2, 3, 4].

[2]To be more accurate, the duration should be application specific. For example, it might be one symbol for coherent detection, two symbols for differential detection, or several symbols for an equalizer [36].

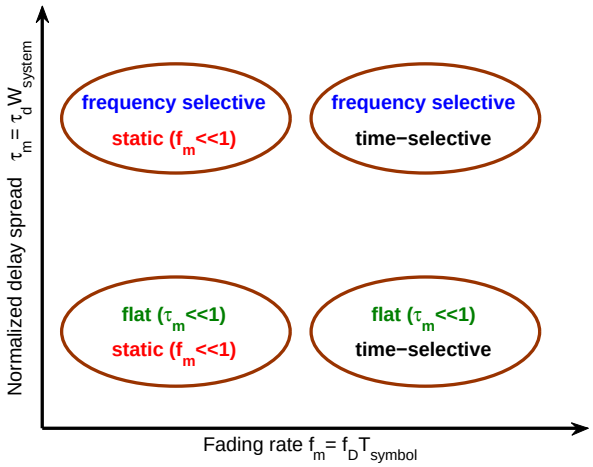

Figure 2.4: Categories of the mobile channel based on fading rate and normalized delay spread. In the labels, f_D is the maximum Doppler frequency, τ_d is the delay spread, T_{symbol} and W_{system} are the symbol duration and system bandwidth, respectively. Specific values of f_m and τ_m separating these channel categories are not well defined.

the time selectivity of the channel. $f_m \ll 1$ represents a static fading channel, and otherwise the channel is time-selective (i.e., fast fading).

Similarly, when the delay spread τ_d is normalized by the system bandwidth, W_{system}, another metric is obtained to describe the frequency selectivity of the channel. The metric, $\tau_D W_{system}$, is called the normalized delay spread and denoted here as τ_m. $\tau_m \ll 1$ represents a flat channel in the frequency domain, and otherwise the channel is frequency-selective.

The mobile channel can be categorized into four types based on the two metrics: static, flat fading; static, frequency-selective fading; time-selective, flat fading; and time-selective, frequency-selective fading, as depicted in Figure 2.4.

The static, flat fading channel is the simplest scenario. The static, frequency-selective channel does not usually occur for moving terminals, but can be observed from a stationary radio or sonar channel. Most channels for cellular communications, e.g., Global Systems for Mobile communications (GSM, originally *Group Speciale Mobile*), are both time-selective and frequency-selective. For frequency-selective channels, it is common to assume Wide Sense Stationarity and Uncorrelated Scattering (WSSUS) [3, 44]. With these assumptions, the frequency-selective channel can be divided into several uncorrelated flat channels, as in orthogonal frequency division multiplexing (OFDM). In this thesis, the signal and phase

models are defined for the time selective, flat fading channel, but can be applied to each flat channel in a frequency-selective channel.

2.1.4 Bandwidth of the Mobile Channel

The concepts and definitions of bandwidth are manyfold. For example, in wireless communications, the information-theoretic bandwidth is the RF bandwidth (including guard bands) in Hertz. However, for network engineers, the bandwidth is often expressed as the capacity, in bits/sec. This section discusses bandwidth of the mobile channel.

The propagation channel has essentially infinite bandwidth, in the sense that the propagation can be modeled at any frequency. However, the bandwidth of the mobile channel is evaluated by the coherence bandwidth, which equals approximately the reciprocal of the delay spread of the signal channel [36].

By comparing the coherence bandwidth of the channel with the bandwidth of a mobile system, the mobile system can be defined as a *narrowband system* or a *wideband system*. Specifically, if the channel coherence bandwidth is much larger than the system bandwidth, the mobile system is referred to as a narrowband system. Otherwise, it is a wideband system [3]. Whether a mobile system is narrowband or wideband is equivalent to defining whether a channel is flat or frequency-selective.

The above concepts and definitions for the mobile channel are fundamentally different from those in RF engineering, where the bandwidth of a system is described by the frequency band over which the power spectral density (for RF circuits) or the match (for antennas) remains within a specified range [4]. By comparing the system bandwidth with the carrier frequency as a percentage, the RF system can be categorized as a narrowband system (usually less than 5 to 10%) or a wideband system. Owing to these different bandwidth concepts, a narrowband antenna could work in a wideband mobile system, but a narrowband mobile system might require a wideband antenna.

In wireless ultra wideband (UWB) systems, one definition of bandwidth is similar to those for RF engineering: if the system bandwidth is larger than 20 percent of the carrier frequency, then the system is UWB [45]. However, there are other definitions, for example: if the system has an absolute bandwidth of more than 500MHz then it is UWB [45].

The literature refers to the narrowband channel, wideband channel, and ultra wideband channel when modeling and characterizing the mobile channel [3, 4]. It is understood that these bandwidth categories require knowledge of the communications system bandwidth.

2.2 Well-Defined Rice Channel

In this thesis, the interest is the channel phase for a narrowband system, i.e., the mobile channel is assumed to have time selective, flat fading. In this section, the models and statistics for such a mobile channel are provided.

2.2.1 Definition and Modeling

The physical mobile channel behavior allows the modeled channel to be considered in perspective. If there is an electrical LOS (meaning that there is Fresnel clearance and the antenna patterns illuminate the Fresnel zone) between the mobile and the BS, and if the mobile trajectory is linear, then the channel model with only short-term fading suggests a *well-defined Rice process* and the channel is called here the *well-defined Rice channel*.

In a well-defined Rice channel, the scenario is assumed to comprise a fixed mobile antenna pattern illuminated by fixed, diffuse scatterers and a single, dominant source with fixed amplitude, phase and direction. A scatterer creates a signal component at the receiver and this component is part of the signal describing the channel. Note that in the terminology here, a dominant *source* (physical scatterer) creates a dominant *component* of the channel CAG. For the Rayleigh channel, these scatterers represent diffuse components, and for a well-defined Rice channel, it is emphasized that there is a single, dominant component received from a fixed, dominant scatterer, added to the diffuse components, as illustrated in Figure 2.5.

When modeling a flat fading channel, the mobile is considered as surrounded by *effective scatterers*, - so called because they include the effect of the antenna patterns, propagation, resolvability, polarization and other physical effects [4]. From now on, "scatterer" and "effective scatterer" are interchangeable in this thesis unless otherwise mentioned. The scatterers are modeled only in the horizontal plane, as in the tradition of vehicular mobiles. Physical scatterers at elevated angles can be projected onto the horizontal plane.

The time-varying, well-defined channel CAG, also referred to simply as the "channel", is the signal representing the sum of the components from these effective scatterers; its notation is

$$h(t) = A\exp[j(2\pi f_D t\cos(\beta_0)+\varphi_0)] + \sum_{i}^{N_d} a_i \exp[j(2\pi f_D t\cos(\theta_i)+\alpha_i)] \tag{2.4}$$

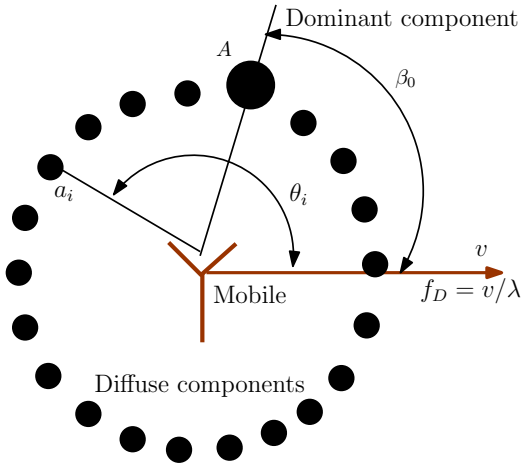

Figure 2.5: Illustration of channel modeling with isotropic scattering. The scattering is not necessarily isotropic. An illustration to the directional scattering is in Figure 2.9.

where A, β_0, and φ_0 are the magnitude, the AOA w.r.t. the mobile trajectory, and the initial phase of the dominant component, respectively; f_D is the maximum Doppler frequency (given by the ratio of the mobile velocity, denoted v, to the carrier wavelength, denoted λ); a_i, θ_i, and α_i are respectively the complex amplitude, the AOA, and the initial phase of the ith diffuse component. α_i is uniform over $[-\pi, \pi)$, and can be absorbed into a_i.

The physical scatterers are assumed to be in the far field of the mobile trajectory. As a result, the angles of the scatterers to the mobile trajectory, θ_i, are assumed not to change during the observation interval (time or distance). Clearly, for this assumption to hold, the observation interval of the time-varying channel is limited by the physical layout of the roads and surroundings. For vehicular mobiles, the valid observation interval may be several meters, but for handheld terminals, it would be smaller owing to their less smooth trajectory.

The observation interval, denoted here by T, is often normalized by the maximum Doppler frequency. Mathematically, $f_D T = \frac{v}{\lambda} t = \frac{z}{\lambda} = L$, where z is the distance the mobile travels during the observation interval T, and L represents the observation interval as either distance in wavelengths, or as duration in maximum Doppler frequency periods. The distance in wavelengths, L, is used in this thesis for denoting the observation interval.

One variation of the phase term in (2.4) is given as follows. $2\pi f_D t \cos(\theta_i) = \frac{2\pi}{\lambda} \cos(\theta_i) v t = u_i z$, where $u_i = \frac{2\pi}{\lambda} \cos(\theta_i)$ is called the *spatial Doppler frequency* in rads/m [4] and is determined only by the multipath environment. $u_i v = 2\pi f_D \cos(\beta_0)$ is the usual *Doppler*

frequency in rads/sec. These two types of Doppler frequency are used depending on the contexts in mobile communications.

In the absence of a dominant component, the channel CAG, denoted by $s(t)$, follows the notation

$$s(t) = \sum_{i}^{N_d} a_i \exp[j2\pi f_D t \cos(\theta_i)] = x(t) + jy(t) = a(t)\exp[j\phi(t)] \tag{2.5}$$

where $x(t)$ and $y(t)$ are the real and imaginary parts of the channel CAG, and each can be modeled as a Gaussian process (based on the central limit theorem (CLT)) with a zero mean and a variance of σ^2. $x(t)$ and $y(t)$ are also known as the inphase and quadrature components of the channel, respectively [1]. Since they have the same statistics, they are sometimes referred to as the "component" of the channel in the discussion of this thesis.

The magnitude, $a(t)$, is modeled by the Rayleigh distribution [1, 3],

$$p_a(a) = \frac{a}{\sigma^2}\exp[-\frac{a^2}{2\sigma^2}] \tag{2.6}$$

The wrapped phase, $\phi(t)$, has a uniform distribution [1, 3],

$$p_{uni}(\phi) = \frac{1}{2\pi},\ \phi \in [-\pi, \pi) \tag{2.7}$$

Note that $\phi(t)$ here is the time-varying version of ϕ_{rand} in (2.3). The Rayleigh magnitude and the uniform wrapped phase are dependent in a signal sense [4, 24], but are statistically independent, i.e., $p(a, \phi) = p_a(a)p_{uni}(\phi)$.

With a dominant component present, the channel is the well-defined Rice channel and the channel CAG can be rewritten as

$$h(t) = A\exp[j(2\pi f_D t\cos(\beta_0) + \varphi_0)] + x(t) + jy(t) = r(t)\exp[j\phi(t)] \tag{2.8}$$

The well-defined Rice channel is usually characterized by the Rice factor. The Rice factor is defined by $K = A^2/(2\sigma^2)$. It is often denoted by K and is also called the K factor [1, 2, 3, 4]. In this thesis other than Chapter 5, K is expressed in dB except for $K = 0$ (which corresponds to $-\infty$dB).

For the well-defined Rice channel, the envelope and wrapped phase signals are dependent in a signal sense and are statistically dependent [4, 24]. The Rice envelope, $r(t)$, is calculated

by $r(t) = \sqrt{A^2 + a^2(t)}$, and modeled by

$$p_r(r) = \frac{r}{\sigma^2} \exp[-\frac{r^2 + A^2}{2\sigma^2}] I_0(\frac{rA}{\sigma^2}) \tag{2.9}$$

where $I_0(x)$ is the modified Bessel function of the first kind and zeroth order. Or in terms of the K factor [4],

$$p_r(r) = \frac{r}{\sigma^2} \exp[-K - \frac{r^2}{2\sigma^2}] I_0(\frac{r}{\sigma}\sqrt{2K}) \tag{2.10}$$

The Rice phase, $\phi(t)$, can be calculated by

$$\phi(t) = \text{atan2}\, \frac{y(t) + A\sin(2\pi f_D t\cos(\beta_0) + \varphi_0)}{x(t) + A\cos(2\pi f_D t\cos(\beta_0) + \varphi_0)} \tag{2.11}$$

where `atan2` is the inverse tangent over $[-\pi, \pi)$ in four quadrants. The Rice phase is modeled by [2],

$$p_{Rice}(\phi; K, \varphi_0; t) = \frac{1}{2\pi} \exp[-K]\{1 + \sqrt{\pi K}\cos(\phi - 2\pi f_D t\cos(\beta_0) - \varphi_0) \times$$
$$\exp[K\cos^2(\phi - 2\pi f_D t\cos(\beta_0) - \varphi_0)](1 + \text{erf}\left(\sqrt{K}\cos(\phi - 2\pi f_D t\cos(\beta_0) - \varphi_0)\right))\} \tag{2.12}$$

where $\text{erf}(x) = \frac{2}{\sqrt{\pi}} \int_0^x \exp(-t^2)dt$. The Rice phase distribution, in general, is not stationary. It becomes stationary either when $K = 0$, i.e., when there is no dominant component present, or when $\beta_0 = 90^o$, i.e., when the dominant source is broadside to the velocity of the mobile over the observation interval.

2.2.2 Categories of Well-Defined Rice Channels

The well-defined Rice channel can be categorized into two groups based on the characteristics of the dominant source. If the dominant source is broadside to the velocity of the mobile (i.e., $\beta_0 = 90^o$) over the observation interval, then the dominant component has a zero spatial Doppler frequency (in rad/m). Here, the dominant component is present as a constant in the channel CAG making the Rician channel with a fixed K factor. This channel is referred to as the *stationary* well-defined Rice channel in this thesis.

If the dominant source is from a direction other than broadside, then the dominant component has a non-zero, constant spatial Doppler frequency. If the mobile travels with

constant velocity, the dominant component has a constant Doppler frequency (in rad/sec). In this case, the dominant component has a constant amplitude and its phase has a constant rate of change. This channel is the general case of the well-defined Rice channel.

On the other hand, if the mobile has a variable velocity (i.e., v is changing), then even if the K factor is fixed, the mobile channel is not a well-defined Rice channel because the Doppler frequency of the dominant source is changing. Similarly, if the dominant source is moving within the scenario w.r.t. the mobile trajectory (i.e., β_0 is changing), then the channel is again not a well-defined Rice channel, even if K is fixed. These cases are not considered here.

In practice, and especially for hand-held terminals, the mobile pattern can be changing drastically (w.r.t. geographical coordinates) with time and position. All the components, including any LOS component, take on a random character because of the pattern changes. In non-line-of-sight (NLOS), there can still be a local dominant component within the local scatterers, and its direction, phase, and amplitude, change with time and with position of the mobile. These practical scenarios are not considered in this thesis.

2.2.3 Second-Order Statistics Given Isotropic Scattering

The channel CAG can be presented as either the real and imaginary parts, or the envelope and phase. Since the dominant component in the well-define Rice channel CAG is deterministic, the Rayleigh channel CAG, $s(t)$, is used to analyze the statistics for these channel variables in this section. An example of these random channel variables for a Rayleigh process is illustrated in Figure 2.6.

The modeled channel CAG is wide-sense stationary over the observation interval, so the correlation function of $s(t)$ is a function only of time difference (or distance difference, for a fixed mobile velocity) [1, 3, 4]. The autocorrelation function of $s(t)$ is given by [3, 46],

$$R_{ss}(\tau) = E[s(t)s^*(t+\tau)] = 2\sigma^2 \int_{-\pi}^{\pi} p(\theta) \exp[j2\pi f_D \tau \cos(\theta)] d\theta \tag{2.13}$$

where $p(\theta)$ is the angular distribution of (effective) scattering in mobile channels, and used to model the directionality of the scattering.

Similar to the autocorrelation function of $s(t)$, the second-order statistics of other channel variables are also affected by the angular distribution of the scattering. It is emphasized here the scattering includes the effects of antennas, and the scattering is taken only in the

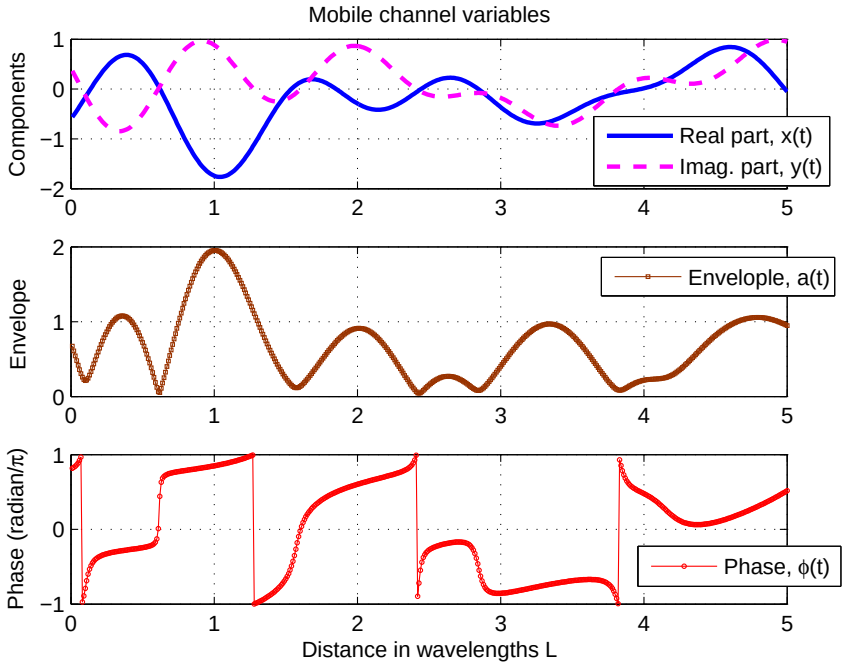

Figure 2.6: An example of time-varying channel variables for a Rayleigh process. They include the real and imaginary parts, the envelope, and the phase of the channel.

horizontal plane. In this section, the second-order statistics of each channel variable are reviewed in the presence of isotropic scattering.

With isotropic scattering (refer to Figure 2.5), $p(\theta) = 1/(2\pi)$, and the autocorrelation function of $s(t)$ becomes [47],

$$R_{ss}(\tau) = 2\sigma^2 J_0(2\pi f_D \tau). \tag{2.14}$$

The corresponding power spectral density (PSD), a.k.a., the Doppler spectrum, is given by [1, 3, 47]

$$S_{ss}(f) = \begin{cases} \frac{2\sigma^2}{\pi\sqrt{f_D^2 - f^2}} & |f| \le f_D \\ 0 & f > f_D \end{cases} \tag{2.15}$$

This spectrum has a U-shape, and is also called as the Clarke spectrum.

The components, $x(t)$ and $y(t)$, have the same autocorrelation function and PSD function as $s(t)$, except that the variance of the component equals half of the variance of $s(t)$

[2]. Mathematically,

$$R_{xx}(\tau) = R_{yy}(\tau) = \sigma^2 J_0(2\pi f_D \tau). \tag{2.16}$$

The corresponding PSD is

$$S_{xx}(f) = S_{yy}(f) = \begin{cases} \frac{\sigma^2}{\pi\sqrt{f_D^2 - f^2}} & |f| \leq f_D \\ 0 & f > f_D \end{cases} \tag{2.17}$$

The autocovariance function of the envelope of the channel, $a(t)$, is [1, 40, 47],

$$C_{aa}(\tau) = E[a(t)a(t+\tau)] - E[a(t)]E[a(t+\tau)] = \frac{\pi\sigma^2}{8} J_0^2(2\pi f_D \tau) \tag{2.18}$$

The PSD of $a(t)$ is [1, 40],

$$S_{aa}(f) = \begin{cases} \frac{\sigma^2}{8\pi f_D} K\left(\sqrt{1 - (\frac{f}{2f_D})^2}\right) & |f| \leq 2f_D \\ 0 & f > 2f_D \end{cases} \tag{2.19}$$

where $K(\gamma) = \int_0^1 \frac{1}{\sqrt{(1-x^2)(1-\gamma^2 x^2)}} dx$ is the complete elliptic integral of the first kind.

The autocorrelation function of the channel phase, $\phi(t)$, is given by, [4, 47],

$$R_{\phi\phi}(\tau) = E[\phi(t)\phi(t+\tau)] = \frac{4\pi^2}{3}\{\frac{3}{2\pi}\arcsin(\rho(\tau))[1 + \frac{1}{\pi}\arcsin(\rho(\tau))] - \frac{1}{8}\Omega(\rho(\tau))\} \tag{2.20}$$

where $\rho(\tau) = J_0(2\pi f_D \tau)$ and $\Omega(\rho(\tau)) = \frac{6}{\pi^2}\sum_{n=1}^{\infty} \frac{\rho(\tau)^{2n}}{n^2}$ with $\Omega(1) = 1$.

The correlation coefficient functions of the channel CAG, the components, the envelope and the phase equal, respectively, (2.14), (2.16), (2.18) and (2.20) normalized by their corresponding variances, and are respectively denoted as $\rho_{ss}(\tau)$, $\rho_{xx}(\tau)$ (or $\rho_{yy}(\tau)$), $\rho_{aa}(\tau)$, and $\rho_{\phi\phi}(\tau)$. The theoretical and simulated correlation coefficient functions and PSDs for these three channel variables are plotted in Figure 2.7 and Figure 2.8, respectively. Figure 2.7 shows that the phase decorrelates faster than both the envelope and the component (x or y) of the channel when the correlation coefficient is larger than around 0.3. Figure 2.8 shows that the cutoff frequency is f_D for the component, and $2f_D$ for the envelope, as expected. The spectrum of the phase has its first drop at f_D, followed by a slowly decaying tail. The first part of the phase spectrum is similar to the spectrum of the component,

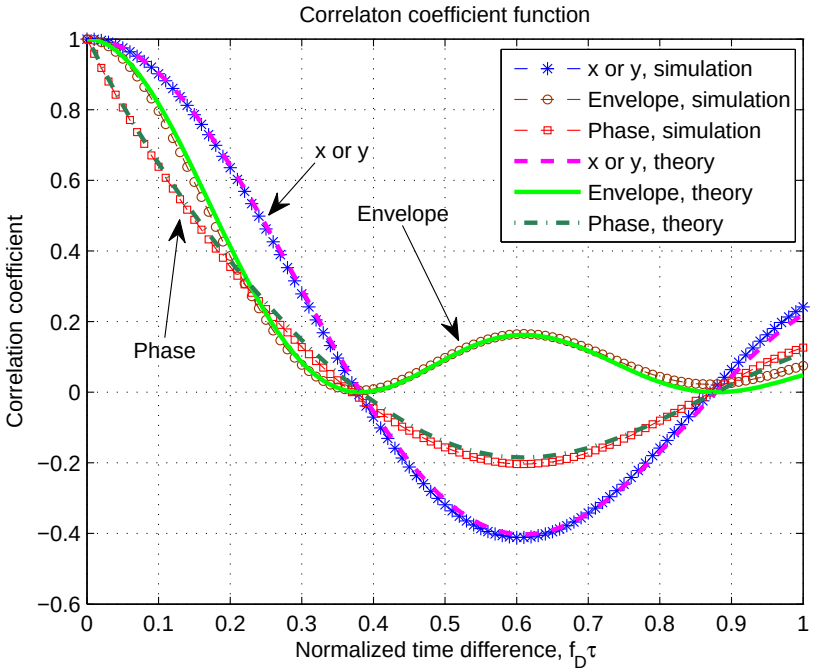

Figure 2.7: Comparison, by theory and simulation, of the correlation coefficient functions of the component (x or y), the envelope and the phase of a Rayleigh channel with isotropic scattering. The Rayleigh channel is simulated using the Algorithm 1 presented in Section 2.3.2.

corresponding to the continuous phase variations. The slowly decaying tail of the phase spectrum corresponds to the fast phase changes when the (wrapped) phase is close to $-\pi$ and π, and results in much wider spectrum than the other two variables.

Besides the correlation coefficient functions of the channel variables discussed above, the power (i.e., $a^2(t)$) correlation coefficient function is often used. The power correlation coefficient function, denoted by $\rho_{a^2a^2(\tau)}$, for a Rayleigh channel is known to have the following relation [4]:

$$\rho_{a^2a^2}(\tau) = |\rho_{ss}(\tau)|^2 \approx \rho_{aa}(\tau) \tag{2.21}$$

This relation says the correlation coefficient of the power equals the magnitude square of the correlation coefficient of the channel CAG, and also approximately equals the correlation coefficient of the envelope. For a Rayleigh channel, these correlation coefficients equal $J_0^2(2\pi f_D \tau)$.

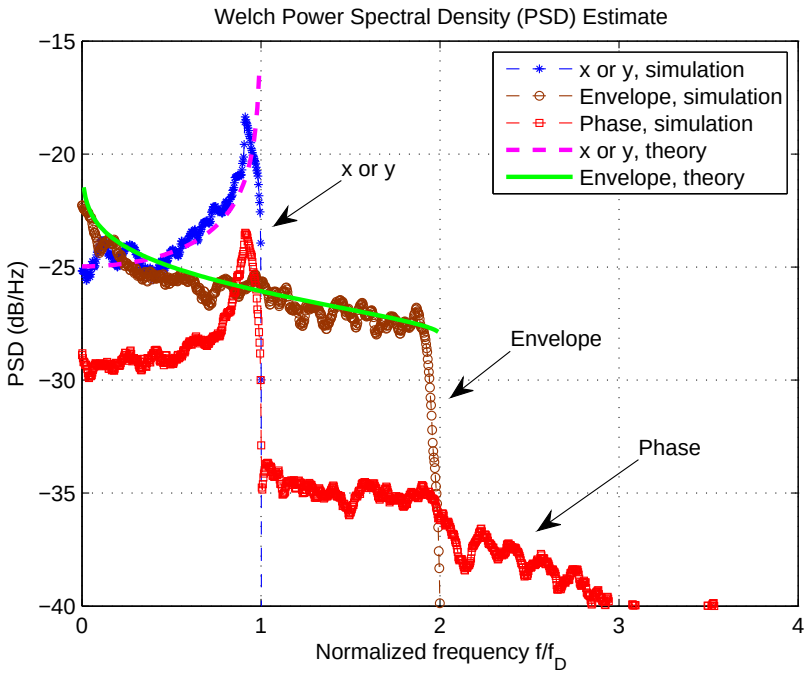

Figure 2.8: Comparison, by theory and simulation, of the PSDs of the component (x or y), the envelope and the phase (simulation only) of a Rayleigh channel with isotropic scattering. The Rayleigh channel is simulated using the Algorithm 1 presented in Section 2.3.2. The PSD is estimated using the Welch's method [48] with a window length of 10^4 samples. Each curve is normalized by the maximum Doppler frequency, and the corresponding variance of each variable.

The power correlation coefficient function of the channel is often used to design the spacing between two points in the multipath field. The two points could be a traveling distance for a mobile, or a spacing between two antennas. Uncorrelated signals or antennas are often required for many applications in mobile communications. Mathematically, the uncorrelated condition is set as the power correlation coefficient function approaching its first zero. By setting $J_0^2(2\pi f_D \tau) = 0$, and solving for $f_D\tau$, it gives $f_D\tau = L = 0.38$. However, in practice, "low" correlation is often taken as an a power correlation coefficient below about 0.5 [4]. This gives $f_D\tau = L = 0.18$. Putting into words, the two signals, or two antennas can be treated as uncorrelated when they are separated by a distance of 0.18 wavelength.

For a fading channel, the level crossing rate (LCR) is defined as the average number of times per second that the channel envelope crosses a given level with positive slope.

The LCR is affected by the scattering directionality, in particular the first and second moment of the channel spectrum. Therefore, the LCR is often used as a benchmark to test the performance of the mobile channel simulator [1, 49, 50]. In this thesis, the LCR for a Rayleigh fading channel is adopted when the proposed channel simulator is evaluated in Section 2.3.2. The normalized (by the maximum Doppler frequency, f_D) LCR for a Rayleigh channel, in the presence of isotropic scattering, is given by [1, 2],

$$N(\varrho) = \sqrt{2\pi}\varrho \exp[-\varrho^2] \tag{2.22}$$

where $\varrho = l_c/E[a(t)^2]$ is the normalized envelope level, l_c is the given level, and $E[a(t)^2]$ is the average power of the channel.

For a well-defined Rice channel, the correlation functions and PSD functions of the channel variables are the same as those for a Rayleigh channel, except for an additive factor from the deterministic dominant component. However, the LCR for a Rician channel is different from (2.22) for a Rayleigh channel, but this is not discussed in this thesis.

2.2.4 Modeling the Channel with Directional Scattering

In mobile communications, the scattering surrounding the receiver is not always isotropic. For example, the multipath signals incident at a BS are often directional, particularly for macrocells. This is seen from classical models where mobiles are located among dense scatterers and the BS is illuminated by the scatterers from a small spread of directions. For a mobile located in dense scatterers, the averaged scenario is often modeled as isotropic, though the local scattering distribution can seldom be expected to be isotropic. For a mobile located in a narrow street, the multipath signals received at the mobile are often directional [51]. For example, Jakes [47] shows a measured example of bi-directional power arrival in an urban street, demonstrating the arrival of power along street canyons can be from both directions. In the applications of smart antennas, the antenna ports often have directional power patterns [52].

Directional here refers to uni-directional. Similar to the discussion above, it is assumed that the scattering includes the antenna effects and in 2 dimensions (one polar angle) only. The directionality of the scattering can be interpreted as either: a directional angular distribution of incident power at an omni antenna; or a directional antenna power pattern in a uniform angular incident power distribution; or a combination of both (the antenna

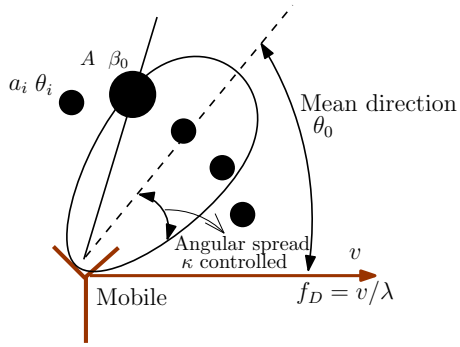

Figure 2.9: Illustration of channel modeling with directional scattering.

power patterns and the incident angular power distribution are multiplicative).

Unlike modeling isotropic scattering, modeling directional scattering requires two more parameters: the mean direction of the scattering; and a measure of the angular spread, as illustrated in Figure 2.9. The mean direction, θ_0, is defined as the angle of the nominal center of the directional scattering relative to the velocity of the mobile. The angular spread, similar to standard deviation of a Gaussian random variable, is measured by κ in the von Mises distribution, as provided in Section 2.2.4.2 below.

2.2.4.1 Directional Model Selection

There are several distributions for modeling directional scattering. Some examples include the cosine-power distribution [53, 54], the uniform [55], the truncated Gaussian [56, 57], and the truncated Laplacian [58, 59].

Except for the truncated Laplacian, these distributions are not founded from the physics of the propagation. So for omni antennas with directional incident power, the remaining models are unlikely to be accurate. However, they are likely to be good enough for many situations, because it tends to be the angular spread rather than the detail of the distribution that impacts communications design.

A common disadvantage of the above directional models is that their approximations to directional scattering are not versatile. For the truncated Gaussian and Laplacian distributions, the approximations to a circular function cause the formulations to be best suited to directional scattering with small to medium angular spreads. The cosine-power distribution better suits large angular spreads. This is because of computational pitfalls such as the power of the cosine becoming high for small angular spreads. The high power factor can

be averted by reducing the period of the cosine function, but then there is the need for keeping an eye on the support limits to ensure a single lobe in the full circular support. The uniform distribution can model the directional scattering with any mean direction and angular spread, but it is the least intuitive model for the AOAs.

Around 2000, the von Mises distribution was introduced for directional scenarios [60]. It is a convenient model owing to its inherent circular support, simple bell-shaped form, and smooth transition among many distributions. It extends the classical omnidirectional scenario to a directional one [46, 51, 61]. This distribution offers simple analysis and simulation in many applications of mobile communications including MIMO [51, 62, 63]. In this thesis, the von Mises distribution is applied for modeling directional scattering.

2.2.4.2 Von Mises Distribution

The von Mises distribution is given by [17]:

$$p_v(\theta;\theta_0,\kappa) = \frac{1}{2\pi I_0(\kappa)} \exp[\kappa\cos(\theta-\theta_0)],\ \theta\in[-\pi,\pi),\ \kappa\geq 0 \tag{2.23}$$

where θ_0 is the mean direction of angular data[3]; κ is called the *concentration parameter* and controls the angular spread of the directional distribution. The meaning of these parameters are depicted in Figure 2.9.

An illustration of the von Mises pdf with $\theta_0 = 0$ and various κ is given in Figure 2.10. κ controls the directional shape and properties of the von Mises pdf, and allows a smooth transition on the circular support from a uniform distribution to a delta-like function. For example, when $\kappa = 0$, the von Mises pdf becomes the uniform distribution between $-\pi$ and π; when $\kappa \to \infty$, the von Mises pdf approaches a delta function at $\theta = \theta_0$; and when κ is sufficient large (i.e., κ >5dB), the von Mises pdf may be thought of as a circular version of the Gaussian distribution.

The simple exponential structure allows the von Mises pdf to produce closed forms for its associated statistical functions. These properties are what make the distribution useful for modeling many different applications involving directional scenarios.

[3] θ_0 should not be confused with β_0, the AOA of the dominant component. They could have the same or different values.

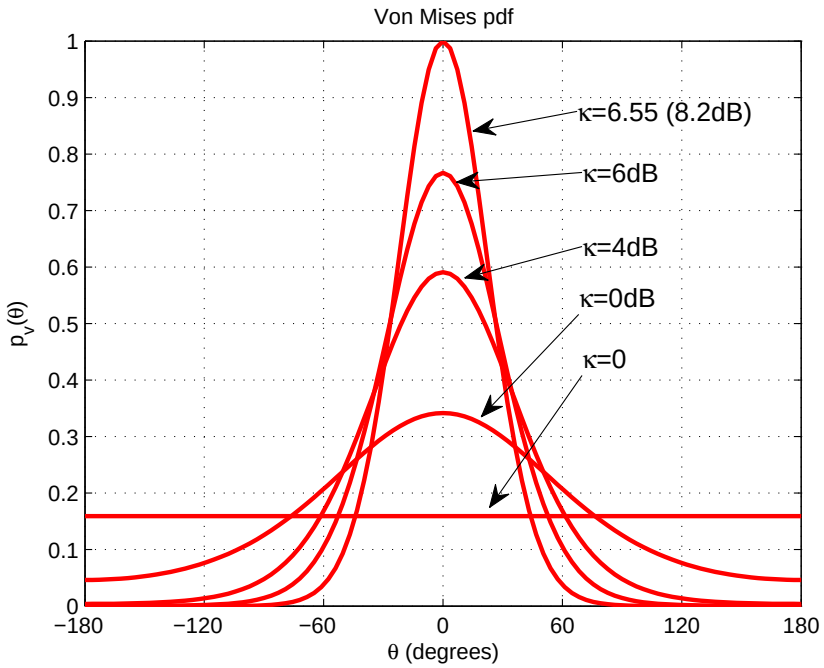

Figure 2.10: Examples of the von Mises pdf with $\theta_0 = 0$ and various κ. The mode is unity when $\kappa = 6.5508$.

2.2.4.3 Second-Order Statistics Given Directional Scattering

In this section, some second-order statistics of the Rayleigh channel with directional scattering, useful for discussions and analysis in this thesis, are reviewed. The directional scattering of the channel is modeled by the von Mises distribution. The channel CAG notation is the same as above: $s(t) = x(t) + jy(t)$.

The autocorrelation function of $s(t)$ is given in [34, 46, 61],

$$R_{ss}(\tau) = \quad 2\sigma^2 \frac{J_0\left(\sqrt{-\kappa^2+4\pi^2 f_D^2 \tau^2 - 4j\pi\kappa f_D \tau \cos(\theta_0)}\right)}{I_0(\kappa)}. \tag{2.24}$$

When $\kappa = 0$, the von Mises pdf reduces to the uniform distribution, and the autocorrelation function in (2.24) reduces to (2.14) for isotropic scattering. When $\kappa = 0$ or $\tau = 0$, $R_{ss}(\tau)$ takes a real value; otherwise, $R_{ss}(\tau)$ takes a complex value.

The relation about the correlation coefficient functions given by (2.21) still holds for the Rayleigh channel with directional scattering. However, the minimum distance for two points in multipath filed being uncorrelated will depend on the directional parameters (i.e.,

θ_0 and κ). The detailed results are discussed in the context of antenna spacing design in Section 6.2.

Two derivatives of the autocorrelation functions at $\tau = 0$ are given as follows [46].

$$\dot{R}_{ss}(0) = -j4\pi\sigma^2 f_D \frac{\cos(\theta_0) I_1(\kappa)}{I_0(\kappa)} \tag{2.25a}$$

$$\ddot{R}_{ss}(0) = -\sigma^2 (2\pi f_D)^2 \left(1 + \frac{\cos(2\theta_0) I_2(\kappa)}{I_0(\kappa)}\right) \tag{2.25b}$$

Other properties related to the autocorrelation functions are,

$$R_{\dot{s}s}(0) = R_{s\dot{s}}(0) = \dot{R}_{ss}(0) \tag{2.26a}$$

$$R_{\dot{s}\dot{s}}(0) = -\ddot{R}_{ss}(0) \tag{2.26b}$$

$$R_{xx}(0) = R_{yy}(0) = \frac{1}{2}\Re\{R_{ss}(0)\} = \sigma^2 \tag{2.26c}$$

$$R_{yx}(0) = -R_{xy}(0) = \frac{1}{2}\Im\{R_{ss}(0)\} = 0 \tag{2.26d}$$

$$R_{\dot{y}x}(0) = R_{x\dot{y}}(0) = -\frac{1}{2}\Im\{\dot{R}_{ss}(0)\} = b^2 \tag{2.26e}$$

$$R_{y\dot{y}}(0) = R_{\dot{y}y}(0) = \frac{1}{2}\Re\{\dot{R}_{ss}(0)\} = 0 \tag{2.26f}$$

$$R_{\dot{y}\dot{y}}(0) = -\frac{1}{2}\Re\{\ddot{R}_{ss}(0)\} = c^2 \tag{2.26g}$$

where $\Re\{\cdot\}$ and $\Im\{\cdot\}$ represents the real and imaginary parts of the argument, respectively,

$$b^2 = 2\pi\sigma^2 f_D \frac{\cos(\theta_0) I_1(\kappa)}{I_0(\kappa)}$$

and

$$c^2 = \frac{\sigma^2}{2}(2\pi f_D)^2 \left(1 + \frac{\cos(2\theta_0) I_2(\kappa)}{I_0(\kappa)}\right).$$

Since $s(t)$ is a circularly symmetric process, its autocorrelation function, $R_{ss}(\tau)$, also has the properties that

$$R_{xx}(\tau) = R_{yy}(\tau) \tag{2.27a}$$

$$R_{xy}(\tau) = -R_{yx}(\tau) \tag{2.27b}$$

$$R_{ss}(\tau) = 2(R_{xx}(\tau) - jR_{xy}(\tau)). \tag{2.27c}$$

For directional scenarios (i.e., $\kappa \neq 0$), $R_{ss}(\tau)$ takes a complex value. In this case, $R_{xy}(\tau)$ no longer equals zero, which means that $x(t)$ and $y(t)$ are now correlated. However, $R_{ss}(\tau)$ is real for $\tau = 0$, independent of κ. In this case, $R_{xy}(0)$ equals zero, which means that $x(t)$ and $y(t)$ are uncorrelated *at the same instant*, independent of κ. This property shows that the scattering directionality does not affect the distribution of the envelope and phase of channel CAG, but changes the second-order statistics of the channel [64].

Denoting the effective scattering distribution by $p(\theta)$, the PSD of the channel CAG is known to be [1, 47],

$$S(f) = \begin{cases} \frac{2\sigma^2(p(\theta)+p(-\theta))}{\sqrt{f_D^2-f^2}} & |f| \leq f_D \\ 0 & f > f_D \end{cases} \tag{2.28}$$

Substituting the von Mises distribution, given by (2.23) for $p(\theta)$, the PSD of the channel CAG becomes

$$S_{ss}(f) = \begin{cases} \frac{\sigma^2(\exp[\kappa\cos(\theta-\theta_0)]+\exp[\kappa\cos(-\theta-\theta_0)])}{\pi I_0(\kappa)\sqrt{f_D^2-f^2}} & |f| \leq f_D \\ 0 & |f| > f_D \end{cases} \tag{2.29}$$

Since $\cos(\theta) = \frac{f}{f_D}$, and $\sin(\theta) = \sqrt{1-(\frac{f}{f_D})^2}$, then

$$\cos(\theta-\theta_0) = \tfrac{f}{f_D}\cos(\theta_0) + \sqrt{1-(\tfrac{f}{f_D})^2}\sin(\theta_0)$$
$$\cos(-\theta-\theta_0) = \tfrac{f}{f_D}\cos(\theta_0) - \sqrt{1-(\tfrac{f}{f_D})^2}\sin(\theta_0).$$

When $\kappa = 0$, (2.29) reduces to (2.15) for isotropic scattering. Similar to the scenario with isotropic scattering, the PSD of the component of the channel is

$$S_{xx}(f) = S_{yy}(f) = \frac{1}{2}S_{ss}(f) \tag{2.30}$$

The LCR is also affected by scattering directionality. Assuming the von Mises distribution is used for modeling directional scattering, the normalized (by the maximum Doppler frequency, f_D) LCR for a Rayleigh channel is given by (*c.f.* Equation (19) in [50]),

$$N(\varrho) = \sqrt{2\pi}\varrho\exp[-\varrho^2]\frac{\sqrt{I_0^2(\kappa) - I_1^2(\kappa) + \cos(2\theta_0)[I_0(\kappa)I_2(\kappa) - I_1^2(\kappa)]}}{I_0(\kappa)} \tag{2.31}$$

When $\kappa = 0$, (2.31) reduces to (2.22), the normalized LCR for a Rayleigh channel with isotropic scattering.

The statistics of the absolute phase (including mean, variance, and pdf) are affected by the scattering directionality. The statistics of the absolute phase in isotropic scattering are presented in Chapter 4, and the mean of the absolute phase in directional scattering is given in Chapter 6.

2.3 Mobile Channel Simulations

2.3.1 Review of Simulation Techniques

Simulation has become the main tool for analyzing and assessing the performance of the algorithms, methodologies, and system designs in communications, and particularly in mobile communications. Simulation results can also reveal unexpected behavior of the system, and bring new opportunities to theory development. For example, in this thesis, all new theoretical results are confirmed using simulations; some results are obtained by simulations, but cannot be solved theoretically. Therefore, the validity of the simulation and its statistical accuracy play an important role in being able to draw conclusions. Speed and memory requirements are also important properties for a simulator.

Generating channel random variates, which satisfy predefined statistics, such as the distributions and correlations mentioned above, is widely required. Four types of techniques for simulating the mobile channel have been proposed:

- the physical channel based sum-of-sinusoids technique [47];
- the time domain based white noise filtering technique using an FIR filter [1, 65, 66];
- the time domain based white noise filtering technique using an IIR filter [49, 67];
- the frequency domain based inverse discrete Fourier transform (IDFT) technique [68, 69].

The physical channel based technique sums multiple sinusoidal variables with each sinusoid modeling one signal component received from one scatterer of the channel [47]. Several variations of this technique also exist by introducing randomness to sinusoids [70]. The summed signal can be modeled as a complex Gaussian using the CLT, and has the Clarke

spectrum if the AOAs of scatterers are uniformly distributed. The physical channel based technique is simple to understand, but its run time complexity is relatively high [69].

The time domain based techniques convolve white Gaussian noise with either an FIR or an IIR filter that satisfies the predefined Doppler filter shape (e.g., the filter is fixed and is the Bessel function for idealized isotropic scattering). To represent complicated shapes such as this Bessel function, the FIR filter needs many filter taps [66, 69], resulting in high computational load. The IIR filter design stems from ill-conditioned Yule-Walker equations, sometimes leading to instability [49]. However, an IIR design is presented in [71].

The frequency domain based IDFT technique multiplies white Gaussian noise with a predefined Doppler spectrum in the frequency domain, and then transforms the spectrally filtered random variates to the time domain. Usage of the FFT makes this type of channel simulator attractive because of its high speed. Owing to the relatively simple shape of the PSD (e.g., the U-shape Clarke spectrum for isotropic scattering), the simulator is easy to design and modify. However, the FFT requires the samples to be produced in large blocks, so this type of channel simulator tends to introduce larger delay and requires more memory than other techniques. Since this type of channel simulator calculates filter coefficients using a discrete spectrum which is approximated from the predefined spectrum, then faithful reproduction of the shape of the predefined spectrum is not guaranteed. Therefore, some second-order statistics, such as the LCR and the zero-crossing rate (ZCR), involving the first and second moments of the spectrum, might not be accurately reproduced using the IDFT technique [49].

Nevertheless, channel simulation based on the IDFT technique is widely used and has been standardized. For example, The package `rayleighchan`, offered by Matlab, generates the Rayleigh random variates with the predefined spectrum using the IDFT technique [72].

Most channel simulators developed so far are based on a 2D isotropic scattering, i.e., for a well-defined Rice channel with the Clarke spectrum. As discussed in Section 2.2.4, the 2D directional scenario, if uni-directional, can be conveniently modeled by the von Mises distribution [34, 46, 51, 61]. In this case, the envelope of the channel CAG is still Rayleigh, but the second-order statistics (e.g., correlation and PSD) change, and non-zero cross-correlation appears between the real and imaginary parts of the signal. Therefore the channel simulators discussed above should be modified or generalized.

In [49], the time domain based white noise filtering technique using an IIR filter is set up for a directional scenario modeled by the von Mises distribution. Several examples show

that the second-order statistics (including correlation and LCR) of the generated channel match the theories very well. In [73], the physical channel based sum-of-sinusoids technique was attempted for simulating the channel with directional scattering but the simulation results depart greatly from the theory. In [73] and [74], the frequency domain based IDFT technique is generalized for the directional scenario modeled by the von Mises distribution with a mean direction of zero. The disagreement between the statistics (the ZCR is used here) of the simulated channel and the theory arises but no explanations are given.

In this Section, a generalized version of channel simulator, using the frequency domain based IDFT technique, is developed based on the one described in [69]. The directional scenario is modeled by the von Mises distribution. The generalized simulator accepts two directional parameters as inputs: κ, related to the angular spread; and θ_0, the mean direction of the directional scenario. The Rice factor, K, is also included in the channel simulator. The performance of the simulator is evaluated using the second-order statistics, including correlation and LCR.

2.3.2 Mobile Channel Simulator in Directional Scenarios Using IDFT

As discussed in [69], the IDFT based simulator finds the Doppler filter coefficients in the frequency domain by sampling the continuous spectrum of the channel component, which is given by (2.29) for directional scenario. If N samples are used, the frequency for each sample is $f = \frac{kf_s}{N}$, where $k = 0, \ldots, N-1$, and f_s is the sampling frequency. The maximum frequency of the spectrum is the maximum Doppler frequency, f_D, so f_s needs to be at least twice f_D in order to prevent aliasing. Mathematically, $f_n = f_D/f_s < 0.5$ where f_n is the maximum Doppler frequency normalized by the sampling frequency. In `rayleighchan` of Matlab, f_n is taken (arbitrarily) as 0.1 [72].

When simulating a communication system in a fading channel with a fading rate of f_m, the channel sampling rate (i.e., f_s) should equal the signaling rate (i.e., $1/T_{symbol}$) so that each signal sample can multiply with a channel sample. This means $f_n = f_m$ when these sampling rates are normalized by the maximum Doppler frequency. When $f_n \neq f_m$, an upsampling technique by a factor of $\lfloor f_n/f_m \rfloor$ if $f_m < f_n$, or a downsampling technique by a factor of $\lfloor f_m/f_n \rfloor$ if $f_m > f_n$, should be followed after channel simulation. Here $\lfloor x \rfloor$ denotes the nearest integer less than or equal to x. The upsampling or the downsampling techniques are not discussed in this thesis.

In the algorithm proposed here, the fading rate, f_m is taken as an input parameter.

When f_m is (arbitrarily) within $[0.001, 0.1]$, it is reasonable to assign $f_n = f_m$. However, if the fading rate is too small (say, $f_m < 0.001$), $f_n = f_m$ would result in a large number of samples used for the IDFT, requiring large memory and slowing simulation speed; if $f_m > 0.1$, $f_n = f_m$ would result in not enough samples for approximating the PSD, sacrificing simulation accuracy. Therefore, f_n might be determined by f_m as follows:

$$f_n = \begin{cases} f_m & 0.001 \le f_m \le 0.1 \\ 0.001 & f_m < 0.001 \\ 0.1 & f_m > 0.1 \end{cases} \tag{2.32}$$

The index for the maximum frequency can be found by

$$k_m = \lfloor \frac{N f_D}{f_s} \rfloor = \lfloor N f_n \rfloor \tag{2.33}$$

The discrete spectrum of the component of the channel CAG, removing constants and normalizing by f_n, becomes

$$S[k] = \begin{cases} \frac{\exp[\kappa a_1] + \exp[\kappa a_2]}{I_0(\kappa)\sqrt{1-(\frac{k}{N f_n})^2}} & |k| \le k_m \\ 0 & k_m < |k| \le N-1 \end{cases} \tag{2.34}$$

where

$$a_1 = \frac{k}{N f_n}\cos(\theta_0) + \sqrt{1 - \left(\frac{k}{N f_n}\right)^2}\sin(\theta_0)$$

and

$$a_2 = \frac{k}{N f_n}\cos(\theta_0) - \sqrt{1 - \left(\frac{k}{N f_n}\right)^2}\sin(\theta_0).$$

When $N f_n$ is an integer, (2.34) becomes infinity at the edge index of k_m. In [69] with isotropic scattering, this singularity is taken care of by assigning a value to the spectrum at k_m with a finite number. The finite number is calculated by setting the area under the discrete spectrum after the modification to equal the area given by the continuous spectrum. In the presence of directional scattering, a finite number could be found using a similar technique but the calculation would be very complicated. With the number of samples, N, usually a power of 2, and f_n a decimal fraction, $N f_n$ is rarely an integer. If N is large enough, the samples in the frequency domain can well represent the continuous spectrum.

Therefore, the "edge effect" (i.e., singularity) is ignored in the following discussion.

With the proof given in [69], the Doppler filter coefficients in the frequency domain are the square root of the discrete spectrum. Therefore, when the filter coefficients are implemented in the positive digital frequency domain, they are

$$F_G[k] = \begin{cases} 0 & k = 0 \\ \sqrt{S(k)} & k = 1, 2, \ldots, k_m \\ 0 & k = k_m + 1, \ldots, N - k_m - 1 \\ \sqrt{S(k-N)} & k = N - k_m, \ldots, N-2, N-1. \end{cases} \tag{2.35}$$

When $\kappa = 0$, (2.35) reduces to Equation (21) in [69], except for the edge values at $k = k_m$ and $k = N - k_m$; and the constant multiplied to the non-zero filter coefficients. These constants are not very important because it is the shape of the spectrum that determines the statistics of the simulated channel. Therefore, (2.35) can be treated as a generalized version of Equation (21) in [69].

When $\kappa = 0$, i.e., for isotropic scattering, the filter coefficients, $F_G(k)$, are symmetric about the digital frequency at π (corresponding $k = N/2$). Therefore, the autocorrelation function of the generated channel CAG in the time domain is real. For nonzero κ, the filter coefficients become nonsymmetric and change with κ and θ_0. Correspondingly, the autocorrelation function becomes complex.

A completed algorithm is described in Algorithm 1. After the IDFT,

$$s[n] = \frac{1}{N} \sum_{k=0}^{N-1} X[k] \exp[j \frac{2\pi kn}{N}]$$

where $X[k]$, in the digital frequency domain, is defined at Line **7**. The variance for each component of $s[n]$, is given by [69]

$$\sigma^2 = \frac{\sigma_k^2}{N^2} \sum_{k=0}^{N-1} F_G^2[k]$$

with σ_k^2 the variance of each generated i.i.d. Gaussian variates at Line **6**. Let $\sigma_k^2 = 1$, then $\sigma^2 = \frac{1}{N^2} \sum_{k=0}^{N-1} F_G^2[k] = \sigma_g^2$, as given by Line **5**. Therefore, by dividing σ_k by σ_g at Line **6**, the variances of $x[n]$ and $y[n]$, i.e., σ^2, generated at Line **8** are both 1. The magnitude of the dominant component is then given by $A = \sqrt{2K}$ at Line **9**, which produces the Rice

factor as $A^2/2\sigma^2 = K$.

Algorithm 1: Simulating the well-defined Rice channel in directional scenarios by the IDFT technique

Input: N: the number of points used for the IDFT;
K: the Rice facor;
β_0: the AOA of the dominant component;
φ_0: the initial phase of the dominant component;
f_m: the fading rate of the mobile channel;
κ: the directionality parameter in the von Mises distribution;
θ_0: the mean direction of the directional scattering;
Output: $h[n]$:N-point samples of the simulated channel CAG with the Rice factor of K.

begin
  Determine f_n by (2.32);
  Find k_m by (2.33);
  Find $F_G[k]$ by (2.35), $k = 0, \ldots, N-1$;
  Calculate $\sigma_g = \frac{1}{N}\sqrt{\sum_{k=0}^{N-1} F_G^2(k)}$;
  Generate two sets of N i.i.d. zero-mean Gaussian variates, $A[k]$ and $B[k]$, each with variance $1/\sigma_g^2$;
  Calculate $X[k] = (A[k] - jB[k])F_G[k]$;
  Calculate the IDFT on N-point $X[k]$. Denote the outputs $s[n] = x[n] + jy[n]$, $n = 0, \ldots, N-1$;
  Add the dominant component: $h[n] = \sqrt{2K}\exp(j2\pi f_n n\cos(\beta_0) + \varphi_0) + s[n]$;
end
Notation: σ_g^2 : the total power of the designed Doppler filter;

To better view the algorithm, the block diagram for simulating the mobile channel in directional scenarios is shown in Figure 2.11, which is similar to Figure 2 in [69].

The number of points used for the IDFT, N, is usually determined by the time/distance required by the simulation. For example, given the distance of interest in wavelengths, L, the number of samples of interest can be calculated by $\lfloor L/f_n \rfloor$. N is taken as an integer close to $\lfloor L/f_n \rfloor$, and is normally a power of two. However, N should not be too small in order to guarantee the accuracy of representing the predefined spectrum with the discrete spectrum. This accuracy is determined by the selected value of the digital frequency index corresponding to the Maximum Doppler frequency, k_m. For example, if $k_m \geq 100$ is required for the accuracy in simulation, N should be an integer larger than $100/f_n$ by (2.33).

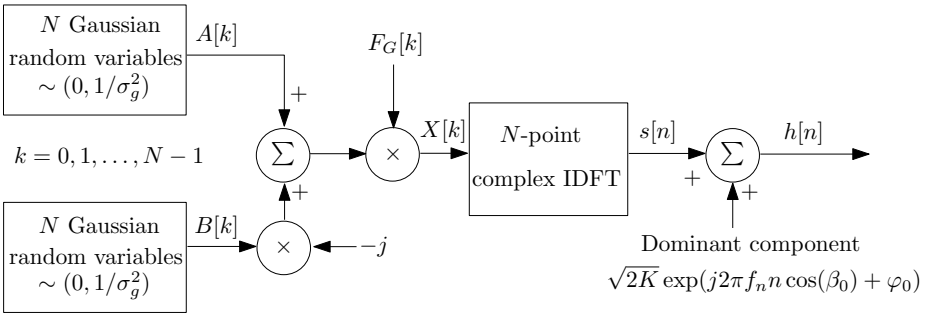

Figure 2.11: Block diagram of the generalized mobile simulator in directional scenarios using the IDFT technique.

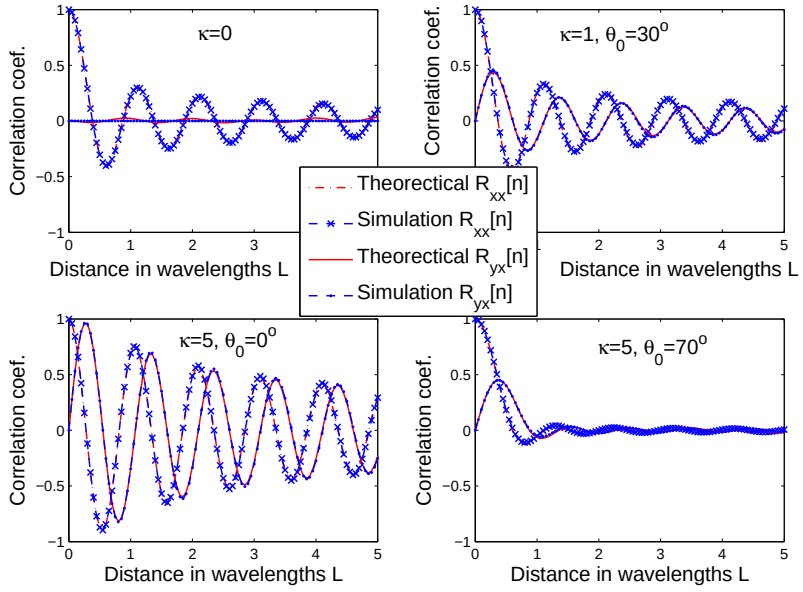

Figure 2.12: Examples of auto- and cross- correlation of the generated channel for different κ and θ_0. The simulated and theoretical curves overlap each other. The lines with markers represent the autocorrelation, and those without markers represent the cross-correlation. The x-label, L, is the distance in wavelengths, and represents $f_D\tau$ in (2.24). L also equals nf_n with n the sample index.

2.3.3 Performance Evaluation

The performance of the generalized channel simulator by the IDFT is evaluated using the second-order statistics of the channel including the correlations and the LCR. Figure 2.12 shows the simulated and theoretical autocorrelation of the real part of the generated channel

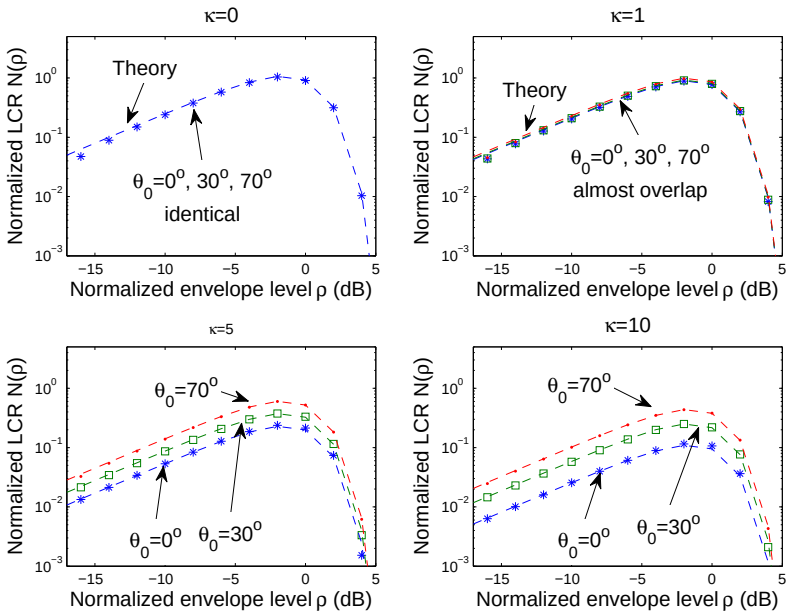

Figure 2.13: Examples of LCR given $\kappa = 0, 1, 5, 10$ and $\theta_0 = 0, 30^o, 70^o$. The theoretical curves are plotted by dashed lines, and the simulated curves are plotted by different markers (stars for $\theta_o = 0$, squares for $\theta_0 = 30^o$, and dots for $\theta_0 = 70^o$).

(i.e, $R_{xx}[n]$); the simulated and theoretical cross-correlation between the imaginary and the real parts of the generated channel (i.e., $R_{yx}[n]$), for different values of κ and θ_0. The theoretical results are based on (2.24) and (2.27). The autocorrelation and cross-correlation vary significantly with κ and θ_0, but the simulation results match the theory very well. There are small discrepancies when the correlation is well away from the main lobe (not shown in the figure). However, in practice, matching the detail of the side lobe region of the correlation function is seldom important. It can be concluded that the mobile simulator by the IDFT technique for directional scenarios is able to reproduce the autocorrelation and cross-correlation of the modeled channel.

Figure 2.13 shows four sets of LCR curves given $\kappa = 0, 1, 5, 10$ and $\theta_0 = 0, 30^o, 70^o$. The simulated LCR curve for $\kappa = 0$ overlaps the LCR curve (not shown here) obtained using the channel simulator by the IDFT described in [69]. The LCR varies with both the mean direction of the directional scenario, θ_0, and the directionality parameter, κ. The variation owing to the mean direction is slight for small κ, but significant for large κ.

The simulated LCR curves do not match the theory very well for small crossing levels

(i.e., $\varrho < -15$dB) when κ is small. A similar observation is made in [49] and also on page 65 in [1] for the case where the physical channel based sum-of-sinusoids technique is used for simulating the channel. The disagreement is because the sampling rate used in the above simulation (i.e., $f_n = 0.01$) is not high enough to capture all the level crossing events. As the sampling rate increases (e.g. $f_n = 0.001$), the simulation converges (slowly) to the theoretical value because less level crossing events are missed.

Another reason for disagreement is that the LCR depends on the first and second moments of the spectrum whereas the IDFT technique cannot guarantee the perfect match to the predefined spectrum shape [49]. This disagreement decreases with increasing κ because the impact of the first and second moments of the spectrum on the LCR is inversely proportional to κ. It is reported in [49], when the white noise filtering technique using an IIR filter is used for simulating the channel, this disagreement is smaller than the one from the IDFT technique because a carefully designed IIR filter can provide a more precise match to the predefined spectrum than the IDFT technique.

The departure of the simulated LCR from the theoretical form of its model, for small crossing levels, demonstrates a limitation of the simulation technique. Nevertheless, the second-order statistics from the simulator are, in general, a good match to the modeled forms, and this is adequate for many simulation requirements.

2.3.4 Summary

Channel simulation by the inverse discrete Fourier transform technique is formulated for directional scenarios, and is summarized in the form of an algorithm in this section. The simulator is only for the well-defined Rice channel, and it is limited to a 2D effective scattering distribution. Nevertheless, it is adequate for many applications. The von Mises distribution is used here for the directionality. It has the usual isotropic form (Clarke spectrum) as a special case. Multi-directional distributions can be synthesized by summing multiple von Mises functions, or by direct synthesis from a different model for the effective scattering distribution. The accuracy of the simulator w.r.t. its mathematical model is limited by the channel sampling rate and the difference of the shape of the predefined spectrum model and its discretized form. This difference causes, for example, small dissimilarities in the side lobe structure of the correlations, and in the LCR for low envelope levels with low directionality. In this thesis, Algorithm 1 is used for simulating the well-defined Rice channel with either isotropic or directional scattering.

Chapter 3

Absolute Phase for a Well-Defined Rice Channel

This chapter introduces a new channel variable, namely the absolute phase, based on the channel modeling presented in Chapter 2. This chapter answers three questions: what is the absolute phase; how to formulate the absolute phase using the channel variables; and how to obtain the absolute phase by simulation, and acquire the absolute phase in practice.

3.1 Introduction to the Absolute Phase

3.1.1 Effects of Propagation on Channel Phase

Figure 3.1 depicts a popular single bounce model of the outdoor channel, where the BS directly illuminates a single set of static, random scatterers around the mobile. As discussed in Section 2.1.2, the scatterers seen by the mobile have random phases but also contain a phase term influenced by the distance between the scatterers and the BS.

Specifically, at position 1, the mobile sees scatterers which all feature a delay related to the distance to the BS, d. The phase of the scatterers includes a distance-dependent term, $e^{j2\pi d/\lambda}$. This term is equivalent to $e^{j\omega_c\tau_1}$, where ω_c is the carrier angular frequency, and τ_1 represents an average delay between the scatterers at Position 1 and the BS. At Position 2, the mobile sees a new set of scatterers whose phase now includes $e^{j\omega_c\tau_2}$, where τ_2 is larger than τ_1. Geometrically, $\tau_1 \approx d/c$ and $\tau_2 \approx (d + \Delta d)/c$. As well as the distance-dependent phase term, the channel phase seen by the mobile, at each position, also includes a random

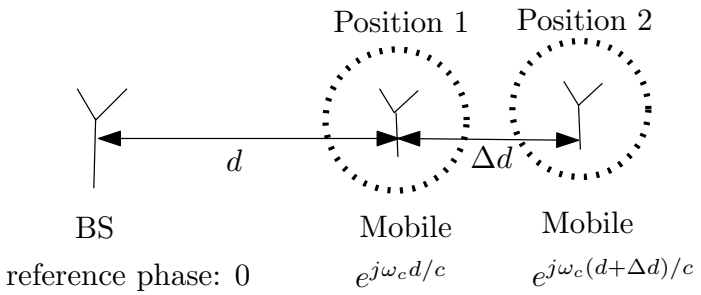

Figure 3.1: A popular outdoor mobile channel model. The channel phase (after unwrapping) increases as the mobile moves away from the BS. ω_c is the carrier angular frequency and c is the speed of light.

term, which is from the summation of random phases of all scatterers.

In an absolute reference system (approximated by having Frequency Standards at both the receiver and transmitter, see Section 3.4.3), as the mobile moves away from a BS, the channel phase (after unwrapping) experiences an average increase while experiencing random phase variation. Similarly, the phase relative to the BS decreases on average as the mobile moves towards the BS. The instantaneous changes are not constant with distance owing to the random nature of the phase, but the mean change rate is essentially constant because it relates to the increasing/decreasing distance.

The channel phase is closely related to the propagation phenomena discussed in Section 2.1.2. The random phase is due to short-term fading, and the distance-dependent phase is due to the signal propagation. The random phase acts as a short-term phase noise added on the deterministic distance-dependent phase. This is analogous to the (random) short-term fading multiplied to the (distance-dependent and deterministic) propagation gain. Another propagation phenomenon is shadowing. If shadowing is multiplicative to short-term fading, it will not affect the random phase. Other types of shadowing[1] will affect the random phase, but they are not considered in this thesis.

For vehicle-to-vehicle channels, there is a similar situation regarding the phase, but one of the vehicles is now the BS and is also typically modeled as having dense local scatterers. In some situations, vehicle-to-vehicle channels are modeled with a keyhole link, or linked with an amplify-and-forward repeater, and the channel becomes so-called double-Rayleigh. This situation is not treated in this thesis.

[1]The detailed shadowing models are discussed in Section 5.1.1 in Chapter 5.

3.1.2 Definition of the Absolute Phase

Instead of the distance-dependent channel phase as described by Figure 3.1, the interest here, for the analysis, is the *absolute phase* of a well-defined Rice channel, i.e., the accumulated *random* phase change from only the (fixed) local scatterers[2].

Recall that with the dominant component present, the channel notation is

$$h(t) = r(t)\exp[j\phi_W(t)] = I(t) + jQ(t)$$

where $\phi_W(t)$ is the same as $\phi(t)$, but the subscript W is used here to emphasize that the phase is "wrapped"; $r(t)$ is the Rice envelope, and $\phi_W(t)$ is the Rice phase in $[-\pi, \pi)$ as given by (2.11); $I(t)$ and $Q(t)$ are the real and imaginary parts of a Rician channel CAG.

The absolute phase is defined as the accumulated (Rice) phase change over the time $(t_0, T + t_0)$, denoted $\phi_A(T; t_0)$, with t_0 the reference time and T the observation interval. The time-varying unwrapped phase without subtracting the phase at time t_0 is called the *continuous phase* $\phi_C(t; t_0)$. Mathematically, $\phi_A(T; t_0) = \Delta\phi_C(T; t_0) = \phi_C(T; t_0) - \phi_C(0; t_0)$. The statistics of $\phi_A(T; t_0)$ are independent of the reference time t_0, so $\phi_A(T)$ is used to denote the absolute phase from here on. Similarly, instead of $(t_0, T + t_0)$, $(0, T)$ is used as the observation time interval of interest in the following discussion. With this formulation, the specific value of the initial phase of the dominant component, φ_0, will not affect the absolute phase, so it is assumed to be zero from hereon.

The observation interval can be normalized by the maximum Doppler frequency, i.e., $f_D T = L$. Similar to $f_D T_{symbol}$ (i.e., f_m) in digital communications, which represents the fading speed of the channel relative to the signaling rate, L is an important parameter to describe the statistics of the absolute phase in the mobile channel.

3.1.3 Absolute Phase Examples

Figure 3.2 shows an example of the real and imaginary parts, the phase of the channel, and its corresponding absolute phase. Owing to unwrapping, the absolute phase does not have abrupt changes at π or $-\pi$ as the wrapped phase does, and has a phase range beyond $[-\pi, \pi)$. The different behaviors fundamentally change the statistics of the absolute phase

[2]The distance-dependent phase can be removed from the received signal, for example, using synchronization techniques.

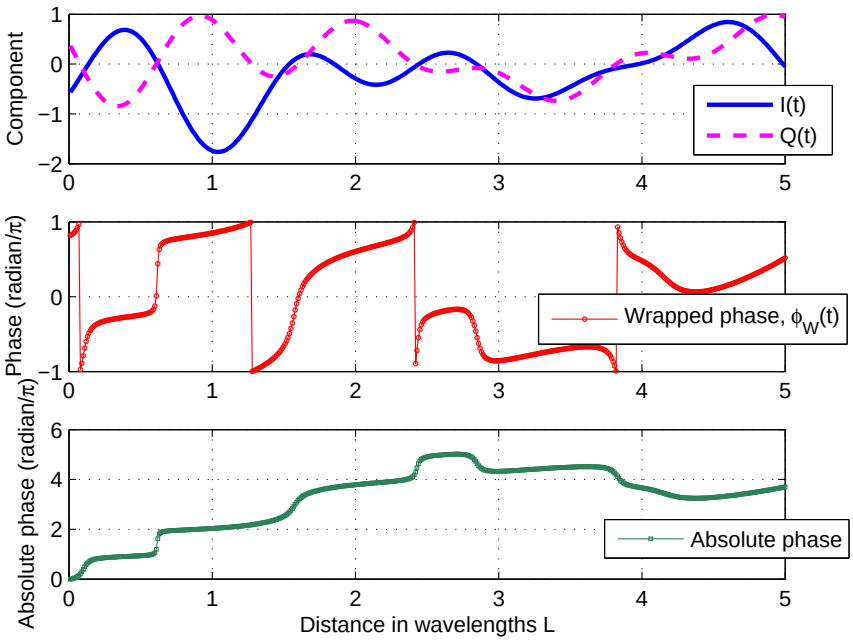

Figure 3.2: Example, from simulation, of the real and imaginary parts, the wrapped phase and the absolute phase for a well-defined Rice channel with $K = 0$.

compared to the wrapped phase.

Figure 3.3 shows an example of the absolute phase trajectories for two users in a well-defined Rice channel with the same weak K factor, but moving in different directions. The different mobile users have different, and in fact independent, absolute phase trajectories due to the moving direction. Moreover, for the well-defined Rice channel, the mean of the absolute phase includes a linear component of the phase from the dominant source that changes proportionally to the distance to that source, even though any distance-dependence to the BS as shown in Figure 3.1 has been omitted. This property is potentially useful in mobile applications such as mobile user localization and tracking.

Figure 3.4 shows another example of the absolute phase trajectories for two users in a well-defined Rice channel moving towards the same direction, but with different K factors. The mean of absolute phase exhibits different slopes, which is related to the value of the K factor. This property can be potentially used for channel characterization in mobile communications. This potential has resulted in a new K factor estimator, which is discussed in Chapter 5.

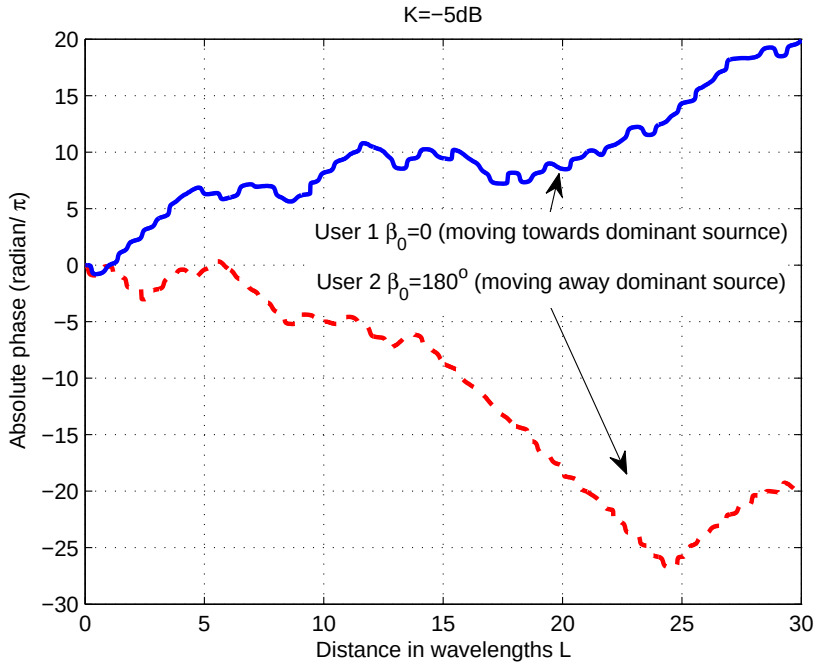

Figure 3.3: Examples, from simulation, of the absolute phase trajectories for two mobile users with the same weak K factor ($K = -5$dB). These examples do not include the distance-dependent effect of Figure 3.1, but show the absolute phase increasing/decreasing on average, for a well-defined Rice channel.

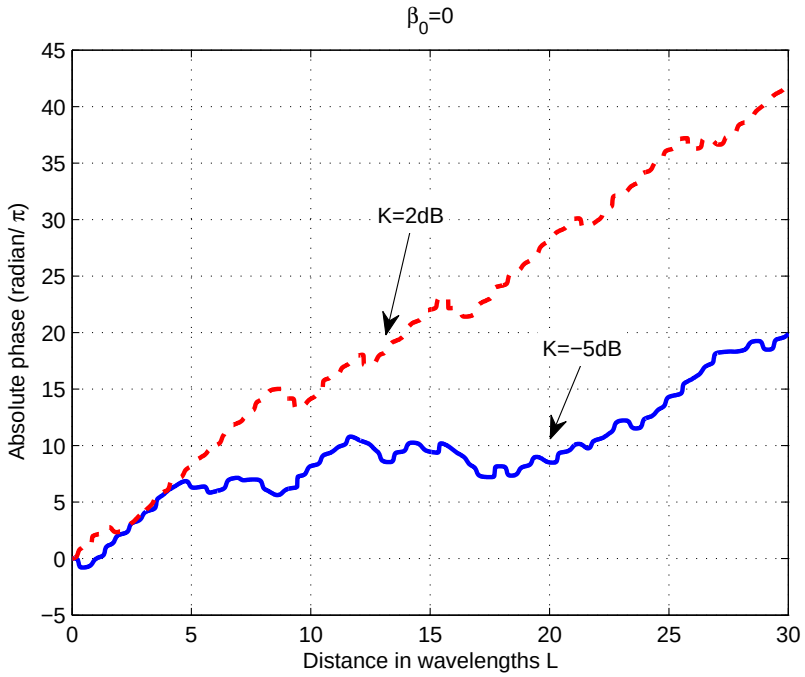

Figure 3.4: Examples, from simulation, of the absolute phase trajectories for two mobile users moving towards the same direction, but with different K factors.

3.2 Formulations of the Absolute Phase

The absolute phase can be obtained by the unwrapping technique as follows. Find the wrapped phase, $\phi_W(t)$, of the channel CAG by circular functions, unwrap $\phi_W(t)$ over the time $(0, T)$, and subtract the initial phase. The unwrapping algorithm is in itself an extensive research area, and has been adopted in many applications, for example, to restore the phase information of images in radar, sonar, and optics [75, 76, 77, 78].

As discussed in Section 1.2, the absolute phase in mobile channels is analogous to the output phase of an FM receiver (e.g. limiter-discriminator-integrator [21]). Several calculation techniques, such as the zero-crossing technique [26], the phase derivative integration technique [20], and the Rice click analysis [15], have been developed to calculate the output phase of the FM receiver. These techniques can be used to formulate the absolute phase in mobile channels.

In this section, these different techniques are discussed using the terminology of mobile channels, and connections between them are made. Here a stationary well-defined Rice channel model (i.e., $\beta_0 = 90^o$) is adopted for discussion, but the results can be generalized to the well-defined Rice channel (i.e., $\beta_0 \neq 90^o$,).

3.2.1 Unwrapping Technique

Given $\beta_0 = 90^o$ and $\varphi_0 = 0^o$, the wrapped phase of (2.11) can be simplified to

$$\phi_{W4}(t) = \text{atan2}\,\frac{y(t)}{x(t)+A} = \text{atan2}\,\frac{Q(t)}{I(t)} \tag{3.1}$$

which is in all four quadrants between $-\pi$ and π. This is the commonest method to find the phase angle in mobile communications.

Given both $Q(t)$ and $I(t)$ are continuous Gaussian processes, the wrapped phase, $\phi_{W4}(t)$, during the time $(0, T)$, calculated by (3.1), might experience a type of phase discontinuity called the 2π *discontinuity*. The 2π discontinuity of the wrapped phase aries when $Q(t)$ changes its sign while $I(t) < 0$, i.e., when the signal trajectory crosses the negative $I(t)$ axis. It is the periodic property of circular functions (i.e., `atan2` in (3.1)) that results in the 2π discontinuity, as illustrated in Figure 3.5. Meanwhile, $\phi_{W4}(t)$ might mathematically experience a phase jump of exactly π, which arises when the signal trajectory crosses the

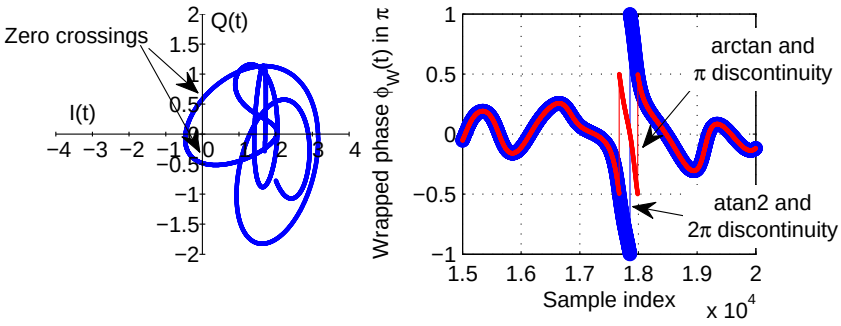

Figure 3.5: Signal trajectory (left) and wrapped phase (right) for a stationary well-defined Rice process. The wrapped phase can have either the 2π discontinuity or the π discontinuity depending on the use of circular functions. The simulation parameters are $K = 5$dB, and $f_n = 0.001$.

origin, i.e., $r(t) = \sqrt{I(t)^2 + Q(t)^2} = 0$. This event strictly has an infinitesimal probability, but in practice, almost-π jumps (and recognized as π *jumps* [4, 16, 29]) are observed whenever $r(t)$ is small, i.e., when the signal moves closely passed the origin. In the mobile channel, deep fades that have no π jump are unlikely.

The continuous phase can be obtained by unwrapping the wrapped phase $\phi_{W4}(t)$ over $(0, T)$. Since the wrapped phase varies relatively slowly and the maximum change is no greater than 2π, the `unwrap` function given, for example, by Matlab, is adopted to implement the unwrapping operation. The `unwrap` function is defined as "correcting the radian phase angles in a vector by adding multiples of $\pm 2\pi$ when absolute jumps between consecutive elements of the vector are greater than the jump tolerance of π radians." In other words, the continuous phase, $\phi_C(t)$, is obtained by adding or subtracting multiples of 2π to the wrapped phase $\phi_{W4}(t)$, as shown in Figure 3.6.

By the unwrapping technique, the absolute phase at time T is formulated as

$$\phi_A^{(u)}(T) = \phi_{W4}(T) - \phi_{W4}(0) + 2\pi N_{2\pi}(0, T) \tag{3.2}$$

where $\phi_{W4}(T)$ and $\phi_{W4}(0)$ are the wrapped phase values within $[-\pi, \pi)$ at time T and 0, respectively, and $N_{2\pi}(0, T)$ represents the cumulative number of 2π corrections during the time period of $(0, T)$. This is written as $N_{2\pi}(0, T) = N_{2\pi+}(0, T) - N_{2\pi-}(0, T)$, where $N_{2\pi+}(0, T)$ and $N_{2\pi-}(0, T)$ are the number of positive and negative 2π corrections respectively.

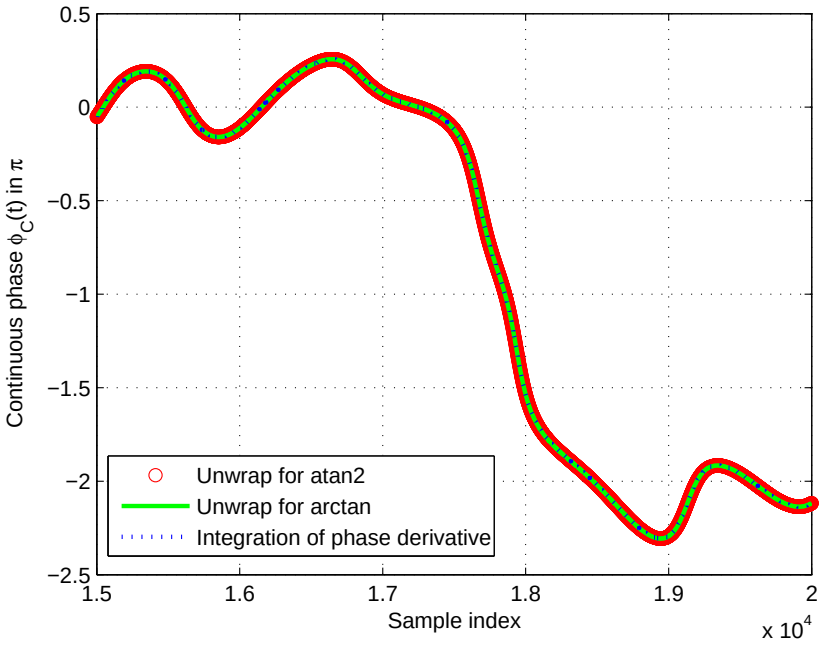

Figure 3.6: The continuous phases calculated using unwrap functions by (3.1) and (3.3), and using the phase derivative integration technique by (3.6), for a stationary well-defined Rice process. The two curves from unwrapping technique are identical, but are slightly different from the curve from the integration. The difference is less than the linewidth in this example.

Note that the 2π correction corresponds to the event that the signal crosses the negative $I(t)$ axis. During the crossing, 2π is added if the sign of $Q(t)$ becomes negative from positive (referred to as the *positive* 2π *crossing event*), and otherwise, 2π is subtracted (referred to as the *negative* 2π *crossing event*).

3.2.2 Zero-Crossing Technique

In early wireless communications phase analysis [20, 26], instead of `atan2`, `arctan` was used to calculate the wrapped phase:

$$\phi_{W2}(t) = \arctan \frac{Q(t)}{I(t)} \tag{3.3}$$

where `arctan` returns the inverse tangent in the range of $[-\pi/2, \pi/2]$. ϕ_{W2} denotes the phase over two quadrants only. As a result, this wrapped phase, $\phi_{W2}(t)$, experiences discontinuities

of π owing to the periodic property of the circular function of `arctan`, each time when $I(t) = 0$, i.e., when the signal crosses the $Q(t)$ axis, as shown by "zero crossings" in Figure 3.5.

In order to obtain the continuous phase, the unwrapping operation is undertaken here by modifying the `unwrap` function given in Matlab. The new `unwrap` function is defined as "correcting the radian phase angles in a vector by adding multiples of $\pm\pi$ when absolute jumps between consecutive elements of the vector are greater than the jump tolerance of $\pi/2$ radians". The continuous phase is shown in Figure 3.6.

The absolute phase can be formulated from ϕ_{W2} through [26],

$$\phi_A^{(z)}(T) = \phi_{W2}(T) - \phi_{W2}(0) + \pi N_\pi(0, T) \tag{3.4}$$

where $N_\pi(0, T)$ represents the cumulative number, counted from time 0 to T, of the real part of signal, $I(t)$, crossing zero.

This formulation is similar to the key idea behind the zero-crossing technique proposed by Blachman [22, 79]. The zero-crossing technique originally comes from the estimation of the phase derivative (i.e., the instantaneous frequency) of a narrowband signal [19]. It relies on the fact that the phase derivative of a narrowband signal can be estimated by the number of zeros of the narrowband signal over an interval.

The continuous phase based on `arctan` is identical to the one based on `atan2`, as shown in Figure 3.6. Since (3.2) and (3.4) are equivalent in calculating the absolute phase by the conversion of `atan2` and `arctan`, only `atan2` is considered here, and $\phi_W(t)$ is used to represent $\phi_{W4}(t)$, when discussing the unwrapping operation, unless otherwise mentioned.

3.2.3 Phase Derivative Integration Technique

In order to avoid the discontinuities caused by `atan2` or `arctan` function, the derivatives of the real and imaginary parts of the signal are taken to calculate the phase derivative, and then this phase derivative is integrated to obtain the continuous phase [20]. This method has been widely adopted in both analog and digital FM receivers [21, 26, 27, 80], where the FM receiver usually consists of a limiter-discriminator plus a low-pass filter.

The discriminator acts as a differentiator, and the output of the discriminator in the FM receiver is proportional to the phase derivative. The phase derivative notation here is

the over-dot, and the formulation is [20, 26]

$$\dot{\phi}_C(t) = \frac{I(t)\dot{Q}(t) - Q(t)\dot{I}(t)}{I(t)^2 + Q(t)^2}. \tag{3.5}$$

Since the analog real and imaginary parts of the signal, $I(t)$ and $Q(t)$, are continuous, the output of the discriminator no longer contains the discontinuity caused by the domain of `atan2` or `arctan`. Mathematically, the phase derivative in (3.5) has the discontinuity only when $I(t) = Q(t) = 0$, i.e., when $r(t) = \sqrt{I(t)^2 + Q(t)^2} = 0$. Similar to the phase jump of exactly π discussed above, the event strictly has an infinitesimal probability.

The low-pass filter in the FM receiver can be approximated by an ideal integrator over a duration from 0 to T. The output of the integrator at time T is the absolute phase, *viz.*,

$$\phi_A^{(i)}(T) = \int_0^T \dot{\phi}_C(t)dt. \tag{3.6}$$

This seems to be the most intuitive way to formulate the absolute phase (given its definition) and this formulation is used by Rice [20] and Middleton [24] for deriving the variance of the output phase in the FM receiver situation.

The resulting continuous phase is shown in Figure 3.6 based on the signal example in Figure 3.5. The continuous phase from the unwrapping technique and from the phase derivative integration technique are almost the same. In Appendix A, these two techniques are compared and it is shown that although they are indeed similar, they can produce different results owing to the sensitivity of (3.5) to small values of $r(t)$.

3.2.4 Rice Click Analysis

As discussed above, the phase discontinuity in the wrapped phase is due to the usage of circular functions. This kind of discontinuity disappears after unwrapping. However, whenever the signal magnitude, $r(t)$, is close to zero, the phase varies dramatically as determined by (3.5). In mobile channels, this corresponds to a deep fade with a corresponding large-peak impulse in the phase derivative [4, 16].

When K is large, the large-peak impulse in the phase derivative becomes highly related to the 2π discontinuity in the wrapped phase. This impulse, appearing after the discriminator in FM receivers, is named as the *click* by Rice [15], because it is heard as a click in analog FM receivers. It is depicted in Figure 3.7. Depending on the trajectory of the signal

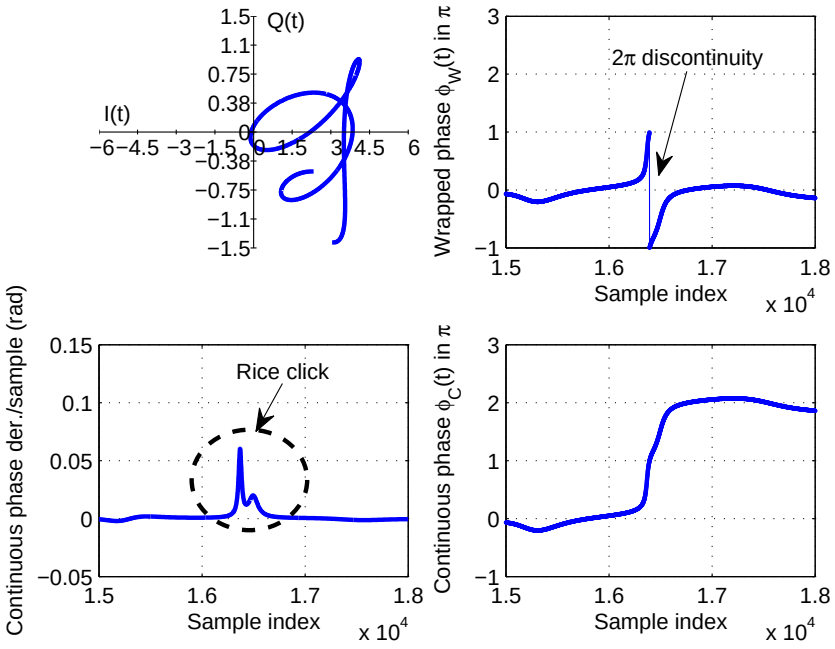

Figure 3.7: An example of the Rice click. The simulation parameters are $K = 8$dB, and $f_n = 0.001$.

completing one 2π trajectory about the origin, the impulse, from hereon called the *Rice click*, can appear as many shapes [81]. The impulse always has an area of 2π, corresponding of course to the phase change of 2π in the continuous phase.

The absolute phase in the mobile channel can be formulated, similar to the formulation of the output phase of an FM receiver using the Rice click [15], as

$$\phi_A^{(c)}(T) = \phi_W(T) - \phi_W(0) + 2\pi N_{r2\pi}(0, T) \tag{3.7}$$

where $N_{r2\pi}(0, T)$ is the cumulative number of the Rice clicks. Note that both $\phi_W(T)$ and $\phi_W(0)$ are calculated through (3.1), and lie in the range of $[-\pi, \pi)$. This formulation is widely used to calculate the output phase in digital FM receivers [27, 80], where the SNR is usually very high.

The Rice click is a complicated random event. However, Rice modeled it as a event of the signal crossing the negative $I(t)$ axis (i.e., the 2π crossing event) when the SNR (*c.f.*, K) of FM receiver is large. With this modeling, (3.7) becomes equivalent to (3.2). However,

when the SNR is not large enough, this modeling becomes inaccurate and then many other clicks, such as the doublet [82] and the false click [82, 83], were observed and discussed in FM receivers. These clicks, especially the false clicks, can appear to be similar to the Rice click, but have different mechanisms and different effects on the mean and variance of the output phase of an FM receiver. The click types, together with their effects on the absolute phase, are summarized and compared in Appendix B.

3.3 Simulation of the Absolute Phase

The statistics of the absolute phase are studied by theory, and the results are verified by simulation. Simulating the absolute phase is based on simulating the mobile channel because the absolute phase is the accumulated channel phase change over an observation interval $(0, T)$. In this thesis, the mobile channel is generated using Algorithm 1 presented in Chapter 2. The parameters used in Chapter 3 to Chapter 5 are as follows: $\varphi_0 = 0$ (initial phase of the dominant component), $\beta_0 = 90^o$ (i.e., the stationary well-defined Rice channel), $\kappa = 0$ (i.e., isotropic scattering), $\theta_0 = 0$ (mean direction of the scattering, any value can be used here for isotropic scattering) , and $f_n = f_m = 0.01$. In Chapter 6, non-zero κ (i.e., directional scattering) and different values of θ_0 and β_0 are considered.

After the channel is generated, the absolute phase $\phi_A(T)$ is then calculated using the formulations described in Section 3.2. For the simulations in this thesis, the `unwrap` function given by Matlab is adopted to calculate the absolute phase.

The absolute phase is a time-varying random variable, and the statistics (e.g., mean or variance) of the absolute phase changes with the observation time. Therefore, ensemble average cannot be replaced by time average when acquiring a sample statistic of the absolute phase [84]. In this thesis, one sample of the absolute phase at time T is acquired by running the channel simulator once. The sample statistics are averaged over at least 10^4 samples.

3.4 On Acquisition of the Absolute Phase

The absolute phase is calculated from the wrapped channel phase, so in this section, the sampling frequency of the wrapped channel phase is first provided. Some possible systems for measuring or estimating the channel phase are then suggested. Finally, some practical considerations for acquiring the absolute phase are discussed.

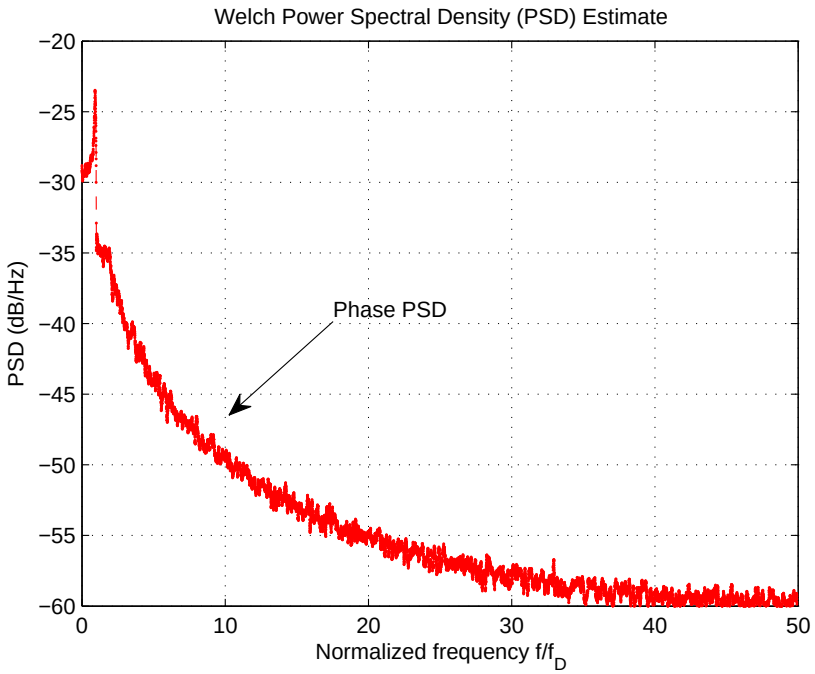

Figure 3.8: The phase PSD, estimated from simulation, against the normalized frequency. The 99 percent bandwidth for the wrapped phase is around $45f_D$. This figure is for the Rayleigh channel, i.e., $K = 0$. A larger K will have a narrower spectrum.

3.4.1 Mobile Channel Phase Sampling Frequency

The channel phase can be calculated from the real and imaginary parts of the channel CAG, or collected directly from the channel phase if available. It is also possible to use the channel envelope to help estimate the phase (refer to Section 7.4 in [4] for detail), but this method is not discussed in this thesis.

As discussed in Section 2.2.3, the channel CAG can be described by three types of variables: real or imaginary part (component); envelope; and phase. They have different spectral properties (refer to Figure 2.8). For the component, the cutoff frequency of the spectrum is f_D, and for the envelope, it is $2f_D$. However, the spectrum of the phase is much wider than those of the component and the envelope. A phase PSD, from simulation, against the normalized frequency, is shown in Figure 3.8. Since the phase PSD has a slowly decaying tail, the 99 percent bandwidth[3] is used here to find its cutoff frequency. Based

[3]The bandwidth that contains 99 percent of the total power [85].

on simulation, the 99 percent bandwidth for the phase is around $45f_D$. By the Nyquist theorem, the minimum sampling frequency for the phase is $90f_D$, which is much larger than the minimum sampling frequencies for the component and the envelope of the channel.

Many communication systems provide only the real and imaginary parts of the channel, and therefore the sampling frequency is usually not high enough to reconstruct the phase without aliasing. In this case, the real and imaginary parts should be interpolated (upsampled) to at least $90f_D$ before the phase is calculated (this is equivalent to requiring the maximum Doppler frequency normalized by the sampling frequency, f_n, to be no larger than 0.01).

3.4.2 Acquisition Systems for Channel Phase

Practical measurement of the absolute phase is suggested as future work. Here, two types of systems are recommended to acquire the absolute phase. Both systems provide samples for the real and imaginary parts of the channel CAG. The absolute phase can then be calculated using these samples.

The first choice is to use a channel sounding system. One such system is described in [86]. In a channel sounding system, the sounding signal is characterized by two time-related parameters: signal duration, denoted T_{signal}, and repetition time or sampling period, denoted T_s [3]. The signal duration determines the achievable resolution in the delay time domain, and can be adjusted based on user requirements, but should not be longer than the coherence time of the channel. Mathematically, this means $f_D T_{signal} < 1$. The sounding signal is used to capture the channel variation in the time domain. The repetition rate of the sounding signal should be at least twice the maximum Doppler frequency to avoid aliasing but the repetition time should be larger than the maximum delay (τ_m) to avoid overlapping of consecutive received pulses. Mathematically, this means $\tau_m < T_s < \frac{1}{2f_D}$. The latter relation is equivalent to $f_n < 0.5$ as discussed in Section 2.3.2. If the sampling frequency of a sounding system is higher than the minimum sampling frequency of the channel phase, interpolation techniques are not required before calculating the absolute phase.

The alternative is to use a communication system capable of channel estimation such as pilot-aided modulations [87, 88] and blind channel estimations [89, 90]. The pilot symbol is similar to the sounding signal in the sounding system. The repetition time of the pilot symbol (i.e., the reciprocal of the pilot symbol rate) should satisfy $f_D T_s < 0.5$. Much larger sampling frequency is preferred for recovering the envelope and phase, but it will decrease

the channel throughput and capacity efficiency. Therefore, interpolation techniques usually follows the channel estimation in these systems [87, 88].

3.4.3 Practical Considerations of Acquiring the Absolute Phase

As discussed in Section 3.1.1, the phase of the channel CAG consists of a distance-dependent term and a random term. To calculate the absolute phase using the random wrapped phase, the distance-dependent phase should be removed.

In practical sounding or communication systems, the distance-dependent phase can be measured and removed from the channel phase using time synchronization techniques. This removal might not be perfect, causing inaccuracy in the wrapped phase measurement. The accuracy of the wrapped phase measurement is also affected by frequency synchronization as discussed below.

The mobile and the BS can be synchronized by their own Frequency Standard oscillators. This technique is experimentally feasible, using, for example, Rubidium Standards, as in many channel sounding systems [86]. In this case, the measured phase difference (found from signal mixing) between the receiver's Standard-derived reference phase and the phase of the received signal from the transmitter's Reference-derived carrier, would be the wrapped phase of the channel. In a communications system with the transmitted carrier phase-modulated, this measured phase would also contain the modulation information. It is assumed here that either there is a dedicated (i.e., unmodulated) pilot tone, or that any angle-modulation can be separated from the channel phase variations.

Normally, a receiver derives its phase reference by locking to the received signal carrier using a phase-locked loops (PLL). Without Frequency Standard oscillators, the measured phase difference would also include a significant phase roll, $\exp(j\Delta\omega_o t)$, where $\Delta\omega_o$ is the radial frequency difference between the transmitter and receiver oscillators, and is a function of time owing to temperature variations in the oscillators. The phase roll is not directly caused by propagation within the mobile channel, but would be part of the measured phase of the mobile channel.

If the PLL tracks the received carrier perfectly and instantaneously, then the derived (instantaneous) frequency reference at the receiver would track the signal carrier perfectly. The measured phase difference at the receiver will include the wrapped channel phase and the phase roll.

With a very stiff (very long time constant) PLL, the receiver's reference oscillator is more

like the Frequency Standard situation in the sense that the fast phase changes (such as from the phase roll) are smoothed out. The received signal phase (which is changing because of the changing channel) and the reference phase (essentially constant) can be subtracted by signal mixing to yield the wrapped channel phase.

In summary, effects such as the phase roll and the changing separation distance, add to other practical issues such as oscillator phase noise, etc., to complicate the acquisition of the wrapped channel phase, and consequently of the absolute phase.

The following chapter develops the statistics of the absolute phase. Therefore, the distance-dependent phase and phase noises such as the phase roll etc. are omitted. The channel phase contains only the absolute phase as defined by contributions from the local, fixed scatterers.

Chapter 4

Statistics of the Absolute Phase with Isotropic Scattering

In this chapter, the theoretical results for the mean, variance and pdf of the absolute phase are provided for the well-defined Rice channel with isotropic scattering. These statistics are fundamental to develop and analyze potential applications related to the absolute phase, such as the Rice factor estimator presented in Chapter 5. Simulations are used to support the analysis and discussion.

4.1 Mean of the Absolute Phase

The mean of the wrapped phase is zero for a Rayleigh channel and for a well-defined Rice channel with a zero initial phase. But the mean of the absolute phase is not always zero. An intuitive way to derive the mean of the absolute phase, as described by Blachman [22, 23], is provided below.

Recalling the channel CAG here for convenience

$$h(t) = A\exp[j2\pi f_D t\cos(\beta_0)] + a(t)\exp[j\phi_W(t)] \tag{4.1}$$

For a stationary well-defined Rice channel (i.e., $\beta_0 = 90^o$), the number of positive and negative 2π crossings are evenly distributed (have the same mean) during the observation interval so that the resulting absolute phase has a mean of zero.

Consider a well-defined Rice channel with a dominant component with a magnitude A,

which rotates the origin with a constant rate. Its phasor is $A\exp[j2\pi f_D t\cos(\beta_0)]$. When the magnitude of the diffuse component, $a(t)$, is smaller than the magnitude of the dominant component, A, then the absolute phase increases with an average rate of $2\pi f_D\cos(\beta_0)$. On the other hand, if $a(t) > A$, then the circumnavigations of the origin are random and so the ensemble average of the absolute phase is zero. Mathematically, the mean of the absolute phase is given by [22]

$$\begin{aligned}\bar{\phi}_A(T) &= T\times[2\pi f_D\cos(\beta_0)]\int_0^A p_a(a)da \\ &= 2\pi f_D\cos(\beta_0)T(1-\exp[-K]) \\ &= 2\pi\cos(\beta_0)(1-\exp[-K])L. \end{aligned} \tag{4.2}$$

The mean of the absolute phase calculated by (4.2) becomes zero when $K = 0$ or when the dominant component has zero spatial Doppler (i.e., $\beta_0 = 90^o$).

Some examples, including both simulation and theoretical results, of the mean of the absolute phase for various K and L are illustrated in Figure 4.1 and Figure 4.2. It can be seen that the mean given by (4.2) is well supported by the simulation results. The sign of the mean is determined by the AOA of the dominant source relative to the mobile velocity: if $\beta_0 \in [0, 90^o)$, the mean is positive, and is negative if $\beta_0 \in (90, 180^o)$. The sign can be used to indicate the quadrant or even specific direction of the dominant source relative to the trajectory of the mobile.

4.2 Variance of the Absolute Phase

In this section, the techniques for calculating the variance of the absolute phase are presented. As discussed in Section 1.2, the absolute phase is analogous to the output phase of an FM receiver. Therefore, various techniques, which have been proposed for analyzing the output phase of an FM receiver, can be applied to the mobile channel to calculate the variance of the absolute phase by reinterpreting the SNR and correlation functions of an FM receiver.

The variance calculation techniques for the output phase of an FM receiver include the correlation technique by Rice [20] and Middleton [24], the zero-crossing technique by Blachman [22], and the click analysis by Rice [15].

In this section, these techniques are examined and compared in the context of the mobile

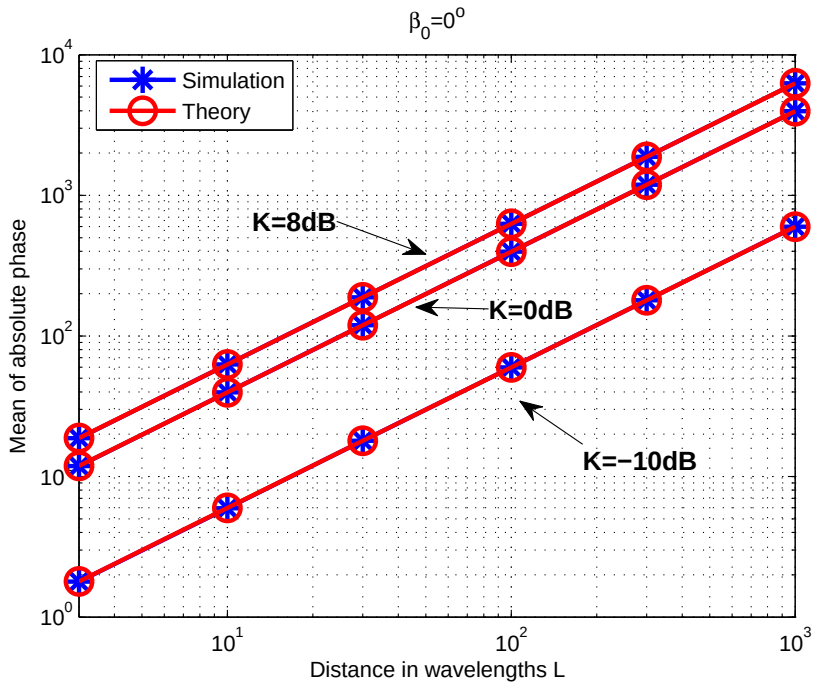

Figure 4.1: Examples of the mean of the absolute phase, against the distance in wavelengths L, given various K and with the AOA of the dominant source $\beta_0 = 0$.

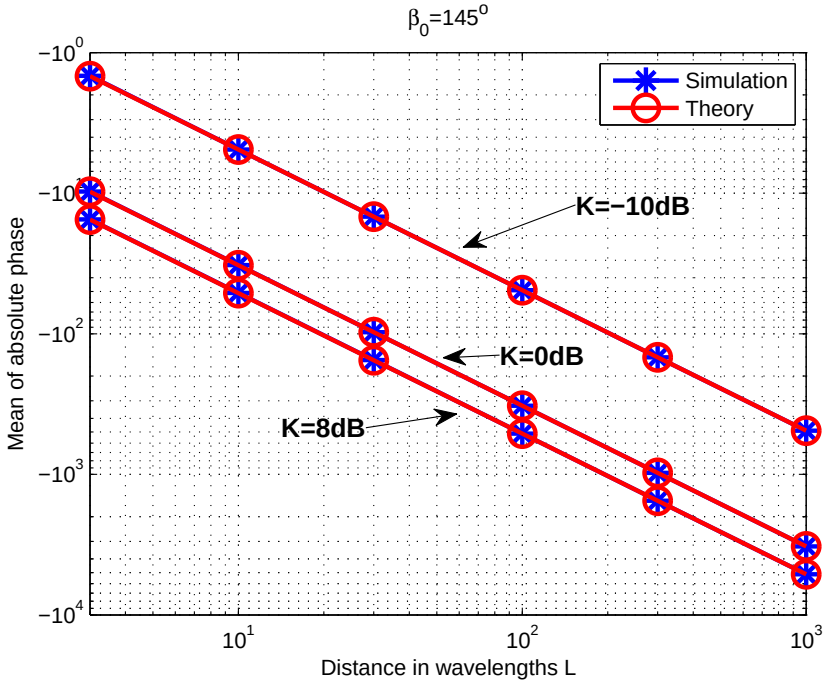

Figure 4.2: Examples of the mean of the absolute phase against the distance in wavelengths L, given various K and with the AOA of the dominant source $\beta_0 = 145^o$.

channel. As shown below, the variances for some situations can be well approximated, and some are complicated. The correlation and zero-crossing techniques are more general and accurate than the Rice click analysis but they provide mathematically attractive forms only for $K = 0$. The Rice click analysis is simple to derive but it approximates well only for K larger than 2dB [15].

4.2.1 Correlation Technique

The correlation technique models the absolute phase as the accumulated phase change, as given by (3.6). Then the variance of the absolute phase can be calculated through the autocorrelation of the phase derivative, which has been derived by Rice [20] and Middleton [24]. Denoting the phase derivative autocorrelation as $R_{\dot{\phi}_C}(\tau)$, then the variance of the absolute phase at the observation time, T, is [91]

$$\sigma^2_{\phi_A^{(r)}}(T) = 2\int_0^T (T-\tau) R_{\dot{\phi}_C}(\tau) d\tau. \tag{4.3}$$

The autocorrelation, $R_{\dot{\phi}_C}(\tau)$, has a closed form only for $K = 0$, which is given by [20]

$$R_{\dot{\phi}_C}(\tau) = \frac{\ddot{\rho}(\tau)\rho(\tau) - \dot{\rho}^2(\tau)}{2\rho^2(\tau)} \log(1-\rho^2(\tau)) \tag{4.4}$$

where $\rho(\tau)$ is the autocorrelation coefficient function for the component of the channel. $\dot{\rho}(\tau)$ and $\ddot{\rho}(\tau)$ are the first and second derivative of the correlation coefficient function, respectively. In the presence of isotropic scattering, the component correlation coefficient function of the channel is given by $\rho(\tau) = J_0(2\pi f_D \tau)$, then

$$\dot{\rho}(\tau) = -2\pi f_D J_1(2\pi f_D \tau)$$

and

$$\ddot{\rho}(\tau) = 0.5(2\pi f_D)^2 (J_2(2\pi f_D \tau) - J_0(2\pi f_D \tau)).$$

More complicated (non-closed) expressions for $R_{\dot{\phi}_C}(\tau)$, with non-zero K, were given by Rice [20], but the results require $\rho(\tau)$ to be non-negative, which is not the case for the vehicular mobile channel model with $\rho(\tau) = J_0(2\pi f_D \tau)$.

4.2.2 Zero-Crossing Technique

The zero-crossing technique is based on the formulation of the absolute phase given by (3.4). The variance of the absolute phase is obtained by the variance of the number of zero crossings over $(0, T)$ multiplied with π^2. The closed-form expression, derived by Blachman, exists only for $K = 0$ [79],

$$\sigma^2_{\phi_A^{(z)}}(T) = \frac{\pi^2}{4} - \arcsin^2[\rho(T)] + 2\int_0^T (T-\tau)\frac{\dot{\rho}(\tau)^2}{1-\rho(\tau)^2}d\tau \tag{4.5}$$

where $\rho(T) = J_0(2\pi f_D T)$. Blachman also provided a mathematically tractable approximation when $\beta_0 = 90^o$ [79, 91],

$$\sigma^2_{\phi_A^{(z)}}(T) = 2\int_0^T (T-\tau)\frac{\dot{\rho}^2(\tau)}{1-\rho^2(\tau)}\exp[-\frac{2K}{1+\rho(\tau)}]d\tau. \tag{4.6}$$

For large T, (4.6) simplifies to [23]

$$\sigma^2_{\phi_A^{(z)}}(T) = 2T\int_0^\infty \frac{\dot{\rho}^2(\tau)}{1-\rho^2(\tau)}\exp[-\frac{2K}{1+\rho(\tau)}]d\tau. \tag{4.7}$$

4.2.3 Rice Click Analysis

Compared with the correlation and zero-crossing techniques, the click analysis proposed by Rice [15] is more intuitive, but it is valid for the well-defined Rice process only with large K. As formulated in (3.7), the number of Rice clicks, $N_{r2\pi}(0, T)$, is modeled as a Poisson distribution for large K [15]. Therefore, the variance of $N_{r2\pi}(0, T)$ is equal to its mean. The general form of the variance of $N_{r2\pi}(0, T)$ for large K is given in [22], but here modified for the modern definition of $\mathrm{erf}(x)$,

$$\begin{aligned}\sigma^2_{N_{r2\pi}} &= f_D\cos(\beta_0)T\exp(-K)\mathrm{erf}[\frac{f_D\cos(\beta_0)\sqrt{K}}{2\pi r_g}] \\ &\quad + \frac{r_g T}{\sqrt{\pi K}}\exp[-\frac{r_g^2 + (f_D\cos(\beta_0))^2}{r_g^2}K]\end{aligned} \tag{4.8}$$

where

$$\mathrm{erf}(x) = \frac{2}{\sqrt{\pi}}\int_0^x \exp(-t^2)dt,$$

and

$$r_g = \frac{1}{2\pi}\sqrt{-\frac{\ddot{\rho}(0)}{\rho(0)}} = \frac{f_D}{\sqrt{2}} \tag{4.9}$$

is the *radius of gyration* of the Doppler spectrum [15], i.e., the measure of Doppler spread [2].

The value of the absolute phase is dominated by the number of Rice clicks, so the variance of the absolute phase at the observation time, T, can be approximated by (4.8) multiplied with $4\pi^2$,

$$\begin{aligned}\sigma^2_{\phi_A^{(c)}}(T) &= 4\pi^2 f_D T\cos(\beta_0)\exp(-K)\mathrm{erf}[\frac{\cos(\beta_0)\sqrt{2K}}{2\pi}] \\ &\quad + \frac{4\pi^2 f_D T}{\sqrt{2\pi K}}\exp[-(1+2\cos^2(\beta_0))K].\end{aligned} \tag{4.10}$$

For the stationary well-defined Rice process, i.e., when $\beta_0 = 90^o$, (4.10) reduces to

$$\sigma^2_{\phi_A^{(c)}}(T) = \frac{4\pi^2 f_D T}{\sqrt{2\pi K}}\exp(-K). \tag{4.11}$$

The other expression for the variance of the absolute phase when $\beta_0 = 90^o$ is given by [15]

$$\sigma^2_{\phi_A^{(c)}}(T) = \frac{4\pi^2 f_D T}{\sqrt{2}}\mathrm{erfc}(\sqrt{K}). \tag{4.12}$$

(4.12) approximates (4.11) for large K as can be seen from

$$\mathrm{erfc}(x) = \frac{e^{-x^2}}{\sqrt{\pi}x}(1 - \frac{1}{2x^2} + \frac{1\cdot 3}{(2x^2)^2} - \cdots). \tag{4.13}$$

4.2.4 Comparisons of Variance Calculation Techniques

The variance calculation techniques are summarized in Table 4.1. Some examples, including both simulation and theoretical results, of the variance of the absolute phase for various K are shown in Figure 4.3 to Figure 4.5. When $K \geq 8$dB as shown in Figure 4.3, both the zero-crossing technique and the Rice click analysis work well and are equivalent for calculating the variance of the absolute phase. These two techniques do not take into account the

	Correlation	Zero-Crossing	Click
Formulation	(3.6)	(3.4)	(3.7)
$K = 0$	(4.3)	(4.5)	
$\beta_0 = 90^o$, large L		(4.6)	
$\beta_0 = 90^o$, large K, L		(4.6)(4.7)	(4.11),(4.12)
$\beta_0 \neq 90^o$, large K, L			(4.10)

Table 4.1: Variance calculation techniques based on various formulations of the absolute phase. The numbers inside parentheses are the equations provided in this thesis. The first row of the table lists the names of three variance calculation techniques, and the second row lists the corresponding formulation of the absolute phase used for calculating the variance. The first column of the table lists the corresponding condition for the variance calculation equation to hold.

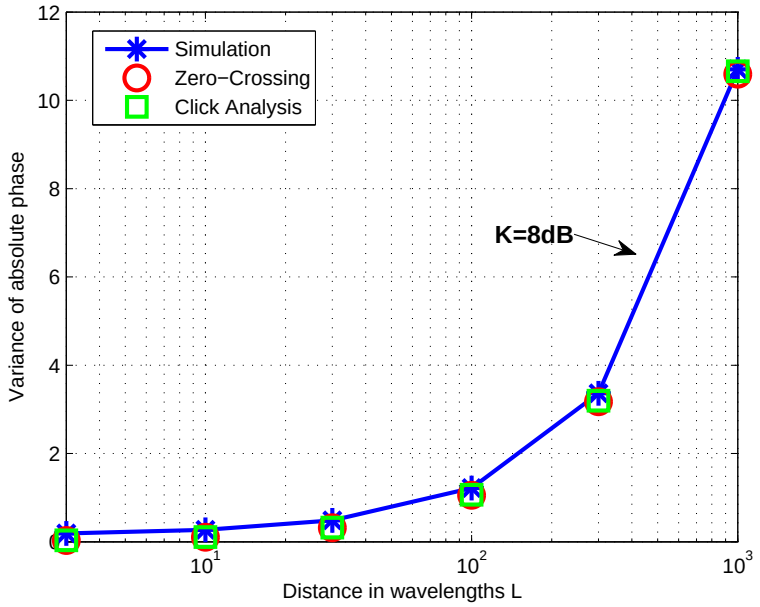

Figure 4.3: The variance of the absolute phase, against the distance in wavelengths L, calculated by different techniques compared with the simulation result. The simulation parameters are K =8dB, $\beta_0 = 90^o$ and $f_n = 0.01$. The distance in wavelengths are $L = 3, 10, 30, 100, 300, 1000$.

variance of the phase difference (i.e., $\phi_W(T) - \phi_W(0)$ in (3.7) and $\phi_{W2}(T) - \phi_{W2}(0)$ in (3.4)). Therefore, both (4.5) and (4.10) are not accurate when the variance of the absolute phase is small (e.g., $L \leq 100$). As L becomes very large (e.g., $L = 1000$), the variance of the phase difference is negligible compared with the variance of the absolute phase.

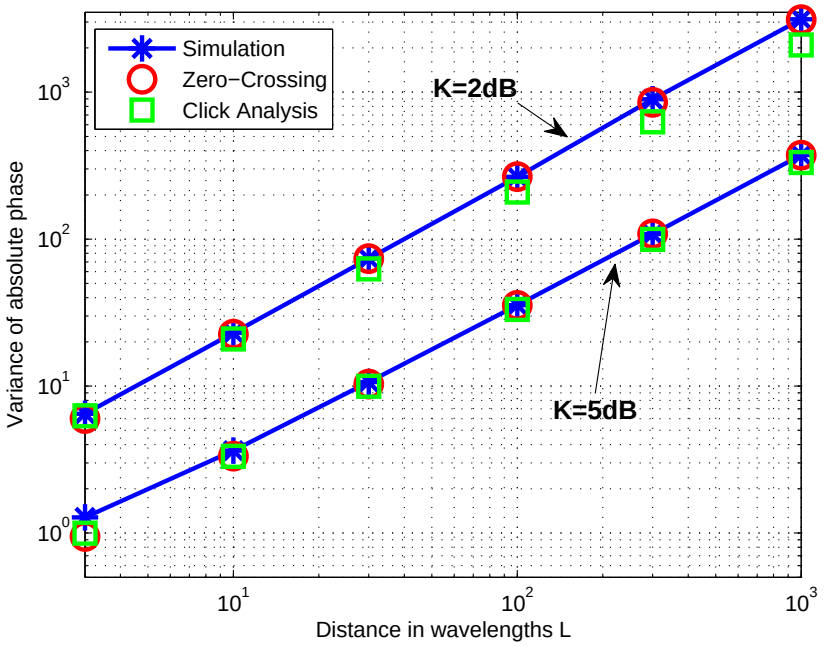

Figure 4.4: Same as Figure 4.3, except $K = 5$dB and $K = 2$dB.

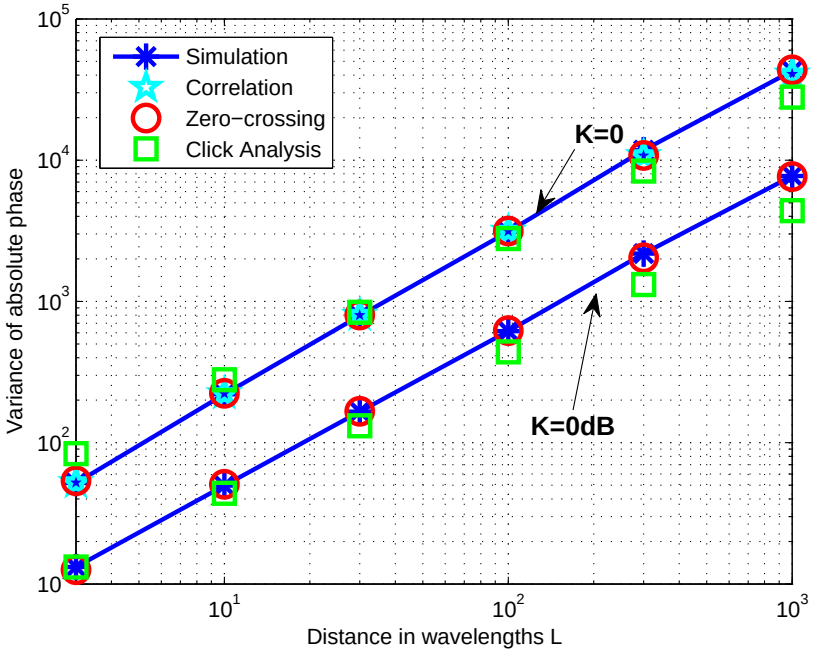

Figure 4.5: Same as Figure 4.3, except $K = 0$dB and $K = 0$ (i.e.,$-\infty$dB).

As K decreases, say to $K = 5$dB as shown in Figure 4.4, the Rice click analysis fails to predict the variance of the absolute phase when $L \geq 100$. The reason is that the false click (Appendix B) starts to appear for medium K. If L is small, the accumulated effect of the false click is small and then it can be neglected compared with the effect of the Rice click, so the variance of the absolute phase based on the Rice click analysis can still work. As K decreases, the valid L, for the Rice click analysis to work, also decreases (e.g., $L \leq 30$ for $K = 2$dB as shown in Figure 4.4).

When K becomes small, the false click becomes dominant compared with the Rice click so that the Rice click analysis cannot predict the variance of the absolute phase, as shown in Figure 4.5. On the other hand, the zero-crossing technique and the correlation technique (only for $K = 0$) are good for calculating the variance of the absolute phase. Figure 4.3 to Figure 4.5 also show that the zero-crossing technique is a more general technique for predicting the variance of the absolute phase given $\beta_0 = 90^o$.

4.3 Modeling pdf of the Absolute Phase

In this section, the pdf of the absolute phase is developed. Similar to the discussion of calculating the variance of the absolute phase, the previous work on modeling the pdf of the output phase of an FM receiver is first reviewed.

4.3.1 Review of pdf Modeling for the Output Phase of an FM Receiver

A rigorous formulation of the output phase of an FM receiver (analogous to the absolute phase of the mobile channel) requires the setup and solution to a Fokker-Planck partial differential equation [92]. This method was applied to find the distribution of the output phase in FM receivers by Campbell *et al.* [25] where it is referred to as the distribution of the "continuous phase" (this continuous phase differs to the definition used in this thesis). Campbell *et al.* assigned the correlation function of the input narrowband noise to be double exponential such that the noise can be modeled as a Gaussian-Markov process. Under this restriction, the general formula of the phase distribution without approximation is still not in an analytically attractive form (*cf.*, Equation (23) in [25]).

Instead of the rigorous derivations, Blachman proposed an approximate solution to the distribution of the output phase of an FM receiver (referred to as the distribution of phase change in [23]) by taking advantage of the CLT. This was based on the output phase being

the sum of many phase derivatives, as given by (3.6). If the correlation function of the narrowband noise decays to zero after certain time (see p.88 in [22] for some examples of the noise correlation and corresponding spectrum), then the phase derivative over $(0, T)$ can be divided into many independent subintervals. The sum of these subintervals, i.e., the output phase of the FM receiver (analogous to the absolute phase), approximates the Gaussian distribution according to the CLT. In the presence of the FM carrier signal (analogous to the dominant component in the mobile channel), the phase in each period is modeled either by the Rice phase pdf with known initial phase, or the convolution of the two Rice phase pdfs with unknown initial phases; and this introduces a periodic fine structure to the broad Gaussian distribution.

Besides these investigations for general values of the FM receiver SNR (analogous to the K factor of the mobile channel), the principal authors, e.g., [26, 27, 28], formulated the distribution of the output phase of an FM receiver based on the click analysis proposed by Rice. This was because analog and digital FM receivers usually operate with large SNR. With large SNR, the output phase can be approximated by the sum of three mutually independent random processes: the initial phase; the final phase; and the discrete click process, as defined in (3.7). Both the initial and the final phase can be modeled by the Rice phase pdf, and the discrete click process can be modeled by the difference of two independent Poisson variables (i.e., positive Rice click minus negative Rice click) [26]. Therefore, the pdf of the output phase of an FM receiver is the convolution of these three random variables.

In high-rate FM digital communications, the short interval between the start and the end of the symbol means that the initial phase and final phase might become correlated [80]. The pdf of the correlated phase difference modulo $[-\pi, \pi)$, given in [93, 94], is adopted to derive the pdf of the output phase of an FM receiver. Under very high SNRs, the probability of the phase difference lying either on $[-2\pi, -\pi)$ or $(\pi, 2\pi]$ is small, so the approximation by taking a modulus of $[-\pi, \pi)$ is acceptable. However, as shown below, it will not be the case for the mobile channel in general.

4.3.2 Properties of the Absolute Phase in Mobile Channels

Despite the analogy to the output phase of an FM receiver, the absolute phase in mobile channels exhibits many different properties.

First, the K factor for the mobile channel (recall this is analogous to the SNR in FM receivers) is often either zero or small. Therefore, the approximated distributions for high

SNR in FM receivers, as given in [26, 27, 28], are not always applicable.

Second, the correlation coefficient of the components for the mobile channel with isotropic scattering is modeled by the Bessel function. Unlike the correlation function of the input noise in the FM receiver, which is always assumed to be positive [22], the Bessel function can be negative. It is shown below that the negative correlation coefficient significantly changes the distribution of the phase difference.

Third, when the final phase and the initial phase for calculating the absolute phase are highly correlated, the K factor of the mobile channel could be small. In this case, the phase difference pdf for the mobile channel will have non-zero values anywhere in $[-2\pi, 2\pi]$. Therefore it is necessary to formulate the distribution of the correlated phase difference without the modulo $[-\pi, \pi)$ condition.

Fourth, if the dominant component of the mobile channel has a time-varying AOA (not the well-defined Rice channel case), then the situation is different from the frequency deviation in FM receivers, where the signal frequency is considered constant during the observation time. However, in the following, the issue is averted by considering only the case of the well-defined Rice channel.

4.3.3 Absolute Phase Formulation Selection for pdf Modeling

The absolute phase is a complicated random process, whose pdf depends on the Rice factor K, the AOA of the dominant source β_0, the observation interval T, the starting and ending phase values, and the signal trajectory from time 0 to T. To acquire the pdf of the absolute phase, a proper formulation of the absolute phase is required.

As discussed in Section 3.2, the absolute phase can be formulated through four techniques based on different mechanisms. They are the unwrapping technique, the zero-crossing technique, the phase derivative integration technique, and the Rice click analysis. These techniques model the absolute phase as the sum of several random processes. If the pdf of each random process, and the correlations among these random processes were known, the pdf of the absolute phase can be calculated. In the following, the four formulations are examined to check if they can be easily used to calculate the pdf of the absolute phase.

- Based on the zero-crossing technique as given by (3.4), the absolute phase is the sum of the zero-crossing event and the difference of two random phases. It has been shown the distribution of the zero crossing (i.e., $N_\pi(0, T)$ in (3.4)) is a largely unsolved

problem (*c.f.*, p. 426 in [24]).

- Based on the Rice click analysis as given by (3.7), the absolute phase is the sum of the Rice click event and the difference of two random phases. The Rice click (i.e., $N_{r2\pi}(0,T)$ in (3.7)) and its modeling have been well treated in the literature of FM receivers [15, 26, 27, 28]. However, as discussed in 3.2.4, the modeling of the Rice click is applicable only for large K.

- Based on the phase derivative integration technique as given by (3.6), the absolute phase is the sum of many phase derivatives, and can be approximately modeled, under some conditions, using a Gaussian distribution. This Gaussian approximation was developed for modeling the pdf of the output phase of an FM receiver [23], as discussed in Section 4.3.1.

- Based on the unwrapping technique as given by (3.2), the absolute phase is the sum of the 2π discontinuity event and the difference of two random phases. This formulation has not been used to develop the pdf of the absolute phase (or the pdf of the output phase of an FM receiver), but, as detailed below, it provides intuitive but relatively accurate models to analyze the pdf of the absolute phase compared with the other three formulations.

The formulations based on both the phase derivative integration technique and the unwrapping technique are adopted to model the pdf of the absolute phase in this thesis. The Gaussian approximation, based on the phase derivative integration technique, together with the approximation condition is discussed in 4.3.5.4. In the next three subsections, the pdf of the absolute phase is developed using the formulation based on the unwrapping technique.

4.3.4 Modeling pdf of the Absolute Phase Using Unwrapping Technique

Following (3.2), the absolute phase is divided into two different events, *viz.*, wrapped phase difference (continuous) and the cumulative number of 2π discontinuities (discrete). The discrete event is the difference of two events (the number of positive 2π crossings, $N_{2\pi+}(0,T)$, minus the number of negative 2π crossings, $N_{2\pi-}(0,T)$). Mathematically, this is

$$\phi_A(T) \quad = \quad [\phi_W(T) - \phi_W(0)] + 2\pi[N_{2\pi+}(0,T) - N_{2\pi-}(0,T)]. \tag{4.14}$$

Intuitively, and borne out by simulation in Section 4.3.7, the continuous event and the discrete event are independent, because given K, the rate of 2π crossings is fixed (as proved in Section 4.3.5), and this rate is not affected by the initial phase and the final phase. Therefore, the pdf of the absolute phase can be modeled by convolving the pdf of the continuous event and the pdf of the discrete event.

This independence assumption differs from the conclusion drawn by Yavuz *et al.* in [95], where both the continuous event and the discrete event are defined based on the phase derivative. The continuous event in [95] is a Gaussian-like noise and is correlated with the discrete event when K is not too large. In our case, both the continuous event and the discrete event are defined based on the phase itself, and the continuous event is the difference of two phases.

When both K and L are large, the initial phase and the final phase for the continuous event are uncorrelated, the number of positive 2π crossings and the number of negative 2π crossings for the discrete event are uncorrelated, and the continuous event and the discrete event are independent. The pdf of the absolute phase can be obtained by the convolution of the pdfs of these four independent events. This is similar to the discussions about digital FM receivers [26, 27, 28].

Other than for both large K and L, the initial phase and the final phase might become correlated, and the positive and the negative 2π crossings might also become correlated. In the following, the pdfs for the discrete event and the continuous event under different scenarios are formulated. The relation between them and the limitations for the uncorrelated assumptions are also discussed.

4.3.5 Modeling the Discrete Event-2π Discontinuity

Inspecting the trajectory of the absolute phase, it is clear that the 2π discontinuities dominate the phase changes. Therefore, the distribution of the discrete event, i.e., the cumulative number of 2π discontinuities, can be expected to dominate the variance of the pdf of the absolute phase. This discrete event was coined the "broad factor" of the phase pdf [23]. As discussed above, the 2π discontinuity event consists of the positive and the negative 2π crossing events.

4.3.5.1 The Number of 2π Crossings

Stationary well-defined Rice channel. The channel is recalled as

$$h(t) = A + x(t) + jy(t) = r(t)e^{j\phi_W(t)}. \tag{4.15}$$

In this case, the number of positive and the number of negative 2π crossings are random variables and follow the same distribution. The event of the positive 2π crossing can be modeled as the event of the signal crossing the negative $I(t)$ axis. Mathematically, it is [15],

$$\begin{aligned} &\text{either: } x < -A, 0 < y < \Delta y, \dot{y} < 0 \\ &\text{or: } r > A, \pi < \phi_W < \pi + \Delta\phi_W, \dot{\phi_W} > 0. \end{aligned} \tag{4.16}$$

Because $x(t)$, $y(t)$, and $\dot{y}(t)$ are uncorrelated Gaussian variables, the joint pdf of $x(t)$, $y(t)$, and $\dot{y}(t)$ is

$$p_{x,y,\dot{y}}(x, y, \dot{y}; t) = \frac{\exp(-\frac{x^2}{2\sigma^2})}{\sqrt{2\pi}\sigma} \times \frac{\exp(-\frac{y^2}{2\sigma^2})}{\sqrt{2\pi}\sigma} \times \frac{\exp(-\frac{\dot{y}^2}{2\nu^2})}{\sqrt{2\pi}\nu}$$

where ν^2 is the variance of $\dot{y}(t)$, and is defined as

$$\nu^2 = -\frac{d^2 r_y(\tau)}{d\tau^2}|_{\tau=0},$$

with $r_y(\tau)$ the autocorrelation function of $y(t)$. When $r_y(\tau) = \sigma^2 J_0(2\pi f_D \tau)$, the variance of $\dot{y}(t)$ is $\nu^2 = 2\sigma^2\pi^2 f_D^2$ [2].

For an arbitrary interval Δt, the average number of positive 2π crossings, $R_+^c \Delta t$, is

$$R_+^c \Delta t = \Delta t \int_{-\infty}^{-A} dx \int_{-\infty}^{0} |\dot{y}| p_{x,y,\dot{y}}(x, y = 0, \dot{y}; t) d\dot{y}. \tag{4.17}$$

Solving (4.17), the positive 2π crossing rate R_+^c is

$$R_+^c = \frac{1}{2} r_g \text{erfc}(\sqrt{K}) \tag{4.18}$$

where $r_g = \frac{\nu}{2\pi\sigma} = \frac{f_D}{\sqrt{2}}$, which is the same parameter as defined in (4.9). The average number

of positive 2π crossings over $(0, T)$ is then

$$R_+^c T = \frac{\text{erfc}(\sqrt{K}) f_D T}{2\sqrt{2}} = \frac{\text{erfc}(\sqrt{K}) L}{2\sqrt{2}}. \tag{4.19}$$

This is how the average number of 2π crossings over duration $(0, T)$ depends on the observation interval L and the Rice factor K. For a fixed L, the signal trajectory with smaller K will have more 2π crossings, as intuitively expected.

Well-defined Rice process channel. When the AOA of the dominant source, β_0, is not 90^o, the average number of positive and negative 2π crossings over $(0, T)$, relative to the dominant component, can be calculated in the similar way [15, 22] (again modified for the modern erf(x) definition),

$$\begin{aligned} R_+^c T = -\frac{1}{2} f_D \cos(\beta_0) T \exp(-K) \text{erfc}[\frac{f_D \cos(\beta_0)\sqrt{K}}{2\pi r_g}] \\ + \frac{r_g T}{2\sqrt{\pi K}} \exp(-\frac{r_g^2 + (f_D \cos(\beta_0))^2}{r_g^2} K) \end{aligned} \tag{4.20}$$

and

$$R_-^c T \;\; = \;\; R_+^c T + f_D \cos(\beta_0) T \exp(-K). \tag{4.21}$$

When $\beta_0 = 90^o$, (4.20) is equivalent to (4.19) after (4.19) is approximated using the expansion for erfc(x) as discussed in Section 4.2. Both (4.20) and (4.21) can be functions of L by substituting $r_g = \frac{f_D}{\sqrt{2}}$ and $f_D T = L$.

The number of 2π crossings over $(0, T)$, resulting by the rotation of the time-varying dominant component, equals $f_D \cos(\beta_0) T$, which has the same direction as $R_+^c T$. Therefore, the average number of the difference between the positive and negative 2π crossings is

$$\Delta R_N \;\; = f_D \cos(\beta_0) T (1 - \exp(-K)) \tag{4.22}$$

which, after multiplying 2π, equals the mean of the absolute phase given by (4.2).

4.3.5.2 pdf of Uncorrelated 2π Crossings

For large K, the positive 2π crossings randomly appear with the average rate of R_+^c and are mutually independent. Therefore, the number of 2π crossings, given the observation time T, can be modeled as a Poisson distribution [23, 96], whose probability mass function (PMF) can be written as

$$p(n_1 = k_1) = \frac{e^{-\mu_1}\mu_1^{k_1}}{k_1!} \tag{4.23}$$

where $\mu_1 = R_+^c T$. Similarly, the PMF for the number of negative 2π crossings can be modeled as (4.23) with $\mu_2 = R_-^c T$. For a stationary well-defined Rice process, $\mu_1 = \mu_2$.

Recall the cumulative number of 2π crossings over $(0, T)$ is given by $N_{2\pi}(0, T) = N_{2\pi+}(0, T) - N_{2\pi-}(0, T)$. For large K (refer to next section for the value of K), the number of positive and the number of negative 2π crossings are assumed to be uncorrelated. Therefore, $N_{2\pi}(0, T)$ is the difference of two uncorrelated[1] Poisson distributions, which is given by the Skellam distribution [23, 26, 98, 97],

$$p(n = k) = e^{-(\mu_1+\mu_2)} \left(\frac{\mu_1}{\mu_2}\right)^{k/2} I_k(2\sqrt{\mu_1\mu_2}) \tag{4.24}$$

where $I_k(z)$ is the modified Bessel function of the first kind and kth order. The Skellam distribution has a mean of $\mu_1 - \mu_2$ and a variance of $\mu_1 + \mu_2$. When $R_+^c T = R_-^c T$, the mean is 0 and the variance is $2R_+^c T$.

Some examples for various L given $K = 5$dB are shown in Figure 4.6. The Skellam distribution resembles the Gaussian distribution when the number of both the negative and positive 2π crossings is large. As seen in (4.19), the number of 2π crossings increases with L but decreases with K. Therefore, larger L is required for larger K in order for the number of 2π crossings to be approximately modeled by the Gaussian distribution.

4.3.5.3 Correlated 2π Crossing Events

The formula for calculating the average number of 2π crossings given in Section 4.3.5.1 hold for any K and L, but the derived distributions discussed in Section 4.3.5.2 are based on

[1]Note here the assumption of independence between two Poissons given in [97] has been relaxed to uncorrelated as developed in [98].

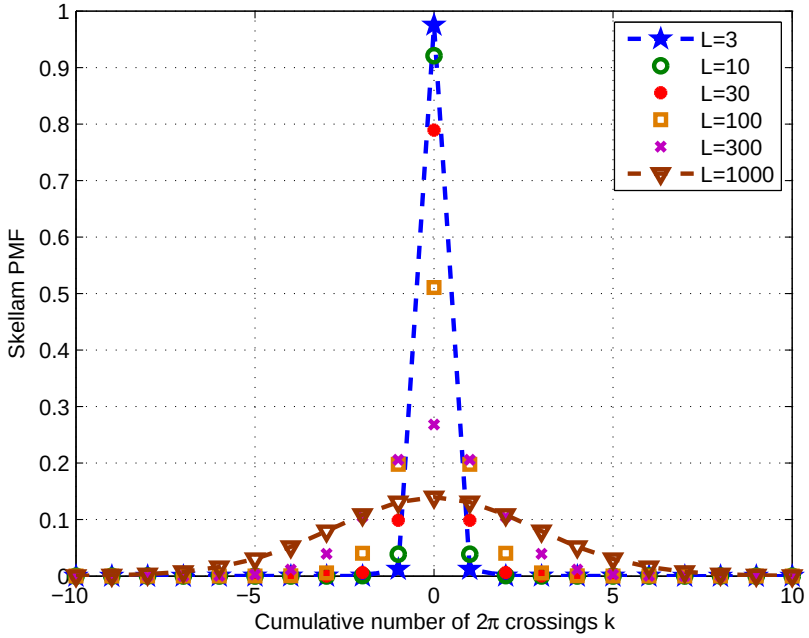

Figure 4.6: The Skellam PMF examples for various L given $K = 5$dB and $\beta_0 = 90^o$. The Skellam PMF resembles the Gaussian shape when L is large.

the assumptions that the positive and the negative crossing events both are uncorrelated, and both events can be modeled as Poisson distributions. These uncorrelated assumptions seem reasonable for large K. When K is not too large, the occurrence of the positive 2π crossings becomes frequent, so that non-zero correlation arises among the positive crossings, and therefore the number of positive 2π crossings can no longer be modeled as the Poisson distribution. The same conclusion is applied to the negative 2π crossing event. For small K, non-zero correlation aries between the positive and the negative crossing events so that the PMF of the discrete event cannot be modeled by the convolution of two individual PMFs. The correlation between the positive and the negative crossing events appears as the false click in the phase derivative, or as two consecutive, opposite 2π discontinuities in the wrapped phase (refer to Appendix B).

Correlations among these events complicate the pdf modeling of the absolute phase. Investigations into these complicated scenarios can be found in the research of FM receivers [82, 83, 95]. These works attempted to calculate the probabilities and correlations of these crossing events, but none of them provide quantitative results. Instead of deriving a general

pdf for the absolute phase in the presence of these correlations, statistical methods based on simulation data are used here to find the conditions for K and L under which the uncorrelated assumptions hold.

Statistical tests. The crossing events through simulation are obtained as follows.

- Generate the complex channel CAG for given K and L as discussed in Section 3.3;
- Find the wrapped phase using (3.1) and then subtract the initial phase $\phi_W(0)$;
- Calculate differences between adjacent phase samples from the last step, and count the total number of the phase differences larger than π (i.e., the number of negative 2π crossings) and smaller than $-\pi$ (i.e., the number of positive 2π crossings);
- Run the simulation 10^6 times, which generates 10^6 independent samples for each of the crossing events.

Two assumptions are required to test whether the discrete event of the absolute phase can be modeled using the Skellam distribution. One assumption is whether the number of positive and negative 2π crossings can be both modeled as the Poisson distribution. A simple check whether a count number can be modeled using the Poisson distribution, is the ratio of the variance to the mean of the simulated data, which is called the *index of dispersion*, I_D. If $I_D = 1$, the simulated data can be modeled as Poisson. Otherwise, the simulated data is overdispersed ($I_D > 1$) or underdispersed ($I_D < 1$) [99]. The other assumption is whether the positive and the negative 2π crossing events can be assumed uncorrelated. If the correlation coefficient, r_c, between these two events is zero, these two events are uncorrelated. Otherwise, they are correlated to certain degree.

The goal is to approximate the crossing events by the uncorrelated Poisson models when possible. So the confidence intervals of the estimates to the parameters (I_D and r_c) will provide more information than the hypothesis tests to these assumptions. Since it is hard to find the statistics of these estimates, the non-parametric bootstrap method is appropriate for calculating the confidence intervals [100]. In the following, the 95% percentile bootstrap confidence interval is used. Owing to the number of samples used for estimating the parameters being as large as 10^6, the confidence interval is very small, as shown below; i.e., the estimates are extremely close to the true values.

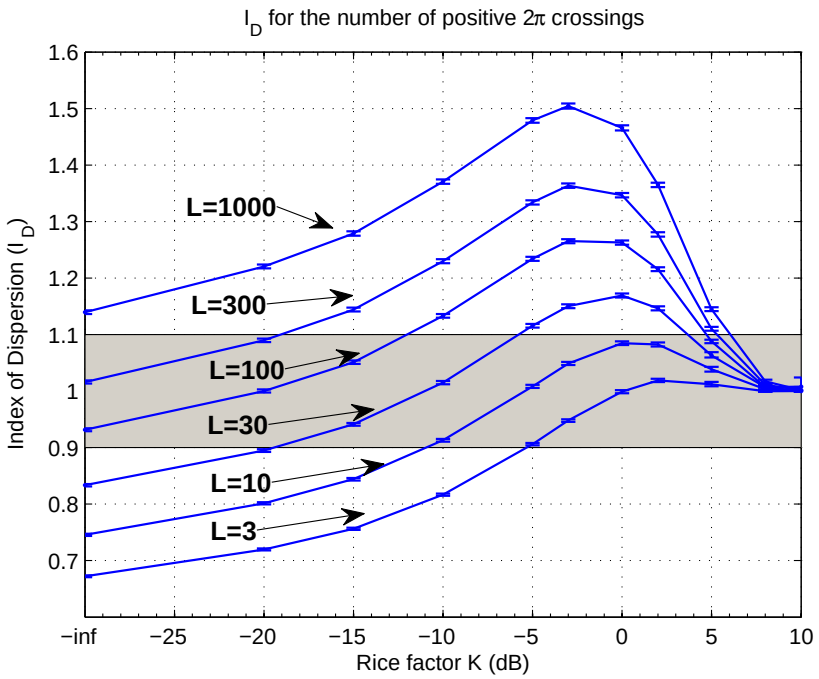

Figure 4.7: Estimate and its 95% percentile bootstrap confidence interval (short horizontal bars) of the index of dispersion for the number of positive 2π crossings at given L, and for various K. The number of samples for estimating the Index of Dispersion is 10^6, and the number of times for random sampling with replacement used in the bootstrapping operation is 10^3. The shaded region represents the cases that can be approximately modeled using a Poisson distribution.

Figure 4.7 presents the estimate to the index of dispersion (I_D), together with the confidence interval, of the number of positive 2π crossings for various K and L. It is shown that I_D is close to 1 and behaves independently of L only when K is larger than 5dB. Given other values of K, I_D increases with increasing L, varying from smaller than 1 (underdispersed) to larger than 1 (overdispersed). Interestingly, the maximum of I_D given fixed L is not at $K = 0$ (Rayleigh case) as intuitively expected. Instead, the maxima are around $K = 0$dB, and moreover, shift gradually from -3dB to 2dB with L decreasing from 1000 to 3. The number of negative 2π crossings follows similar trends as the positive ones, and the results are not presented here.

For the mobile channel, it is acceptable to model the number of positive 2π crossings as the Poisson distribution when $|I_D - 1| < 0.1$. This approximation gives a region of "Poissonness" as shown in the shaded region in Figure 4.7. This validity region includes

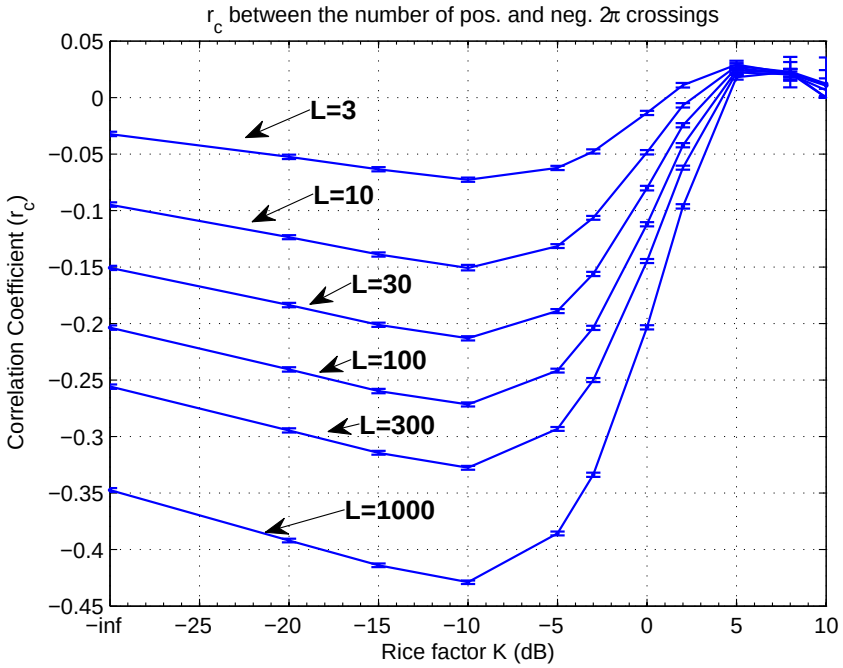

Figure 4.8: Estimate and its 95% percentile bootstrap confidence interval (short horizontal bars) of the correlation coefficient between the number of positive and negative 2π crossings. The statistical parameters used for this figure are the same as those in Figure 4.7.

the cases when $K > 8$dB given any L, $5 < K < 8$dB when $L < 100$, and $K < 5$dB for some special values (different for various K) of L.

Similar to the index of dispersion, the correlation coefficients, r_c, between the number of positive and the number of negative 2π crossings, and their 95% percentile bootstrap confidence intervals for various K and L, are estimated and shown in Figure 4.8. With estimated r_c negative, the number of positive and negative 2π crossings, for fixed L, are negatively correlated. Also of interest, the maximum correlation coefficients are not at $K = 0$ (Rayleigh case), but instead at about $K = -10$dB. Given K smaller than 5dB, the correlation coefficients increase negatively with increasing L from 3 to 1000. When K is larger than 5dB, the correlation coefficients are close to zero, and do not vary with changing L.

For the mobile channel, it is reasonable to assume that the positive and negative 2π crossing events are uncorrelated when $|r_c| < 0.1$. In this case, $K = 2$dB is a lower limit for this assumption to hold. This is the same conclusion, but arrived at in a different way, as

given by Rice in [15].

Summary of uncorrelated conditions. Violating either of the above assumptions prevents us from modeling the discrete events by the Skellam distribution. Based on the simulation results, this requires that K is larger than 5dB. Below 5dB, neither the number of positive nor negative 2π crossings can be modeled as a Poisson distribution for most values of L. When K is smaller than 2dB, the number of the positive and negative 2π crossings become correlated.

4.3.5.4 Summary of Modeling the Discrete Event

When the uncorrelated conditions hold, the number of 2π crossings can be modeled using the Skellam distribution as discussed in 4.3.5.2. Recall that the discrete event of the absolute phase equals the number of 2π crossings multiplied with 2π. So the PMF of the discrete event is scaled version of the Skellam distribution given by (4.24),

$$p(n = 2\pi k) = e^{-(\mu_1+\mu_2)} \left(\frac{\mu_1}{\mu_2}\right)^{k/2} I_k(2\sqrt{\mu_1\mu_2}). \tag{4.25}$$

On the other hand, when the observation interval L is long enough such that the number of 2π crossings is large, the discrete event can be approximated by a Gaussian distribution as discussed by Blachman based on the CLT in [23], without considering the distribution of either the number of positive or negative 2π crossings, and the correlation between them (refer to Section 4.3.1 for reasoning). This Gaussian distribution is given by

$$p(n = 2\pi k) = \frac{2\pi}{\sqrt{2\pi\sigma^2_{\phi_A}}} \exp[-\frac{(2\pi k - \bar{\phi}_A)^2}{2\sigma^2_{\phi_A}}] \tag{4.26}$$

where $\bar{\phi}_A$ is the mean of the absolute phase as given by (4.2), and $\sigma^2_{\phi_A}$ is the variance of the absolute phase and can be calculated using the variance calculation techniques discussed in Section 4.2.

Both the Skellam distribution and the Gaussian approximation are used to model the discrete event of the absolute phase in Section 4.3.7 when comparing the simulation to theoretical results for pdfs of the absolute phase.

4.3.6 Modeling the Continuous Event–Wrapped Phase Difference

The pdf of the wrapped phase difference is continuous from -2π to 2π, but it is repeated each 2π interval, when convolved with the discrete event. It forms a "periodic factor" in the distribution of the absolute phase [23].

4.3.6.1 Wrapped Phase Difference

For a stationary well-defined process, both $\phi_W(T)$ and $\phi_W(0)$ can be modeled by the Rice phase pdf. Define $\zeta(T) = \phi_W(T) - \phi_W(0)$ and note that $\zeta(T)$ has a range of $[-2\pi, 2\pi]$. When K is large, the probability of the phase difference lying either both $[-2\pi, -\pi)$ and $(\pi, 2\pi]$ is close to zero, so the pdf of $\zeta(T)$ can be approximated by the pdf of $\zeta(T)$ modulo $[-\pi, \pi)$, as given in [93, 94]. If $\phi_W(T)$ and $\phi_W(0)$ are uncorrelated, the pdf of the phase difference can by readily derived by convolving two Rice phase pdfs.

However, in general, $\zeta(T)$ is the difference of two *correlated* wrapped phases, and should be defined in a range of $[-2\pi, -2\pi)$. In order to derive the pdf for $\zeta(T)$ when $\phi_W(T)$ and $\phi_W(0)$ are correlated, the joint pdf of $\phi_W(T)$ and $\phi_W(0)$, should be found first. For brevity, $\zeta(T)$, $\phi_W(T)$, $\phi_W(0)$ and $J_0(2\pi f_D T) = J_0(2\pi L)$ are respectively denoted as ζ, ϕ_2, ϕ_1 and ρ in the following analysis. Here $f_D T$ and L are interchangeable.

4.3.6.2 pdf of the Phase Difference

The joint pdf of two Rice phases, ϕ_1 and ϕ_2, when separated by a time interval of T, is given by (p. 419, [24] - note that there is a correction applied here),

$$\begin{aligned} p(\phi_1, \phi_2|T) &= \frac{1-\rho^2}{(2\pi)^2} \exp[-\frac{2K\rho}{1+\rho}] \sum_{l,m,n=0}^{\infty} \varepsilon_l \varepsilon_m \varepsilon_n \frac{\Upsilon^{\frac{l+m}{2}} \rho^n}{l!m!} \\ &\quad \times A_{lm}^{(n)} \cos[l\phi_1] \cos[m\phi_2] \cos[n(\phi_2 - \phi_1)] \end{aligned} \tag{4.27}$$

with

$$\begin{aligned} A_{lm}^{(n)} &= \sum_{q=0}^{\infty} \frac{\rho^{2q}}{q!(q+n)!} \Gamma[\frac{l+n}{2} + q + 1] \Gamma[\frac{m+n}{2} + q + 1] \times \\ &\quad {}_1F_1[\frac{l-n}{2} - q; l+1; -\Upsilon] {}_1F_1[\frac{m-n}{2} - q; m+1; -\Upsilon] \end{aligned} \tag{4.28}$$

where $\Upsilon = \frac{K(1-\rho)}{1+\rho}$, $\Gamma[\cdot]$ is the Gamma function, and ${}_1F_1[\cdot]$ represents the confluent hypergeometric function, also called the Kummer function. The infinite upper limits for l, m, and n are replaced by K-dependent numbers in the calculation (e.g., 5 is good enough for $K < 0$dB, but 30 is required for $K > 5$dB in order to make the approximation accurate).

Since $\zeta = \phi_2 - \phi_1$, the pdf of ζ is given by [84],

$$p(\zeta) = \begin{cases} \int_{-\pi}^{\pi-\zeta} p(\phi_1, \zeta + \phi_1) d\phi_1 & 0 \le \zeta \le 2\pi \\ \int_{-\pi-\zeta}^{\pi} p(\phi_1, \zeta + \phi_1) d\phi_1 & -2\pi \le \zeta < 0. \end{cases} \tag{4.29}$$

Substituting (4.27) into (4.29), the pdf for the difference of two correlated Rice phases can be obtained, *viz.*,

$$p(\zeta) = \begin{cases} C(\zeta) \int_{-\pi}^{\pi-\zeta} \cos[l\phi_1] \cos[m(\zeta + \phi_1)] d\phi_1 & 0 \le \zeta \le 2\pi \\ C(\zeta) \int_{-\pi-\zeta}^{\pi} \cos[l\phi_1] \cos[m(\zeta + \phi_1)] d\phi_1 & -2\pi \le \zeta < 0 \end{cases} \tag{4.30}$$

with

$$C(\zeta) = \frac{1-\rho^2}{(2\pi)^2} \exp[-\frac{2K\rho}{1+\rho}] B(\zeta)$$

where

$$B(\zeta) = \sum_{l,m,n=0}^{\infty} \varepsilon_l \varepsilon_m \varepsilon_n \frac{\Upsilon^{\frac{l+m}{2}} \rho^n}{l!m!} A_{lm}^{(n)} \cos[n\zeta].$$

When $K = 0$, the closed form of (4.30) is

$$p(\zeta) = \frac{1-\rho^2}{(2\pi)^2} \frac{\sqrt{1-\Lambda^2} + \Lambda(\pi - \cos^{-1}\Lambda)}{(1-\Lambda^2)^{3/2}} (2\pi - |\zeta|) \tag{4.31}$$

with $\Lambda = \rho\cos(\zeta)$, which is the pdf for the difference of two correlated Rayleigh phases given by Middleton [24] and Jakes [47].

When K is large, say, $K > 8$dB, the phase difference pdf can be approximated by the pdf of phase difference modulo $[-\pi, \pi)$ [93],

$$p(\zeta) = \frac{1-\rho^2}{4\pi(1-\Lambda^2)^{3/2}} \int_{-(\pi-\cos^{-1}(\Lambda))}^{(\pi-\cos^{-1}(\Lambda))} \exp[-H](1 - H + \frac{2K}{1+\rho})(\Lambda + \cos(\theta)) d\theta \tag{4.32}$$

where $H = \frac{K[1-\Lambda\cos(\zeta)+\Lambda\cos(\theta)-\cos(\zeta)\cos(\theta)]}{1-\Lambda^2}$ and $\Lambda = \rho\cos(\zeta)$.

4.3.6.3 Examples of Phase Difference pdf

Examples of (4.31) are illustrated in Figure 4.9. The pdf shape is governed by the correlation coefficient $\rho = J_0(2\pi L)$. Since ρ periodically oscillates around zero, even a small change of L will change the shape of the pdf. For example, $L = 3$ and $L = 3.5$, corresponding to $\rho = 0.13$ and $\rho = -0.12$, respectively, demonstrate the dissimilarity of the pdfs. When $L = 3.37$, corresponding to $\rho = 0.007$, the pdf resembles a triangle, which is the pdf for the difference of two uncorrelated, uniformly distributed phases.

The example of the phase difference pdf given by (4.30) is illustrated in Figure 4.10. It shows that when K is large, the pdf of the phase difference is dominated by the Rice phase, and therefore it varies with L but does not change as dramatically as when $K = 0$. Compared with the Rice phase pdf, the Rice phase difference expands the range to $[-2\pi, 2\pi]$ and has larger variance.

4.3.7 Examples and Investigations of the Absolute Phase pdf

In this subsection, the simulation is run 10^6 times. The histogram is compiled from the absolute phase at the end of observation interval expressed as distance in wavelengths L. The size of the histogram bins is set as 0.01π.

The theoretical pdf of the absolute phase is obtained by convolving the discrete distribution (the Skellam distribution given by (4.25) or the Gaussian distribution given by (4.26)) and the phase difference pdf (given by (4.30)). As discussed above, the pdf of the continuous event (i.e., the phase difference) can be modeled for any K and any L. However, the pdf of the discrete event (i.e., the cumulative number of 2π crossings) can be modeled by the Skellam distribution only when $K > 5$dB, or when the number of 2π crossings is so large that it can be approximated by the Gaussian distribution. The examples that represents these scenarios are provided in this subsection. Other scenarios are also shown as by simulation examples, but their modeling requires further investigation, and these are not discussed in this thesis.

The figures of this section are displayed on logarithm or linear scales. These are chosen case by case to emphasize the difference between the theoretical and simulation curves. In the figures, the pdf of the absolute phase is denoted by $p(\phi_A)$.

When $K \geq 8$dB, the occurrence probability of the 2π crossing is low. The cumulative number of 2π crossings can be modeled by the Skellam distribution. Figure 4.11 is the

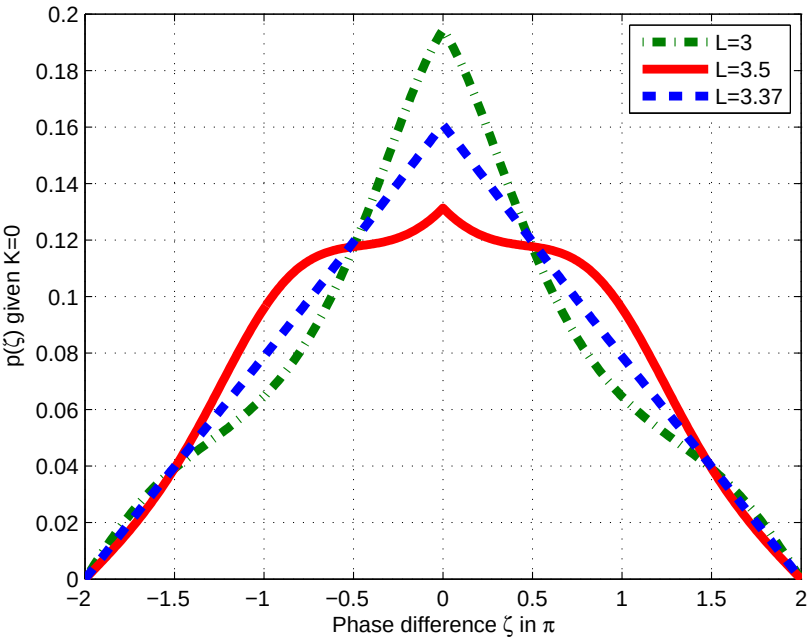

Figure 4.9: Rice phase difference pdf for $K = 0$ and different L. The pdf shape is sensitive to the correlation coefficient, ρ (positive, negative, or close to zero).

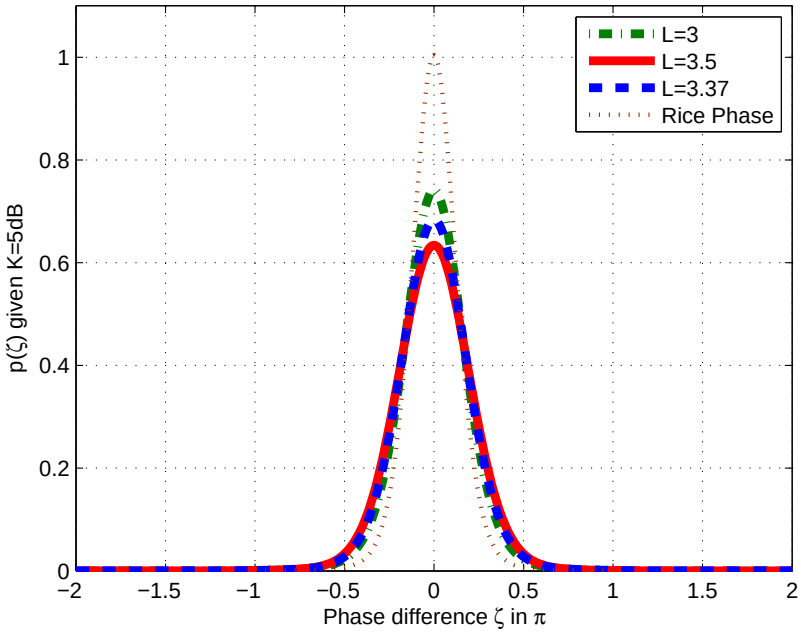

Figure 4.10: Rice phase difference pdf for $K = 5$dB and different L. When K is large, the pdf of the phase difference varies with L but does not change as dramatically as when $K = 0$.

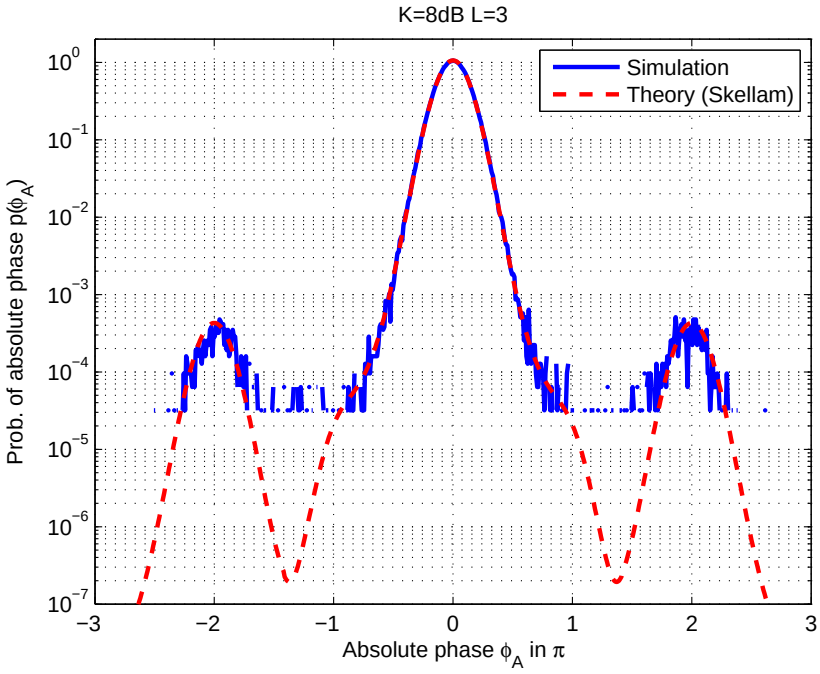

Figure 4.11: Absolute phase pdf by simulation and theory, for $K = 8$dB and $L = 3$.

result from both simulation and theory, which match each other very well. The lower cut-off, $3(10)^{-5}$, appearing on the logarithm scale, is due to the limited simulation size (number of realizations) and selected bin size.

The histogram comprises the number of the samples in each bin scaled by the number of trials and bin size. Mathematically, $p(\phi_A = \phi_{Ai}) = \frac{n_i}{N_{\text{trials}} \times \text{binsize}}$, where n_i is the number of samples in the ith bin. The minimum number of the samples for each bin is 0, which does not display on the logarithm scale. This is why there is a cut-off on the logarithm scale. Its value is $\frac{1}{N_{\text{trials}} \times \text{binsize}} = \frac{1}{10^6 \times 0.01\pi} = 3(10)^{-5}$.

$K = 5$dB is the threshold value where the discrete event for some values of L can be modeled by the Skellam distribution, say $L = 30$ as shown in Figure 4.12, but for some, cannot, e.g., $L = 1000$ as shown in Figure 4.13. Clearly, the theoretical variance given by the Skellam distribution is smaller than the actual variance of the absolute phase given by the simulation. For $K = 5$dB and $L = 1000$, the number of 2π crossings is not large enough, so the Gaussian approximation does not work either, as shown in Figure 4.13.

For $K = 5$dB and $L = 3$, the discrete event of the absolute phase should be modeled

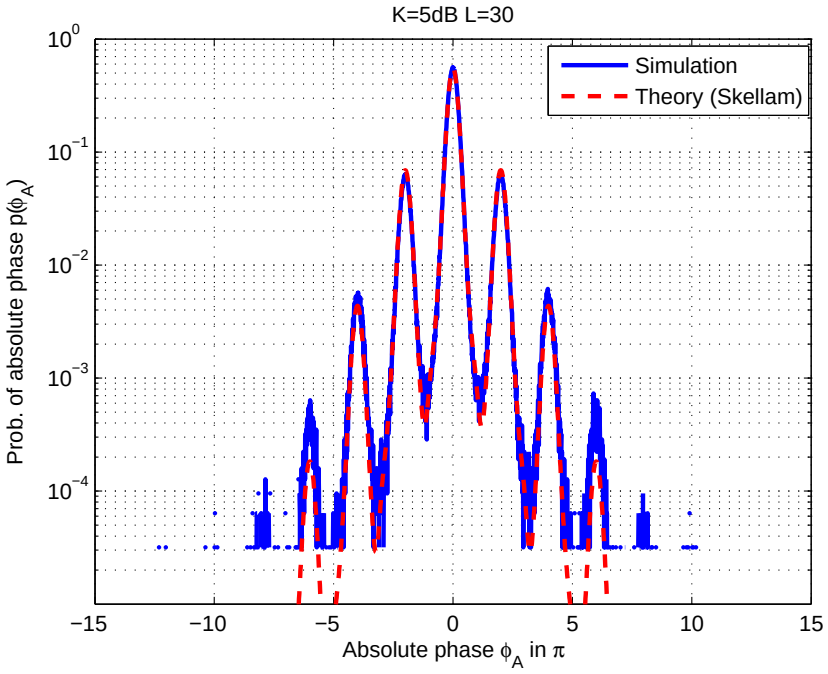

Figure 4.12: Absolute phase pdf by simulation and theory, for $K = 5$dB and $L = 30$.

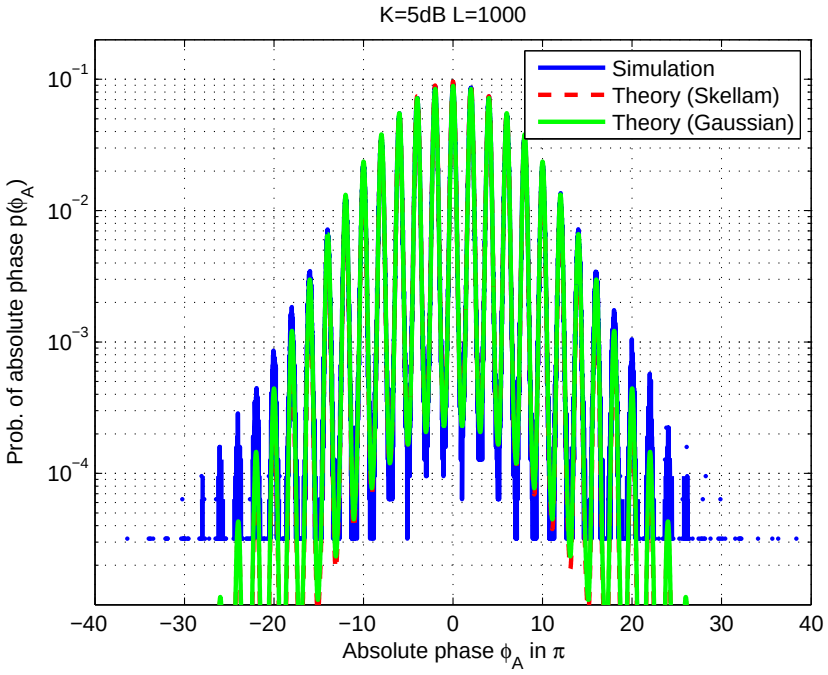

Figure 4.13: Absolute phase pdf by simulation and theory, for $K = 5$dB and $L = 1000$. The lines for the Skellam theory and the Gaussian theory essentially overlap.

correctly by the Skellam distribution based on the discussion in Section 4.3.5.3. Interestingly, although the peak values of the simulations match well to the theory, at the minima and tails the accuracy falls off, as shown in Figure 4.14.

For $K = 0$dB and $L = 300$, the discrete event of the absolute phase can no longer be modeled by the Skellam distribution, as shown in Figure 4.15, because neither the number of positive nor negative 2π crossings follow the Poisson distribution, and there is correlation between them. However, the cumulative number of 2π crossings becomes large such that the Gaussian approximation starts to hold. As shown in Figure 4.16, a magnified portion of Figure 4.15, the peak values of the simulated absolute phase can be modeled better by convolving the continuous event with the Gaussian distribution than with the Skellam distribution.

For $K = 0$ and $L = 300$, the Gaussian approximation works very well to predict the cumulative number of 2π crossings, as shown in Figure 4.17. However, for $K = 0$ and small L, the Gaussian approximation no longer holds. Two examples are shown in Figure 4.18 and 4.19. The variances of the absolute phase at these two setups are similar due to the similar values of L, but the shapes of the distribution of the absolute phase change dramatically owing to the distribution of the phase difference. By convolving the continuous event with the Skellam distribution, the resulting theoretical pdfs do not match the simulation results very well, but are good enough to predict the positions of the peaks and valleys of the pdfs.

This subsection discussed simulation results for the stationary well-defined Rice channel. For the well-defined Rice channel, the mean of the absolute phase is no longer zero, but the pdfs of the discrete and continuous events follow the same trends as discussed above. The simulation results for this more general case are not provided in this thesis.

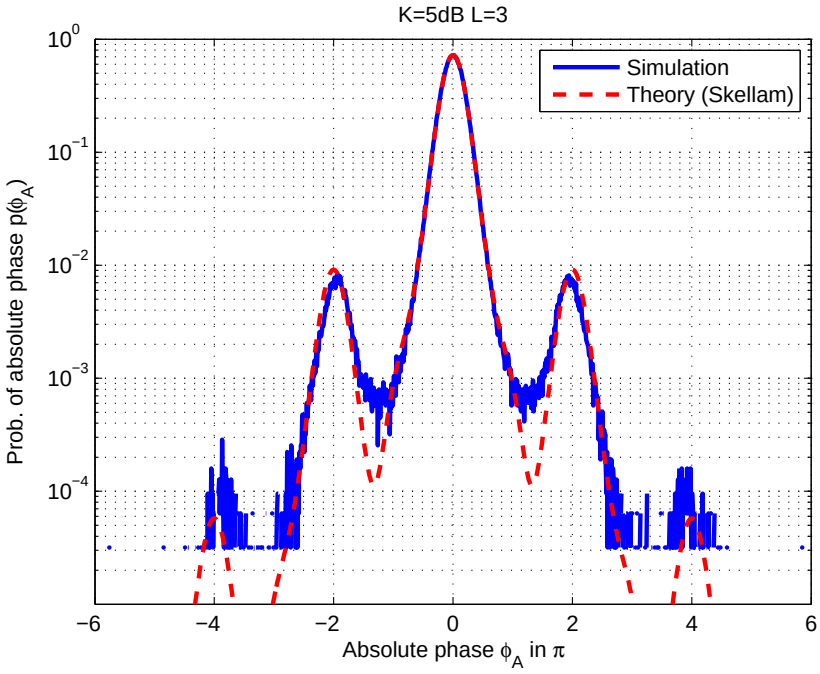

Figure 4.14: Absolute phase pdf by simulation and theory, for $K = 5$dB and $L = 3$.

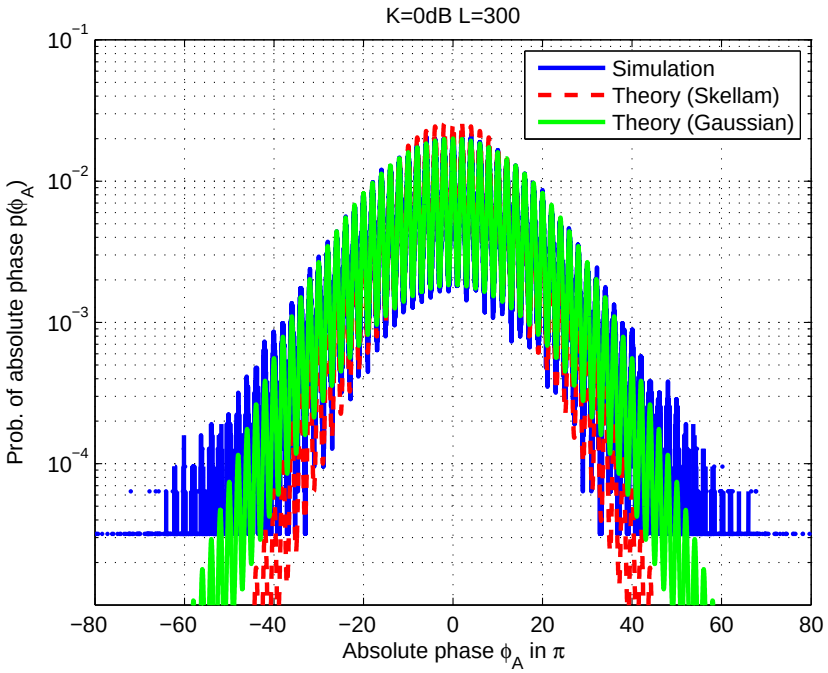

Figure 4.15: Absolute phase pdf by simulation and theory, for $K = 0$dB and $L = 300$.

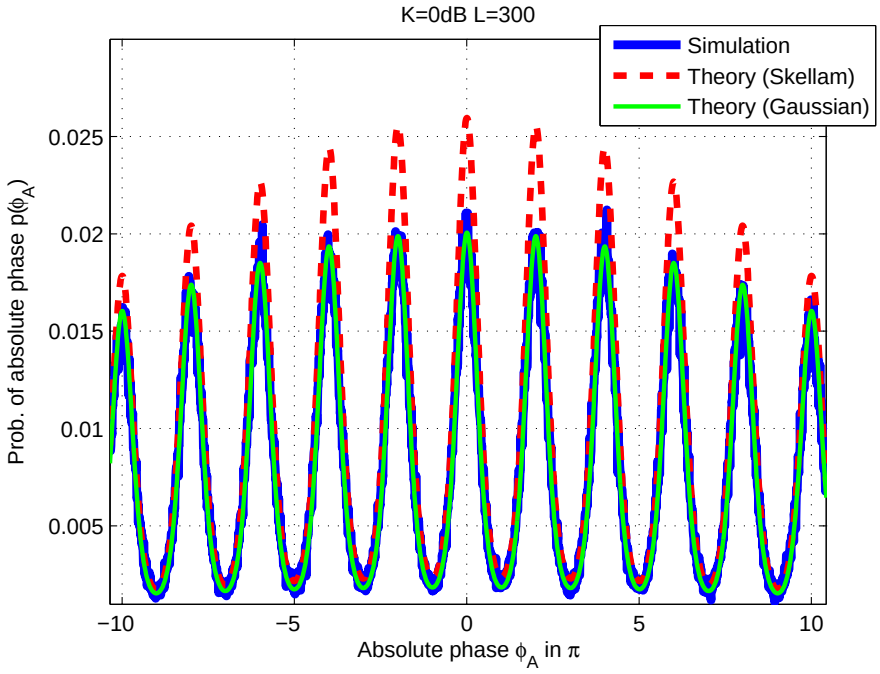

Figure 4.16: Detail of Figure 4.15.

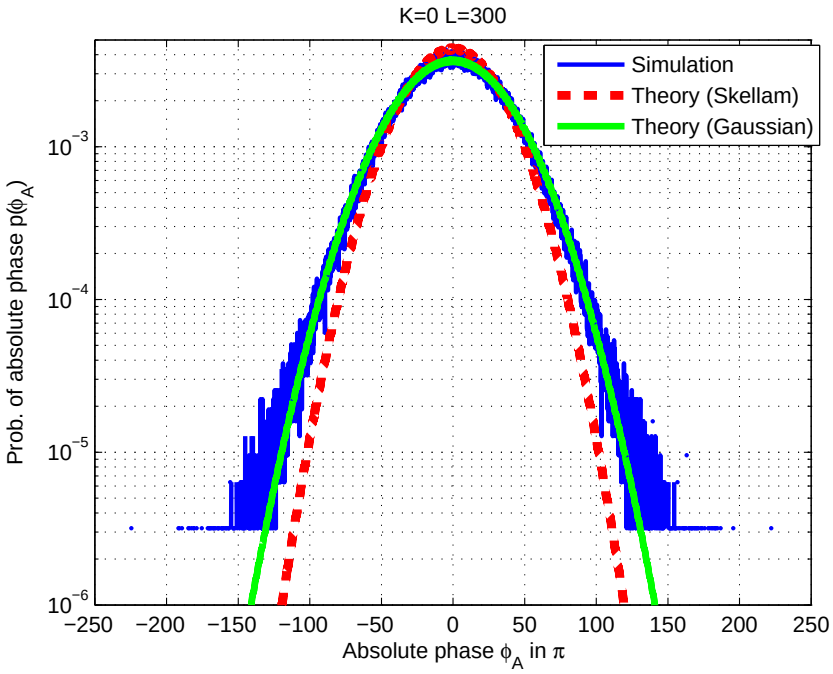

Figure 4.17: Absolute phase pdf by simulation and theory, for $K = 0$ and $L = 300$.

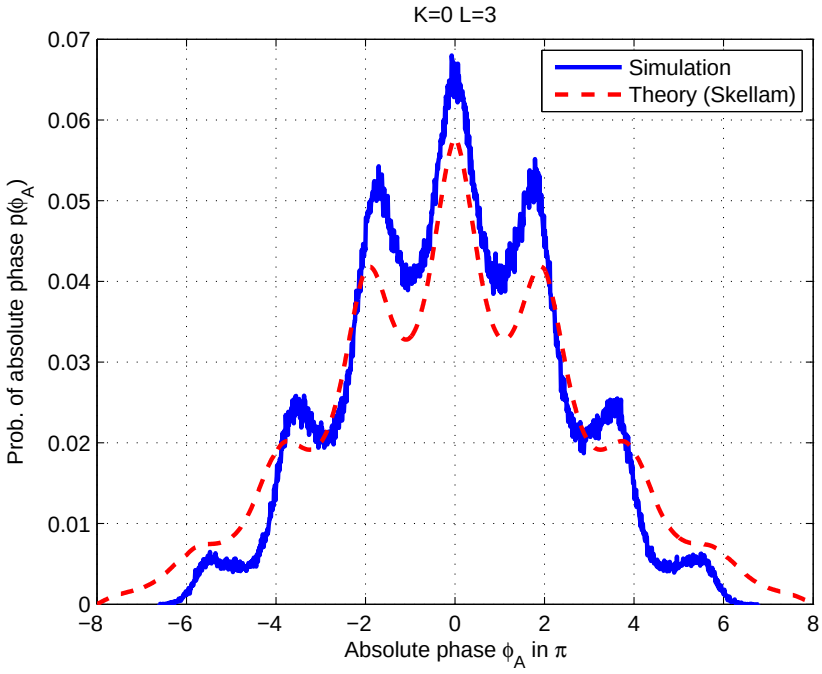

Figure 4.18: Absolute phase pdf by simulation and theory, for $K = 0$ and $L = 3$.

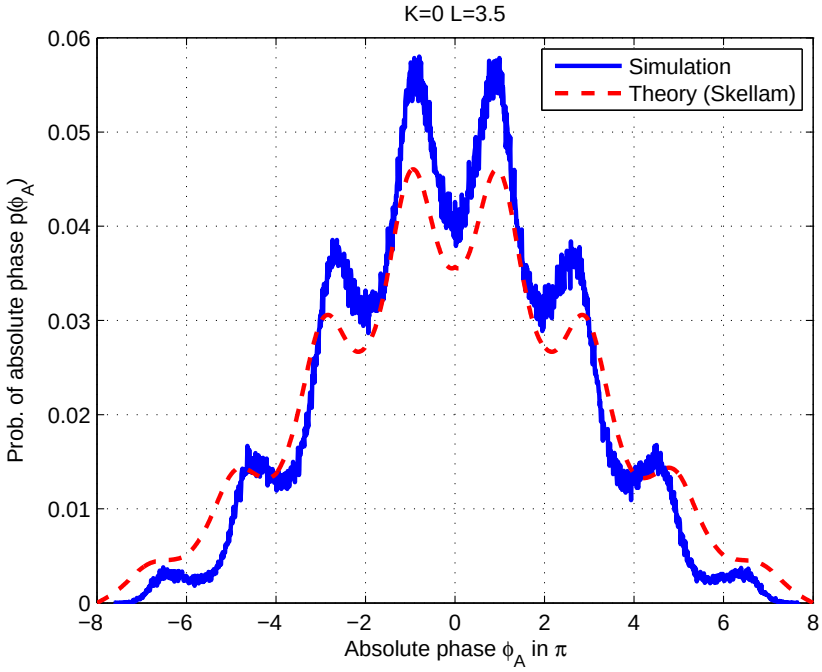

Figure 4.19: Absolute phase pdf by simulation and theory, for $K = 0$ and $L = 3.5$.

Chapter 5

Absolute Phase Based K Factor Estimator

The absolute phase is a new variable that contains more information about the mobile channel than the wrapped phase. Development of the absolute phase will foster new techniques for applications in mobile communications. One such application is to estimate the Rice factor based on the mean of the absolute phase, which is the main topic of this chapter.

5.1 Introduction

5.1.1 K Factor Definition in Mobile Channels

As discussed in Chapter 2, the well-defined Rice channel CAG is the sum of a single, dominant component and a number of diffuse components. The Rice factor, also known as the K factor, is the ratio of the power of the dominant component to the power of the diffuse component. K is an important metric for characterizing channels and is also used as a digital communication parameter, such as in MIMO capacity [4]. Estimating K accurately and easily is an interesting research topic in mobile communications. Simplified models have fostered much published mathematical analysis. Therefore, a literature review is included in next section to cover the different modeling approaches.

The powers used for defining K are considered fixed over the observation interval of interest in the original works of Rice, i.e., for the well-defined Rice channel. More recently, with mobile communications, these powers change with space and time because of the

random nature of mobile patterns and surroundings. As such, the K factor becomes a random variable [101, 102], and this means that the channel is no longer well-defined.

If there is shadowing in the well-defined Rice channel, the definition and interpretation of K require more attention. Shadowing has been modeled as a slow-varying random factor acting: 1) on the dominant component only [41, 103]; 2) on both the dominant and diffuse components with the same random value [39, 40]; or 3) on both the dominant and diffuse components with the same distribution but different random values [104, 105]. As discussed in Section 2.1.2, the second type is the multiplicative shadowing [41], and is the only type of shadowing model that can be removed from the Ricean fading by demeaning the signal [7, 102]. For the other two types of shadowing models, the K factor is not fixed and an averaging technique is required for its definition and computation [106].

5.1.2 Related Work on the K Estimator

Most existing K estimators are developed for the well-defined Rice channel in the absence of shadowing using a single receive antenna. Many of these estimators find K using only the data of the Rice envelope [7, 107, 108, 109]. In [7], K is estimated by comparing the pdf of the collected envelope data to the Rice envelope pdf using goodness-of-fit tests. This statistical method requires a large set of data and is hard to be applied in real-time applications. Similarly, a standard maximum-likelihood estimator (MLE) of K is proposed based on the Rice envelope pdf (referred to here as the *envelope-based MLE*) in [107]. Besides requiring the second moment of the envelope data, this estimator needs a root search of a complicated equation (*c.f.* Equation (10) in [107]) for K. An expectation-maximization algorithm [110] could be adopted to alleviate the computation load of the envelop-based MLE.

To reduce the computational complexity, moment-based methods are proposed in [107] and [108], and then are generalized in [109]. The moment-based methods take advantage of the ratio of two different moments[1] of the Rice envelope being a (complicated) function of only K. K can then be obtained by finding the root of the ratio function. The commonly used moment order pairs are $(1, 2)$ [107] and $(2, 4)$ [108]. The $(1, 2)$ moment-based method is proved to have the best performance in terms of asymptotic variance, of all moment-based methods, for moderate and large K [109]. However, it requires numerically inverting

[1]A moment of the Rice envelope pdf is a function of both the channel variance and K. For any two moments, by equating the product of the moment order and the power of the moment function, for each moment, the channel variance cancels when taking their ratio.

the complicated ratio function. A polynomial fit to the ratio function could be used to simplify the function inversion [111], but the $(1, 2)$ moment-based method still has a higher computational load than the $(2, 4)$ moment-based method. The $(2, 4)$ moment-based method allows a closed-form function between the envelope moments and K, hence leading to a much easier, albeit with a relatively larger estimation variance, implementation [112].

The Rice phase pdf is stationary only when the dominant component is constant. In this special case, the Rice phase pdf alone can be used to find an MLE of K (referred to here as the *phase-based MLE*). However, because the Rice phase pdf is in a more complicated form than the Rice envelope pdf, a simple, but approximate, solution exists only when K is large (i.e., $K >\sim 5$) [113]. When the dominant source is other than broadside (i.e., $\beta_0 \neq 90^o$), the Rice phase pdf, although mathematically well-defined, is no longer strictly stationary and is not suitable for estimating K.

The estimators based on neither the Rice envelope nor the Rice phase alone, use the full information provided by the (complex) channel CAG. Therefore, *complex-signal-based* MLEs were proposed by [11, 113] (using a polar signal representation) and [109] (using a cartesian signal representation) and found to have an improved performance in terms of the Cramer-Rao bound (CRB). The two types of complex-signal-based MLEs, derived from different coordinate systems, are equivalent as shown in [11]. The complex-signal-based MLE has been proved to have the CRB lower than those estimators based on the Rice envelope alone [109]. This MLE is consistent but biased for a finite number of samples. The bias can be removed by adjusting the estimator formulation [11]. However, finding the unbiased MLE requires the knowledge of the exact number of uncorrelated samples used in the estimator.

As well as the distributions of the channel CAG, the second-order statistics (e.g., the autocorrelation functions) also contain information of K, hence leading to another set of correlation-based K estimators such as the one proposed in [114]. The advantages of this correlation-based K estimator are: that it considers the correlation of transmit data symbols and therefore allows a non-data-aided estimator of K; and that it can jointly estimate K and the local average SNR using the same channel samples and therefore allows a channel with additive Gaussian noise. However, this estimator is limited in that it is based on the autocorrelation functions derived from the assumption of isotropic scattering (i.e., the Clarke spectrum), and therefore is sensitive to the physical scattering distribution; and it lacks the robustness to large (larger than 52^o as reported in [11]) AOA of the dominant

component.

Most existing K estimators [11, 107, 108, 109, 110, 111, 112, 113] assume that there is no shadowing , but some [4, 7, 102, 106, 115] account for some form of shadowing . Any type of shadowing changes the estimated envelope distribution, and then the modeled pdf is no longer Rician. Demeaning the channel CAG before estimating K is a common method to remove the shadowing effects on the Rice fading [4, 7, 102]. The demeaning operation in the mobile channel assumes the long-term shadowing is a slow-varying mean multiplied to the short-term fading signal, and therefore will not affect the K factor estimation. But this assumption is valid only for the multiplicative shadowing.

Instead of demeaning the channel CAG, the authors in [115] construct a K estimator using only the statistics of channel phase derivative (a.k.a., instantaneous frequency). The involved statistics are the mean (first moment) and ZCR (second moment related) of the phase derivative, which require a complicated receiver structure for implementation. The authors claim by simulation that this estimator is robust to shadowing. Actually, here the shadowing refers to multiplicative shadowing. Since the second moment (i.e., ZCR) function used in the estimator is derived based on isotropic scattering, the error in estimating K increases with increased directionality of the scattering.

For other shadowing models, the shadowing affects the dominant and the diffuse components independently, hence making the K factor change with time and position. In this case, the K factor could be defined as the ratio of the average power of the dominant component to the average power of the diffuse components. Two generalized moment-based estimators for this definition of K are proposed in [106]. These estimators are based on a shadowed Rice envelope model given in [41], which models the shadowing with the dominant component envelope having a Nakagami distribution (for mathematical convenience). Owing to the more complicated envelope distribution, the derivations and calculations of these estimators have higher complexity.

All the aforementioned K estimators require a large number of uncorrelated samples to achieve reasonable accuracy. As discussed in Section 2.2.3, for an idealized isotropic scenario, the minimum spacing for two signals to be uncorrelated (i.e., the power correlation coefficient approaches its first zero) is 0.38 wavelength at the carrier frequency[2]. Therefore,

[2]The required distance in wavelengths can be smaller or much larger than 0.38 for a nonisotropic scenario [34, 47].

each wavelength of distance provides only around 3 uncorrelated samples[3]. Requiring a large number of uncorrelated samples is equivalent to requiring the physical channel (i.e., AOA and magnitude of the dominant source, power of the scatterers, etc.) to remain unchanging for a relatively long physical distance (e.g., 30 wavelengths for around 100 uncorrelated samples), and this is unlikely to happen in the real-word mobile channel, in particular for a handheld terminal.

5.2 Absolute Phase Based K (APK) Estimator Using Multiple Receive Channels

In this section, a new K estimator using MIMO channels is proposed based on the absolute phase, and is called here as the *absolute phase based K (APK) estimator*. The APK estimator concerns the fixed K estimation over an observation interval for a well-defined Rice channel with isotropic scattering. The APK estimator uses only the channel phase, and therefore is robust to the effects of the distance-dependent path gain and multiplicative shadowing. It requires the mean of absolute phase (i.e., no amplitude involved), and therefore allows a simple receiver structure compared with other real-time estimators, such as the (2,4) moment-based estimator and the complex-signal-based MLE. The APK estimator is only applicable when the K factor is small and medium (i.e., $K <\sim 7$), but for small K (i.e., $K <\sim 1$), it can outperform the (2,4) moment-based estimator and achieves a comparable performance to the complex-signal-based MLE with a small (e.g., 4) number of uncorrelated channels and within a short distance in wavelengths (e.g., 10).

5.2.1 Derivation of the APK Estimator

The absolute phase for a well-defined Rice channel has complicated statistical behavior including the variance and pdf, as discussed in Chapter 3. However, its mean for the channel with isotropic scattering is relatively simple, and is given by (4.2). For convenience, it is repeated here,

$$\bar{\phi}_A(T) \quad = \quad 2\pi f_D \cos(\beta_0) T(1 - \exp[-K]). \tag{5.1}$$

[3]This is consistent with the calculated result given in [11]. The number of uncorrelated samples usually differs from the number of available samples. The latter approximately equals $\frac{1}{f_D T_s}$ for each wavelength, where f_D the maximum Doppler frequency and T_s the sampling period.

It shows that the mean of the absolute phase becomes zero when $K = 0$ or when the dominant component is broadside to the mobile velocity over the observation interval (i.e., when $\beta_0 = 90^o$). As discussed in Chapter 3, the absolute phase, and hence its mean, are not affected by the multiplicative shadowing and the distance-dependent propagation gain.

Solving (5.1), the K factor is readily derived as

$$K = -\log\left[1 - \frac{\bar{\phi}_A(T)}{2\pi f_D \cos(\beta_0) T}\right]. \tag{5.2}$$

Denoting T_{sp} as the sampling period of the channel phase[4], the time interval T can be represented by $T = nT_{sp}$ with n the sample index corresponding to time T ($n = 0$ when $T = 0$). Given $T = 0$, the absolute phase $\phi_A(0) = 0$, so the estimator starts working from the sample index of 1. The digital equivalent of (5.2) is

$$K = -\log\left[1 - \frac{\bar{\phi}_A(n)}{2\pi f_D \cos(\beta_0) n T_{sp}}\right], \ n \geq 1. \tag{5.3}$$

This result means that the K factor can be estimated if both the mean of the absolute phase, $\bar{\phi}_A(n)$, and the Doppler frequency of the dominant source, $f_D \cos(\beta_0)$, are known, provided $\beta_0 \neq 90^o$. The Doppler frequency of the dominant source can be estimated from the wrapped phase samples using FFT techniques as presented in [11, 109]. From now on, the Doppler frequency of the dominant source, $f_D \cos(\beta_0)$ is assumed as a known parameter.

Estimating the mean of the absolute phase requires uncorrelated absolute phase samples (in space) at the same time. This has become possible with a multiple antenna (e.g., MIMO) system. Assuming multiple uncorrelated receive channels are available, with all having the same $f_D \cos(\beta_0)$ and the same K factor, then at any time $T = nT_{sp}$,

$$\hat{\bar{\phi}}_A(n) = \frac{1}{M} \sum_{i}^{M} \phi_{A_i}(n) \tag{5.4}$$

where M is the number of uncorrelated receive channels. In a MIMO system, $M = M_{tx} M_{rx}$ where M_{tx} and M_{rx} are the number of properly designed (uncorrelated) transmit and receive antennas. For example, for a single transmit antenna, $M = M_{rx}$. From now on, only this simple case is considered, i.e., M is the number of receive antennas and this is the same

[4] T_{sp} is usually different from T_s, but they are taken as the same in this chapter because T_s used here is small enough (i.e., $f_D T_s = 0.01$) to capture the variation of the phase.

as the number of uncorrelated channels. A larger M produces a better estimate of K at a particular time T.

By substituting (5.4) into (5.3), the APK estimator at time $T = nT_{sp}$ is obtained,

$$\hat{K}_{AP} = -\log\left|1 - \frac{\frac{1}{M}\sum_i^M \phi_{A_i}(n)}{2\pi f_D \cos(\beta_0) n T_{sp}}\right|, \quad n \geq 1 \tag{5.5}$$

where $|\cdot|$ represents the absolute value. As discussed in Chapter 4, the variance of the absolute phase is relatively large especially for small K. If the number of uncorrelated antennas is limited, the estimated mean of the absolute phase fluctuates around the true value, and sometimes may become larger than $2\pi f_D \cos(\beta_0) n T_{sp}$. In this case, the argument of the logarithm becomes negative, producing a complex-valued result. To avoid the negative argument of the logarithm, the absolute value of the argument is taken before the logarithm is calculated.

In the following discussion, the normalized parameters are used: the sampling frequency is $f_n = f_D T_{sp}$; the distance in wavelengths the mobile travels from time 0 to time T is $L = z/\lambda = n f_n$ with z the physical distance in meter. Correspondingly, the denominator in the estimators above can be written as $2\pi f_D \cos(\beta_0) n T_{sp} = 2\pi f_n \cos(\beta_0) n = 2\pi L \cos(\beta_0)$.

With these normalization parameters, the estimator given by (5.5) is a function of the number of uncorrelated antennas (M), the observation interval as distance in wavelengths (L), and the AOA (β_0).

5.2.2 Performance Analysis of the APK Estimator

The APK estimator given by (5.5) is consistent when analyzed using large sample theory [116]. The consistency property means that the estimator is asymptotically unbiased and has a variance of approximately zero when the sample number M goes to infinity.

However, for a finite sample size, i.e., a limited number of uncorrelated antennas, the estimated mean of the absolute phase differs from the true value. The error introduced by estimating the mean of the absolute phase, given by (5.4), is propagated to the estimate of K. Denote

$$\hat{\bar{\phi}}_A(n, K) = \bar{\phi}_A(n, K) + \epsilon_\phi(n, K) \tag{5.6}$$

where $\epsilon_\phi(n, K)$ is the estimate error of the absolute phase mean for a given K at the time

instant nT_s owing to the finite number of samples M, and the argument K is used to emphasize that the true mean ($\bar{\phi}_A$), the mean estimate ($\hat{\bar{\phi}}_A$), and the error (ϵ_ϕ), are all dependent on K.

Substitute (5.6) and (5.1) into (5.5),

$$\begin{aligned}
\hat{K}_{AP} &= -\log\left|1 - \frac{\bar{\phi}_A(n,K) + \epsilon_\phi(n,K)}{2\pi L\cos(\beta_0)}\right| \\
&= -\log\left|\exp[-K] - \frac{\epsilon_\phi(n,K)}{2\pi L\cos(\beta_0)}\right| \\
&= K - \log\left|1 - \frac{\epsilon_\phi(n,K)\exp[K]}{2\pi L\cos(\beta_0)}\right| \\
&= K + K_{bias} \qquad (5.7)
\end{aligned}$$

where K_{bias} is the estimator bias due to a finite sample size, and is affected by the error of estimating the absolute phase mean (ϵ_ϕ), the distance in wavelengths (L), the AOA of the dominant source (β_0), and the Rice factor (K). The first and second moment of K_{bias} are the bias and Mean Square Error (MSE) of the APK estimator, respectively.

When M is large, ϵ_ϕ can be modeled as Gaussian by the CLT. This approximated Gaussian has a mean of zero, and a variance of $\sigma^2_{\phi_A}/M$, where $\sigma^2_{\phi_A}$ is the variance of the absolute phase and M is the number of uncorrelated antennas. By modeling ϵ_ϕ as Gaussian, the argument of the logarithm in (5.7) is also Gaussian with the mean of 1 and the variance of

$$\sigma^2_\epsilon = \frac{\sigma^2_{\phi_A}\exp[2K]}{M(2\pi L\cos(\beta_0))^2}.$$

Then the pdf of K_{bias}, denoted by $p(K_b)$, is given by

$$p(K_b) = \frac{1}{\sqrt{2\pi}\sigma_\epsilon}\{\exp[K_b - \frac{(\exp[K_b]-1)^2}{2\sigma^2_\epsilon}] + \exp[K_b - \frac{(\exp[K_b]+1)^2}{2\sigma^2_\epsilon}]\}. \qquad (5.8)$$

An example of the statistics of ϵ_ϕ and K_{bias} against K is given[5] in Figure 5.1, where $L = 10$, $\beta_0 = 0$, and $M = 32$. When $M = 32$, ϵ_ϕ can be modeled as Gaussian with a mean of zero. The standard deviation of ϵ_ϕ, from simulation, monotonically decreases with K (crossed line). The argument of the logarithm in (5.7) is still Gaussian, but with a mean of 1 and modified standard deviation (circled line). Owing to the nonlinearity of $\exp[K]$,

[5]Finer lines are used for this plot and the succeeding plots of this chapter, for clarity.

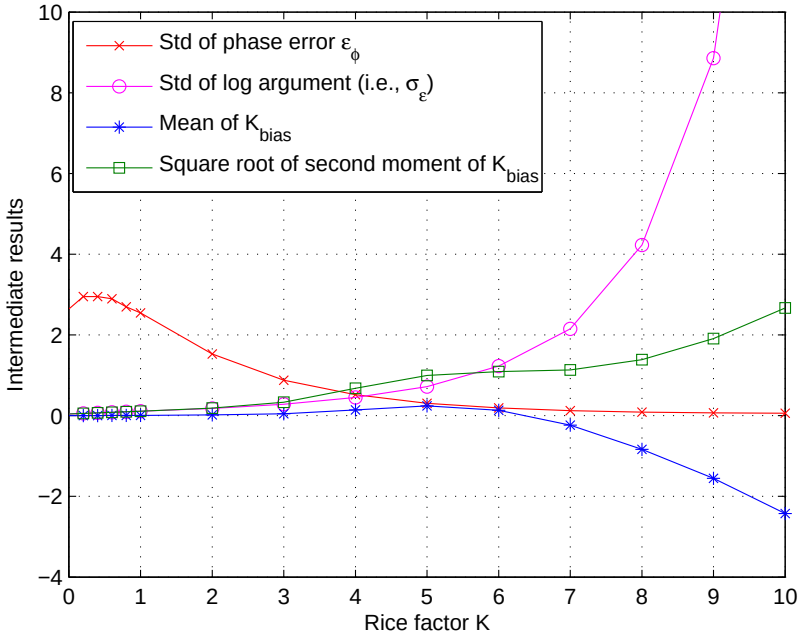

Figure 5.1: The intermediate results: simulated standard deviation of phase error, ϵ_ϕ (crossed), standard deviation of the logarithm argument in (5.7), formulated as σ_ϵ (circled), mean of K_{bias} (starred), and square root of the second moment of K_{bias} (squared), given $L = 10$, $\beta_0 = 0$ and $M = 32$ for various K.

this modified standard deviation monotonically increases with K. After taking the absolute value and the logarithm, K_{bias} is not Gaussian, but its numerically evaluated mean (equal to the bias of the APK estimator, starred line) and square root of the non-central second moment (equal to the root mean square error (RMSE) of the APK estimator, squared line) change nonlinearly with K.

The changing trends of the bias and RMSE of the APK estimator against K are hard to predict due to these nonlinear transformations, even when the phase error ϵ_ϕ can be modeled as Gaussian for large M (e.g., 32 in this example). For small M, they become more complicated because the Gaussian approximation no longer holds, as illustrated by simulation results in the next section.

5.3 Numerical Results and Discussion

5.3.1 Performance Analysis Using Simulation

The performance of the APK estimator is affected by the Rice factor (K), the observation interval as distance in wavelengths (L), and the AOA of the dominant component (β_0). In a practical measurement, a signal is transmitted through the channel with additive noise, and the received signal is used to estimate the K factor, so the SNR also determines estimation accuracy of the K factor. The SNR is established by the anti-aliasing filters and the sampling accuracy of the components (i.e., I and Q). It is assumed there are sufficient statistics, after digitization, to interpolate the component signals in order to calculate the phase signal without adding further noise.

The effects of these parameters, including the SNR, are analyzed by simulation below, for a number of uncorrelated antennas (M). The major criteria to evaluate and compare the estimator performance are the estimator bias and the root mean square error (RMSE). For the simulations in this subsection, the number of trials is 5000, the number of uncorrelated antennas is $M = 1, 2, 4, 8, 32$, and the normalized sampling rate is $f_n = f_D T_{sp} = 0.01$. $K = 1$, $\beta_0 = 0$, and $L = 10$ are used as examples for these parameters in following discussion when necessary. Other values of these parameters, if applicable to the APK estimator, have similar trends as with the parameter examples, and they are not presented here.

As given by (5.5), the K factor can be estimated using the mean of the absolute phase at any observation time. However, the APK estimator performance differs for different observation intervals. Figure 5.2 shows how the bias and RMSE vary with increasing L (time) given $\beta_0 = 0$ and $K = 1$. For small numbers of antennas (e.g., $M = 1, 2$), the bias and RMSE decrease rapidly when L increases from 2 to 20. For more than 4 antennas and $L >\sim 5$, the performance does not improve much. After $L \simeq 50$, all curves continue to decay slowly. A practical configuration for the APK estimator is $M = 4$ and $L = 10$, which trades off performance with a simple system.

Figure 5.3 illustrates the bias and RMSE of the APK estimator against K for different sets of antennas given $L = 10$ and $\beta_0 = 0$. The trends of mean and RMSE against K, given by the simulation results, are complicated and hard to predict as discussed in the last section. Given $M = 32$, the theoretical curves of mean and RMSE (dashed lines), based on the assumption that ϵ_ϕ can be reasonably modeled as Gaussian, match well the simulation results, although there is small departure for K from 5 to 8. For a smaller M, the Gaussian

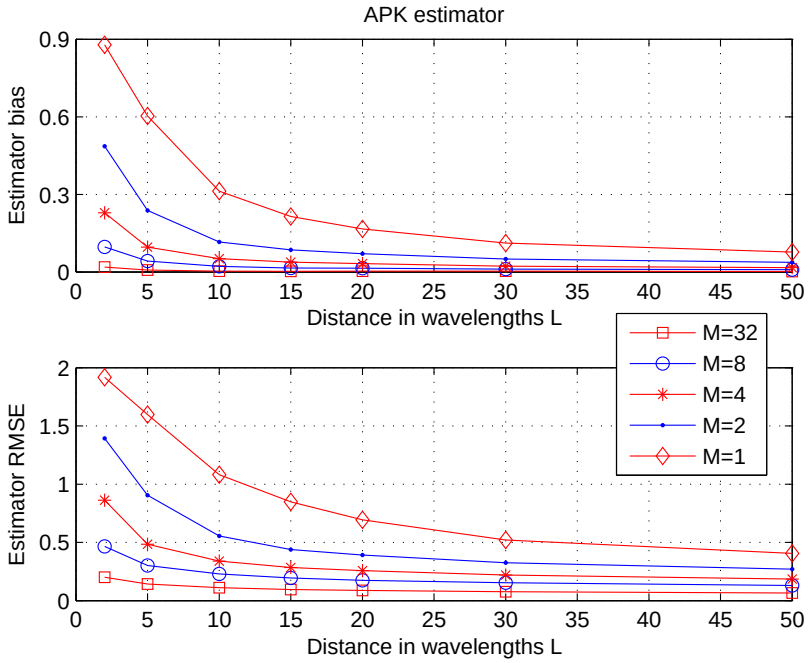

Figure 5.2: The bias and RMSE of the APK estimator against the distance in wavelengths, L, given $K = 1$ and $\beta_0 = 0$.

assumption loses validity for a larger range of K, so the corresponding theoretical curves (not shown) have a large discrepancy with the simulated ones. Interestingly, the APK estimator bias at $K \simeq 5$ and the RMSE at $K \simeq 6$ are almost independent of the number of antennas in this simulation setup.

An example of the APK estimator given $M = 4$, $L = 10$ and $\beta_0 = 0$, with a confidence region represented by the RMSE, is illustrated in Figure 5.4. In this example, the APK estimator performs very well for K smaller than 2, and becomes less accurate for K between 2 to 6. For $K >\sim 6$, the estimated value of K stays around 6 so that the estimator bias, shown in Figure 5.3, linearly decreases as K increases. This is because when $K >\sim 6$, the mean of the absolute phase is almost independent of K owing to the term $(1 - \exp[-K])$ in (5.1). Based on this observation, the APK estimator can work for K from 0 up to around 7. For $K >\sim 7$, both bias and RMSE become so large that the APK estimator is no longer applicable.

As discussed above, the APK estimator cannot work when the AOA of the dominant source is $\beta_0 = 90^o$. Figure 5.5 shows the APK estimator performance against AOAs for

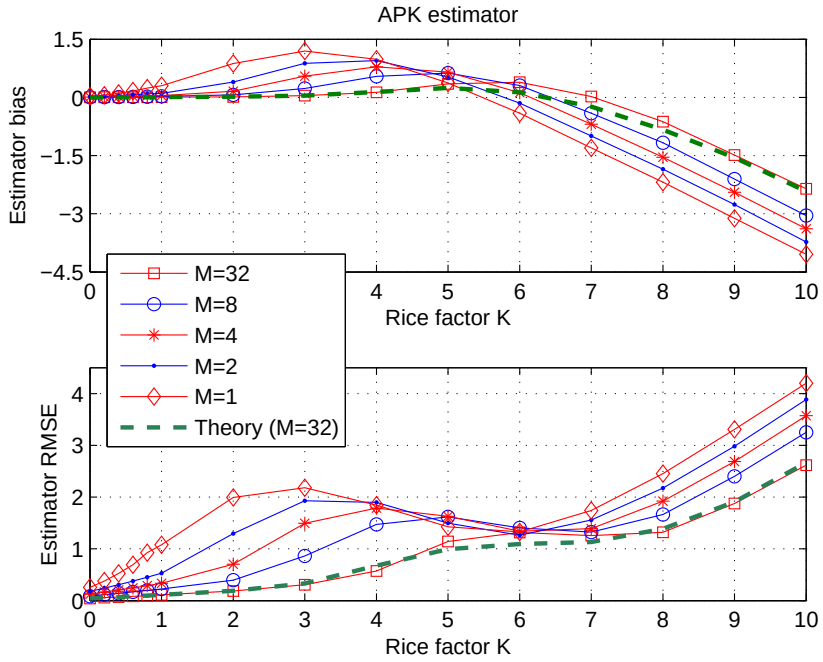

Figure 5.3: The bias and RMSE of the APK estimator against the Rice factor K, given $L = 10$ and $\beta_0 = 0$. The theoretical curves for $M = 32$ are also shown.

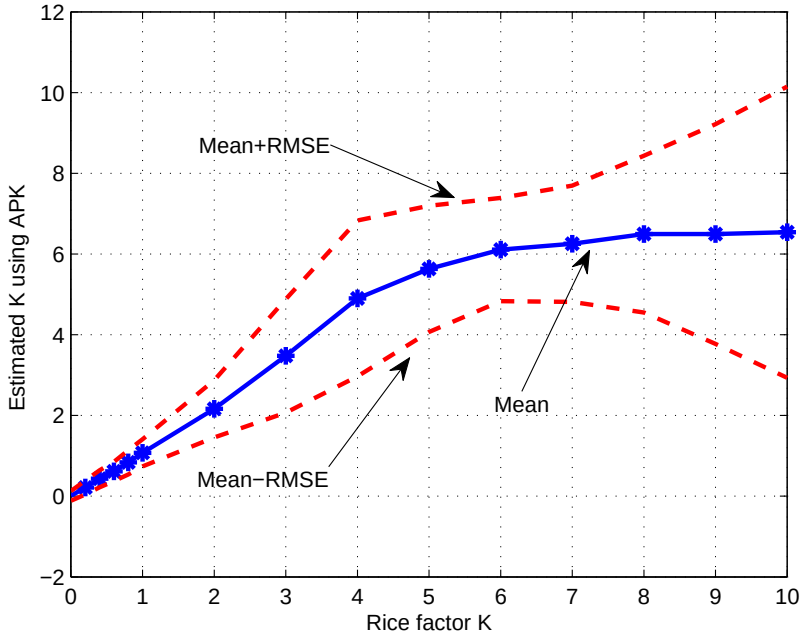

Figure 5.4: The mean of the APK estimator against the Rice factor K, given $M = 4$, $L = 10$ and $\beta_0 = 0$. The upper and lower values, represented by (mean±RMSE), show estimation accuracy using the APK estimator for the given parameters.

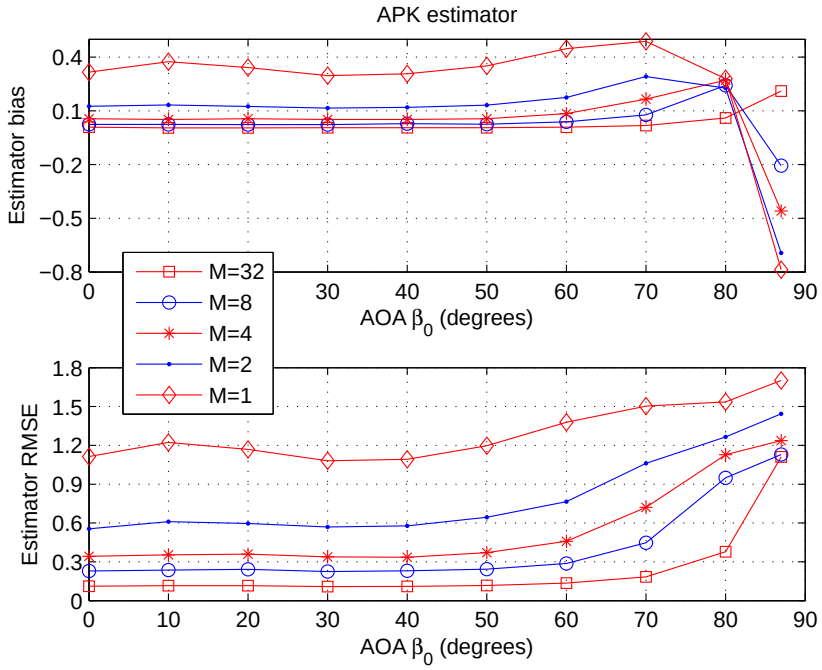

Figure 5.5: The bias and RMSE of the APK estimator against the AOA of the dominant source, β_0, given $K = 1$ and $L = 10$.

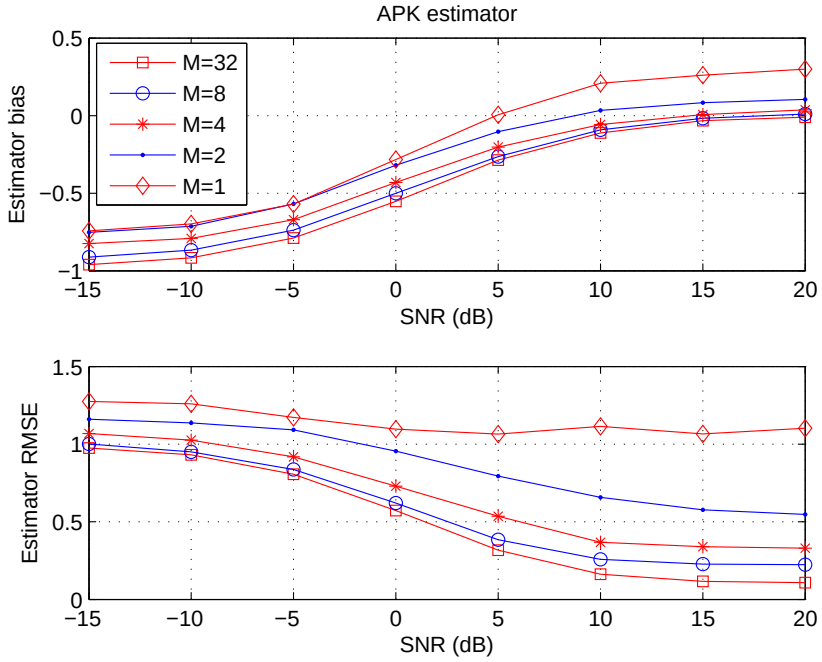

Figure 5.6: The bias and RMSE of the APK estimator against the SNR given $K = 1$, $\beta_0 = 0$ and $L = 10$.

the example of $L = 10$ and $K = 1$. The bias and RMSE start to increase from $\beta_0 = 50^o$ when the number of antennas, M, is 1 or 2, but given $M = 4$, these performances are almost unchanging until $\beta_0 = 60^o$ and become unacceptable when $\beta_0 > 80^o$. More antennas extend the applicable range of AOA towards 90^o. When $\beta_0 = 90^o$, the channel becomes the stationary well-defined Rice channel. In this case, K can be easily estimated using any other methods if the AOA can be estimated a priori. AOA estimation is not discussed here.

Figure 5.6 illustrates the bias and RMSE of the APK estimator against the SNR for different sets of antennas given $K = 1$, $L = 10$ and $\beta_0 = 0$. The APK estimator performance improves with increasing M and/or increasing SNR. When the SNR is larger than 15dB, both the bias and the RMSE of the APK estimator level out. This means that the effect of the SNR on performance of the APK estimator can be ignored when the SNR is larger than 15dB.

5.3.2 Estimator Comparisons

In this subsection, the APK estimator is compared to those that can be implemented in real time and have relatively simple receiver structure, i.e., the (2,4) moment-based estimator [108, 109], and the complex-signal-based MLE [11, 109].

The (2,4) moment-based estimator is given by [109]

$$\hat{K}_{24} = \frac{-2\hat{\mu}_2^2 + \hat{\mu}_4 - \hat{\mu}_2\sqrt{2\hat{\mu}_2^2 - \hat{\mu}_4}}{\hat{\mu}_2^2 - \hat{\mu}_4} \tag{5.9}$$

where $\hat{\mu}_p$ is the estimated pth moment of the signal envelope, $r(n)$, and can be obtained by

$$\hat{\mu}_p = \frac{1}{N_s}\sum_{n=0}^{N_s-1} r^p(n) \tag{5.10}$$

with N_s the number of available samples.

The complex-signal-based MLE is given by [109]

$$\hat{K}_{ML} = \frac{\hat{A}^2}{2\hat{\sigma}^2} \tag{5.11}$$

with

$$\hat{A} = \left| \frac{1}{N_s}\sum_{n=0}^{N_s-1} r(n)\exp[j(\phi_W(n) - 2\pi n T_{sp} f_D \cos(\beta_0))] \right|$$

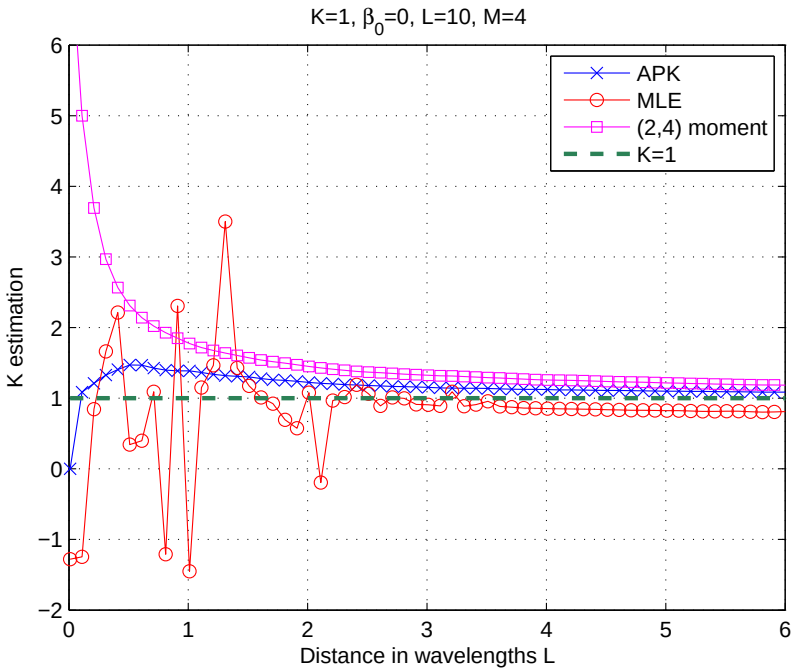

Figure 5.7: Comparison of averaged (over 5000 trials) results from three estimators for the example of $K = 1$, $L = 10$, $\beta_0 = 0$, and $M = 4$ in a sliding window mode. The length of the sliding window is $L = 10$ (corresponding to 1000 samples when $f_n = 0.01$, and about 30 uncorrelated samples with isotropic scattering for each antenna). For $L < 10$, the estimators use all the available samples for estimation.

and

$$2\hat{\sigma}_2 = \hat{\mu}_2 - \hat{A}^2.$$

In the simulations, the samples up to time nT_{sp} from multiple antennas are collected and then used for estimating K by different estimators. The trial number used to estimate the bias and RMSE is 5000. Here $M = 4$ is used as an example for performance comparisons of these three estimators. More antennas produce similar performance curves for each estimator but with smaller bias and RMSE. The bias and RMSE of the APK estimator for $M = 32$ are also illustrated in the following figures. It shows that the APK estimator with a large number of antennas can sometimes perform comparably to the other K estimators with a small number of antennas. The examples of $L = 10$, $K = 1$, and $\beta_0 = 0$ are used when necessary for discussion, but the conclusions are applied to other parameter combinations.

Figure 5.7 is the averaged output of the three estimators with a sliding window of $L = 10$.

For $L < 10$, the estimators use all the available samples for estimation. For small L (i.e., $L <\sim 3$, corresponding to fewer than 10 available uncorrelated samples), neither the (2,4) moment based estimator nor the complex-signal-based MLE works and the latter exhibits very large variation, including negative values of K. On the contrary, the APK estimator approaches the actual value of K quickly and smoothly. This difference is because the former two estimators are required to estimate the sample moments which does not work well when the number of available uncorrelated samples is small. When $L >\sim 3$, all three estimators work well with the APK having the smallest bias. This is confirmed by the performance comparison result at $L = 10$ given in Figure 5.8.

To get a feel for the computation time, the calculation duration is counted from time 0 to time at $L = 15$, during which each estimator is run 1500 times. Using Matlab on a PC, the average calculation durations (over 5000 trials) are 0.88, 0.98, and 1.16 seconds for the APK, the MLE, and the (2,4) moment-based estimator, respectively.

In summary, the APK estimator provides a more stable output at the beginning of the adaptive output than the complex-signal-based MLE and the (2,4) moment-based estimator, and also requires less memory and less computation time. Since no amplitude involved in the APK estimator, it requires a simple receiver structure compared with the other two estimators.

The performance of the three estimators against the distance, L, is shown in Figure 5.8. Given small K ($K = 1$ in this example), and when $L \geq 5$, the APK estimator has similar but smaller bias, and similar but slightly larger RMSE than the complex-signal-based MLE. The (2,4) moment-based estimator always has the largest bias and the largest RMSE across all the distances of interest among the three estimators. In this setup, the APK estimator with more antennas (e.g., $M = 32$, dashed lines) has much smaller bias and RMSE than the other two estimators with $M = 4$.

The performance of the three estimators against K, given $L = 10$, $\beta_0 = 0$ and $M = 4$, is shown in Figure 5.9. The bias here is shown as the value relative to its actual K. It is clear that the (2,4) moment-based estimator is not applicable for K smaller than 1, but both the APK estimator and the complex-signal-based MLE have similar performance in this range. From $K \simeq 1$, the relative bias and RMSE of the APK estimator start to increase, become larger than those of the MLE, but smaller than those of the (2,4) moment-based estimator before $K \simeq 2$, and finally exceed those of the other two estimators when $K >\sim 2$. However, the maximum relative bias for the APK estimator is less than 20% (0.2 in the

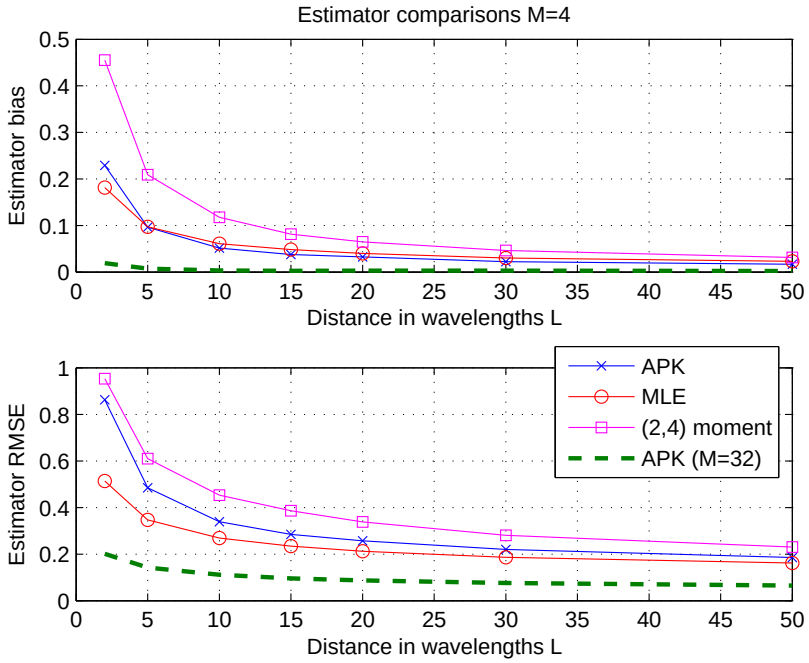

Figure 5.8: Comparison of the bias and RMSE of three estimators for various L given $K = 1$, $\beta_0 = 0$, and $M = 4$. Also shown are the bias and RMSE of the APK estimator for $M = 32$ (dashed lines).

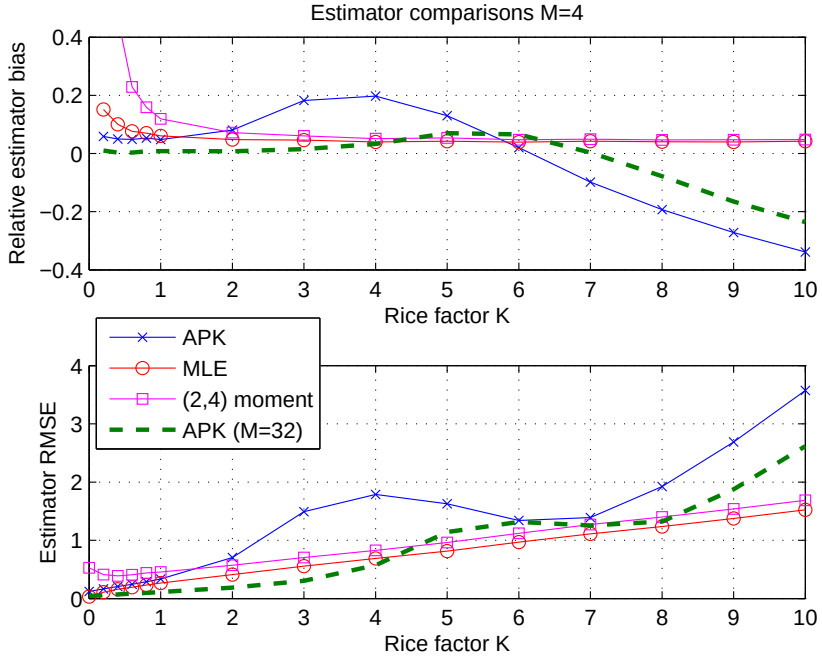

Figure 5.9: Comparison of the relative bias and the RMSE of three estimators for various K given $L = 10$, $\beta_0 = 0$, and $M = 4$. Also shown are the relative bias and the RMSE of the APK estimator for $M = 32$ (dashed lines). The relative bias at $K = 0$ becomes infinity and hence cannot be displayed.

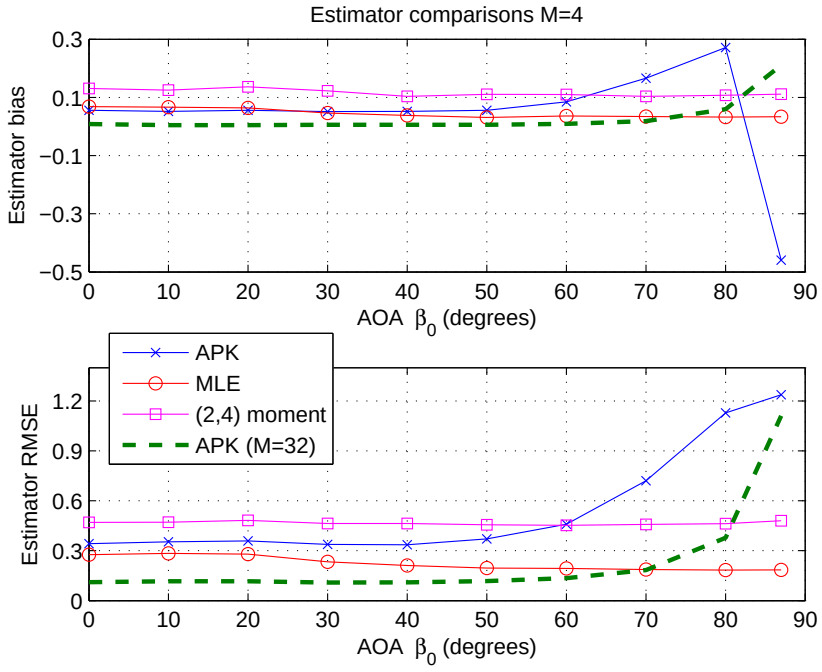

Figure 5.10: Comparison of the bias and RMSE of three estimators for various AOA given $K = 1$, $L = 10$, and $M = 4$. Also shown are the bias and RMSE of the APK estimator for $M = 32$ (dashed lines).

upper plot of Figure 5.9) for K from 0 to ~ 8 given $M = 4$. This percentage decreases as more uncorrelated antennas (e.g., $M = 32$, dashed lines) are used, especially for the region of K from around 3 to 5.

The performance of the three estimators against AOA, β_0, given $K = 1$, $L = 10$, and $M = 4$, is shown in Figure 5.10. As expected, the performance of both the (2,4) moment-based and the complex-signal-based estimators is not affected by the AOA, β_0. However, from the $\cos(\beta_0)$ term in the estimator, the bias and RMSE of the APK estimator start to increase at $\beta_0 = 50^o$, but become similar to those given by the (2,4) moment-based estimator until $\beta_0 = 60^o$, and diverge to large values when $\beta_0 > 80^o$. As discussed for Figure 5.5, more available uncorrelated antennas (e.g., $M = 32$, dashed lines) will move the largest applicable AOA towards 90^o.

The performance of the three estimators against the SNR, given $K = 1$, $L = 10$, $\beta_0 = 0$ and $M = 4$, is shown in Figure 5.11. The effect of the SNR on the estimation performance is similar for all the K estimators. Specifically, both the bias and RMSE of all the estimators

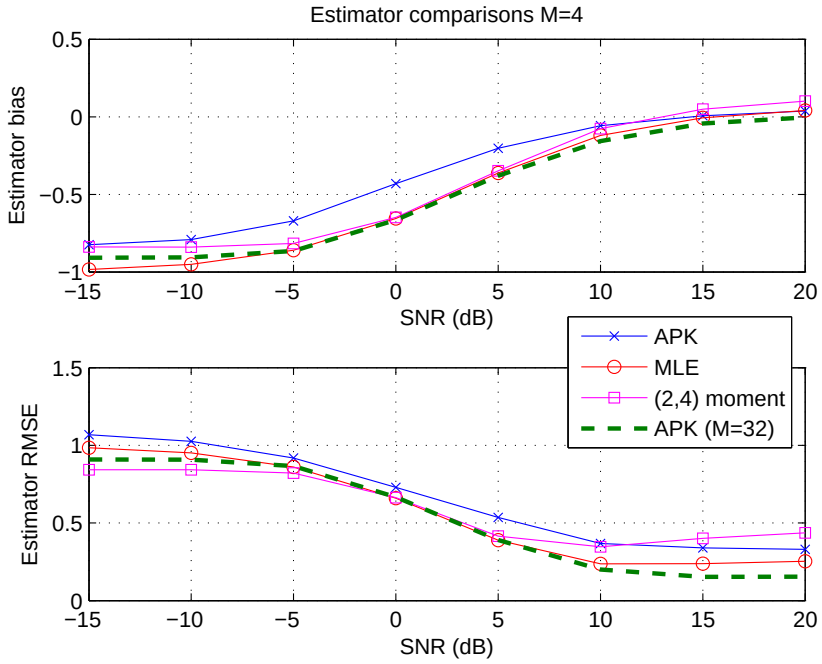

Figure 5.11: Comparison of the bias and RMSE of three estimators for various SNR given $K = 1$, $\beta_0 = 0$, $L = 10$, and $M = 4$. Also shown are the bias and RMSE of the APK estimator for $M = 32$ (dashed lines).

decrease as the SNR increases, but level out when the SNR is larger than 15dB. More uncorrelated antennas (dashed lines for $M = 32$) increase the estimation accuracy of the APK estimator, but will not change the effect of the SNR on the estimator. Another observation is that the bias owing to the SNR for all K estimators is negative. This is because the noise, additive to the channel, acts as the diffuse component of the channel CAG, and then reduces the estimated value of K.

5.4 Summary

The problem of estimating the Rice factor, K, has been an interesting research topic in mobile communications. Much analysis has resulted from models which simplify the physical channel mechanisms. Estimating K requires a large number of uncorrelated samples for good accuracy. However, the fast-changing K of the physical mobile channel limits the number of available uncorrelated samples with fixed K. A multiple antenna system, such

as MIMO, is a good candidate to reconcile these two requirements.

Existing K estimators which are easy to implement are based on the Rice envelope and Rice phase pdfs. They require to estimate different moments of the Rice envelope and are therefore sensitive to the changing K and are also sensitive to any kind of shadowing.

The channel phase based K estimator proposed in this chapter is derived from the mean of the absolute phase. The K factor can be estimated after simple operations on the mean of the absolute phase collected from multiple receive channels. Compared to other K estimators, the proposed estimator requires less memory, less computation, and a simpler receiver structure.

The performance (bias and RMSE) of the proposed phase based estimator, is analyzed and simulated. The performance of this estimator improves when more uncorrelated receive channels (M) and longer electrical observation interval (L) are available. A combination of $M = 4$ and $L = 10$ is shown in this chapter as a practical configuration with acceptable performance.

Similar to many K estimators derived from the Rice phase and/or Rice envelope pdf, the proposed phase based estimator requires a mobile channel which is noise-free or with very high SNR (i.e., SNR$>$ 15dB). Low SNR will degrade the performance of this estimator in a similar way to the performance of other estimators.

The proposed K estimator is based on the mean function of the absolute phase with isotropic scattering. In the presence of directional scattering, non-zero correlation appears between the real and the imaginary part of the channel CAG, and will thus influence the mean as discussed in Chapter 6. In other words, the scattering directionality will introduce estimation errors to this proposed estimator.

Nevertheless, the proposed absolute phase based estimator provides a different and simple way to estimate the Rice factor. The elegant properties of the proposed K factor estimator stem from the absolute phase, the new channel variable. By taking advantage of the absolute phase, other applications, such as mobile localization and tracking, can be developed, and these are left as future work.

Chapter 6

Effects of Directional Scattering on Mobile Channels

The research presented in Chapter 4 and Chapter 5 is based on the assumption that the scattering surrounding the receiver is isotropic. However, as discussed in Section 2.2.4, the directionality of the scattering alters the second-order statistics of the channel, hence changing some of the results which were based on isotropic scattering. It is emphasized again that the directional scattering is assumed to be uni-directional and in a 2D plane, and directionality is the combination of both scatterers and antennas. In this chapter, two effects of scattering directionality on the mobile channels are investigated: the mean of the absolute phase; and antenna spacing design.

6.1 Mean of the Absolute Phase with Directional Scattering

As discussed in Chapter 3, the absolute phase can be calculated by

$$\phi_A(T) = [\phi_W(T) - \phi_W(0)] + 2\pi \left[N_{2\pi+}(0,T) - N_{2\pi-}(0,T)\right] \tag{6.1}$$

where $\phi_W(T)$ and $\phi_W(0)$ are the wrapped phase values within $[-\pi, \pi)$ at time T and 0, respectively, and $N_{2\pi+}(0,T)$ and $N_{2\pi-}(0,T)$ are the number of positive and negative 2π crossings during the observation interval of $(0,T)$, respectively.

As a random variable, the mean of the absolute phase can be obtained by taking its

expectation,

$$\begin{aligned}\bar{\phi}_A(T) &= E[\phi_A(T)] \\ &= E[\phi_W(T)] - E[\phi_W(0)] + 2\pi E[N_{2\pi+}(0,T)] - 2\pi E[N_{2\pi-}(0,T)]. \end{aligned} \quad (6.2)$$

Since $E[\phi_W(T)] = E[\phi_W(0)] = 0$, then the mean of the absolute phase is determined by the average number of cumulative 2π crossings.

6.1.1 2π Crossing Rate Owing to a Time-Varying Dominant Component

In this subsection, the 2π crossing rate is evaluated for a well-defined Rice channel with a time-varying dominant component. As discussed in Section 4.1, the mean of absolute phase with isotropic scattering is the result of the cumulative 2π crossings due to the time-varying dominant component rotating with a increase rate of $2\pi f_D \cos(\beta_0)$. This type of 2π crossing rate can be intuitively derived from the relationship between the time-varying dominant component and the envelope of the diffused components modeled by the Rayleigh distribution. In the presence of directional scattering, this relationship does not change, so the mean of the absolute phase with directional scattering contains a term given by (4.2),

$$\bar{\phi}_A^{(1)}(T) = 2\pi f_D \cos(\beta_0) T(1 - \exp[-K]) \quad (6.3)$$

If $\beta_0 = 90^o$, (6.3) becomes zero, which represents that the contribution of the dominant component to the mean of the absolute phase is zero when the dominant component is stationary. In the presence of directional scattering, $x(t)$ and $y(t)$ at the same instant (i.e., zero lag) remains uncorrelated, but non-zero cross-correlation appears between $x(t)$ and $\dot{y}(t)$. This cross-correlation contributes another term to the 2π crossing rate, and hence to the mean of the absolute phase.

6.1.2 2π Crossing Rate Owing to Scattering Directionality

In this subsection, the 2π crossing rate is evaluated for a well-defined Rice channel with a stationary dominant component (i.e., $\beta_0 = 90^o$) and directional scattering. In this case, the channel CAG can be written as $h(t) = A + x(t) + jy(t)$. The derivation is similar to those presented in Section 4.3.5.1.

In Section 4.3.5.1, it is shown that, for an arbitrary interval Δt, the number of the

positive 2π crossings, $R_+^c \Delta t$ is

$$R_+^c \Delta t = \int_{-\infty}^{-A} \int_{-\infty}^{0} \int_{0}^{\Delta y} p_{x,y,\dot{y}}(x, y, \dot{y}; t) dy d\dot{y} dx \tag{6.4}$$

Denoting $Z^T(t) = [\ x(t) \quad y(t) \quad \dot{y}(t)\ ]$, the joint pdf of $x(t)$, $y(t)$ and $\dot{y}(t)$ is

$$p_{x,y,\dot{y}}(x, y, \dot{y}; t) = \frac{1}{(2\pi)^{3/2}\sqrt{\det(C_h(0))}} \exp[-\frac{1}{2} Z(t)^T C_h^{-1}(0) Z(t)]$$

where $C_h(0)$ is the autocovariance of $Z(t)$, which is given by

$$\begin{aligned} C_h(0) &= E[Z(t)Z^T(t)] \\ &= \begin{pmatrix} R_{xx}(0) & R_{xy}(0) & R_{x\dot{y}}(0) \\ R_{yx}(0) & R_{yy}(0) & R_{y\dot{y}}(0) \\ R_{\dot{y}x}(0) & R_{\dot{y}y}(0) & R_{\dot{y}\dot{y}}(0) \end{pmatrix} \end{aligned}$$

When the directional scattering is modeled by the von Mises distribution, these second-second order statistics are given by (2.26). Substituting (2.26) into above equation produces

$$C_h(0) = \begin{pmatrix} \sigma^2 & 0 & b^2 \\ 0 & \sigma^2 & 0 \\ b^2 & 0 & c^2 \end{pmatrix}.$$

and

$$Z(t)^T C_h^{-1}(0) Z(t) = \frac{1}{d^2}\{x(t)^2 c^2 - 2x(t)\dot{y}(t)b^2 + \dot{y}(t)^2\sigma^2 + \frac{y(t)^2 d^2}{\sigma^2}\} \tag{6.5}$$

where $b^2 = 2\pi\sigma^2 f_D \frac{\cos(\theta_0) I_1(\kappa)}{I_0(\kappa)}$, $c^2 = \frac{\sigma^2}{2}(2\pi f_D)^2 \left(1 + \frac{\cos(2\theta_0) I_2(\kappa)}{I_0(\kappa)}\right)$, and $d^2 = \sigma^2 c^2 - b^4$. The determinant of $C_h(0)$ is calculated as $\det(C_h(0)) = \sigma^2 d^2$.

Equation (6.5) suggests that the integral of $y(t)$ can be calculated independently from $x(t)$ and $\dot{y}(t)$. Then (6.4) becomes

$$R_+^c \Delta t = \Delta t \int_{-\infty}^{-A} \int_{-\infty}^{0} |\dot{y}| p_{x,y,\dot{y}}(x, y = 0, \dot{y}; t) d\dot{y} dx \tag{6.6}$$

Solving (6.6), the positive 2π crossing rate with directional scattering modeled by the von Mises distribution is

$$\begin{aligned} R_+^c &= \frac{d^2(1-\mathrm{erf}(\frac{cA}{\sqrt{2}d}))}{4\pi\sigma^3 c} + \frac{b^2\exp[-\frac{A^2}{2\sigma^2}]}{4\pi\sigma^2} \\ &+ \int_{-\infty}^{-A} \frac{b^2}{4\pi\sigma^4}\exp[-\frac{A^2}{2\sigma^2}]\mathrm{erf}(\frac{xb^2}{\sqrt{2}\sigma d})dx \end{aligned} \tag{6.7}$$

If the scattering is isotropic, $b^2 = 0$ and $\frac{c}{\sigma} = \sqrt{2}\pi f_D$. In this case,

$$R_+^c = \frac{c(1-\mathrm{erf}(\frac{A}{\sqrt{2}\sigma}))}{4\pi\sigma} = \frac{\mathrm{erfc}(\sqrt{K})f_D}{2\sqrt{2}},$$

which is the same as (4.18), the positive 2π crossing rate with isotropic scattering.

Similarly, the negative 2π crossing rate is given by

$$\begin{aligned} R_-^c &= \frac{d^2(1-\mathrm{erf}(\frac{cA}{\sqrt{2}d}))}{4\pi\sigma^3 c} - \frac{b^2\exp[-\frac{A^2}{2\sigma^2}]}{4\pi\sigma^2} \\ &+ \int_{-\infty}^{-A} \frac{b^2}{4\pi\sigma^4}\exp[-\frac{A^2}{2\sigma^2}]\mathrm{erf}(\frac{xb^2}{\sqrt{2}\sigma d})dx. \end{aligned} \tag{6.8}$$

R_-^c differs from R_+^c only by the second term, so the cumulative average number of 2π crossings owing to scattering directionality equals

$$\Delta R_N = (R_+^c - R_-^c)T = \frac{b^2 T}{2\pi\sigma^2}\exp[-\frac{A^2}{2\sigma^2}]. \tag{6.9}$$

Substituting for b^2 in the above result, then the mean of the absolute phase for a well-defined Rice channel with a stationary dominant component is obtained as,

$$\begin{aligned} \bar{\phi}_A^{(2)}(T) &= 2\pi\Delta R_N \\ &= 2\pi f_D T\exp[-K]\cos(\theta_0)\frac{I_1(\kappa)}{I_0(\kappa)} \end{aligned} \tag{6.10}$$

where κ and θ_0 are respectively the directionality parameter and the mean direction of the directional scattering. If $\kappa = 0$, i.e., with isotropic scattering, $I_1(\kappa) = 0$. Then (6.10) becomes zero and is independent of the value of θ_0, as expected.

6.1.3 Mean of the Absolute Phase with Directional Scattering

With directional scattering, the mean of the absolute phase is the sum of (6.3) and (6.10),

$$\bar{\phi}_A(T) = 2\pi f_D T \times \{\exp[-K]\cos(\theta_0)\frac{I_1(\kappa)}{I_0(\kappa)} + \cos(\beta_0)(1-\exp[-K])\}. \tag{6.11}$$

The mean of the absolute phase with directional scattering is determined by the maximum Doppler frequency (f_D) and the AOA (β_0), of the dominant component, the mean direction (θ_0) and the directionality parameter (κ), of the directional scattering, the Rice factor (K), and the observation time interval (T).

Two extreme cases can be examined. The first case is for a highly directional scenario, where the AOA of the dominant component and the mean direction of the scattering can be assumed to be the same. When κ is large, $I_1(\kappa)$ is approximately equal to $I_0(\kappa)$. Then the mean of the absolute phase reduces to $2\pi f_D T\cos(\beta_0)$. This means in highly directional scenarios, the concentration of the diffuse sources becomes equivalent to the dominant source. The second case is for an isotropic scattering (i.e., $\kappa = 0$) and without the dominant component present (i.e., $K = 0$). The mean of the absolute phase becomes zero, as expected.

6.1.4 Simulation Results and Discussion

The directional channel is simulated using Algorithm 1 as presented in Section 2.3.2. The simulation parameters for this section are set up with the following examples: $f_n = f_m = 0.01$ (normalized sampling frequency); K=0dB (Rice factor); $L = 50$ (distance in wavelengths, replacing $f_D T$ in (6.11)); $N = 20L/f_n$(number of samples used for the IDFT, converted to an integer of power of two); $\varphi_0 = 0$ (initial phase of the dominant component); $\kappa = [0, 1, 3, 5, 7, 9, 10]$ (directionality of scattering); $\theta_0 = [0, 15^o, 30^o, 45^o, 60^o, 75^o, 90^o]$ (mean direction of scattering); and $\beta_0 = [0, 30^o, 45^o, 60^o, 90^o]$ (AOA of the dominant component).

The first set of simulations compares the effects of the mean direction of scattering (i.e., θ_0) and the AOA of the dominant component (i.e., β_0) on the mean of the absolute phase with fixed $\kappa = 3$. Both the simulated and theoretical results are plotted in Figure 6.1. Given a fixed β_0, the mean of the absolute phase decreases as θ_0 increases from 0 to 90^o because the Doppler frequency of the diffuse scatterers decreases to zero as θ_0 goes to 90^o. Similarly, given a fixed θ_0, the mean of absolute phase decreases as β_0 increases from 0 to 90^o. In a modeled directional scenario, θ_0 might be, but is not necessarily, the same as β_0.

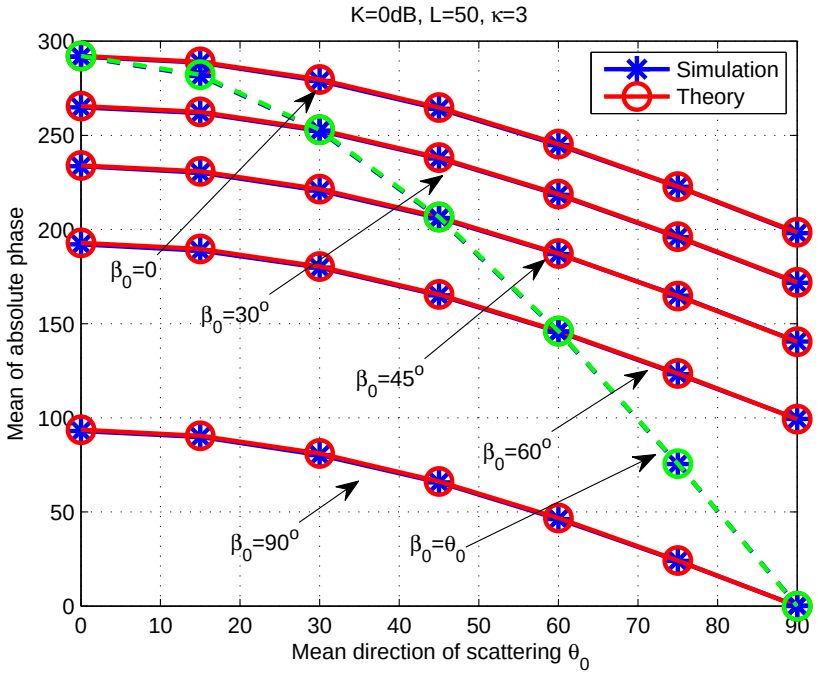

Figure 6.1: Mean of the absolute phase against the mean direction of scattering, θ_0, at different values of AOA of the dominant component, β_0, with K =0dB and $\kappa = 3$.

The curve (dashed line) for $\beta_0 = \theta_0$ is also shown in Figure 6.1. One special point is at the right lower corner of this figure, and represents that the mean of the absolute phase is zero when $\theta_0 = \beta_0 = 90^o$, as expected.

The second set of simulations compares the effect of the directionality of scattering (i.e., κ) on the mean of the absolute phase with fixed $\beta_0 = 0$. Both the simulated and theoretical results are plotted in Figure 6.2. Except for $\theta_0 = 90^o$, the mean of the absolute phase increases quickly as κ increases from 0 to 3, but gradually approaches a limit when $\kappa > 3$. This makes sense because when the directionality increases, the concentration of the diffuse scatterers acts similarly to a dominant component. When $\kappa = 0$, $\beta_0 = 90^o$, and $K = 0$dB, the mean of the absolute phase is 200, the same result shown in Figure 4.1 for the mean with isotropic scattering. When $\theta_0 = 90^o$, all diffuse scatterers have zero Doppler frequency, and do not contribute to the mean of the absolute phase. Thus, the mean of absolute phase when $\theta_0 = 90^o$ remains unchanged and independent of the directionality of scattering.

There are small discrepancies between the simulation results in Figure 6.2 and the theory given by (6.11) for small κ, although they are not easily visible on the displayed scale.

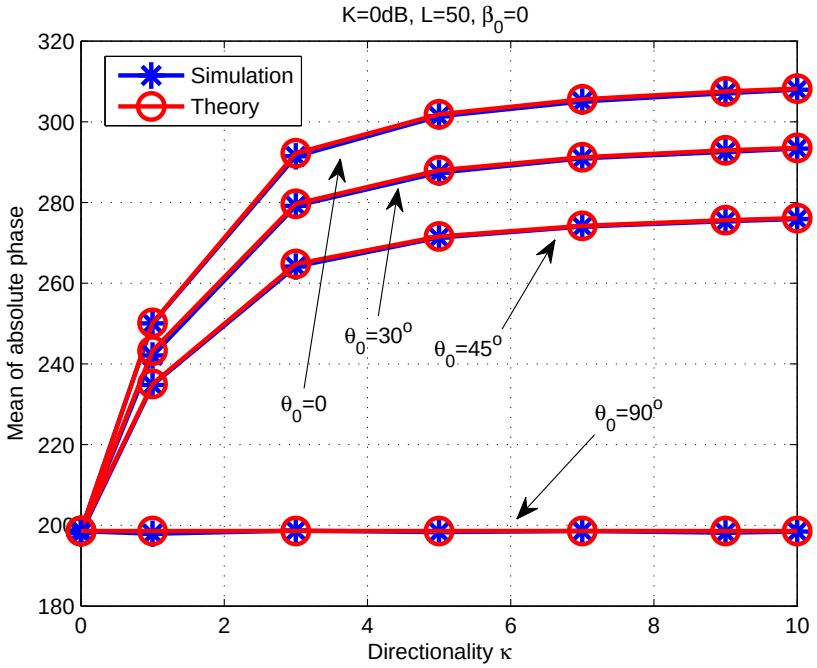

Figure 6.2: Mean of the absolute phase against the directionality of scattering, κ, at different mean directions of scattering , θ_0, with K =0dB and $\beta_0 = 0$.

These discrepancies result from the IDFT based channel simulator used for simulations. As discussed in Section 2.3.3, either insufficient channel phase sampling rate or inaccurate reproduction of the first and second moment of the Doppler spectrum influences simulation results of some second-order statistics, including the mean of absolute phase.

6.1.5 Summary

The directionality of scattering changes the second-order statistics of the mobile channel, including the mean and variance of the absolute phase. A closed form for the mean of absolute phase is derived in this section, and is confirmed by the simulation. This closed form can be used as guidance for applications that require the mean of the absolute phase in the presence of directional scattering. The variance of the absolute phase for the mobile channel with isotropic scattering is complicated as discussed in Section 4.2, and becomes much more complicated for the mobile channel with directional scattering, which is identified as interesting future research.

6.2 Antenna Spacing Design with Directional Scattering

In previous chapters, the investigations are focused on the statistics of the mobile channel. The angular power density model can be applied to antenna spacing design. In this section, the minimum spacing for uncorrelated antennas in a directional scenario is analyzed using the von Mises distribution. It is shown that the resulting antenna spacings are well-defined for any mean directions and angular spreads, including its limiting omnidirectional form as expected.

6.2.1 Motivation

For space diversity or MIMO, the antennas need to be as compact as possible, but also be able to retrieve signals with uncorrelated multipath fading. A compromise is to settle for a low, rather than zero, correlation between the antennas. For small-N diversity and MIMO, "low" correlation is often taken as a power correlation coefficient below about 0.5 [4]. For large-N MIMO, the correlation coefficient threshold should be lower if possible because the increased capacity efficiency (the point of MIMO) is more sensitive to the finite correlation and the associated mutual coupling losses.

The minimum spacing requirement for uncorrelated antennas is well known in situations where both the scatterers and the antenna patterns are omnidirectional, or their combination is omnidirectional. As discussed in Section 2.2.3, the required spacing is about 0.18 wavelength at the carrier frequency for a power correlation coefficient of about 0.5. This spacing is dependent only on the carrier frequency, and is a result of the 2D omnidirectionality.

Uncorrelated multiple antennas are required both for BSs and for mobiles in directional scenarios. Similar to modeling the directional channel, characterizing the minimum antenna spacing for space diversity or MIMO in a directional scenario needs two other parameters: the mean direction of the scenario; and a measure of the directionality. These two parameters can be described by many directional models, as discussed in Section 2.2.4.1. In [60], comparisons of the von Mises distribution to other directional distributions are provided, and the arguments on the choice of the von Mises distribution are detailed. More complicated scenarios using the von Mises distribution for correlation functions have been discussed, e.g., [51, 117]. However, the von Mises distribution has not been used to specifically analyze minimum antenna spacings for space diversity or MIMO in directional scenarios.

6.2.2 Directionality Measure Using the Von Mises Distribution

For a directional scenario, the directionality is often measured by the angular spread, while for a directional antenna, the directionality is often measured by the half-power beamwidth. These equivalence of the two parameters are discussed as follows.

The angular spread is an important parameter for characterizing the directional scenario. When modeled by the von Mises distribution, one definition of the angular spread is the standard deviation of the von Mises distribution,

$$\sigma_\theta \text{ (rads)} = \sqrt{\int_{-\pi+\theta_0}^{\pi+\theta_0} \theta^2 p_v(\theta;\theta_0,\kappa)d\theta - \theta_0^2}. \tag{6.12}$$

The angular spread depends only on κ and is independent of the mean direction θ_0. There is no closed-form solution to (6.12), but when κ is larger than 3 (i.e., $\sim$ 4.8dB), the angular spread can be approximated by [17, 61]

$$\sigma_\theta \text{ (rads)} \simeq 1/\sqrt{\kappa}, \;\; \kappa > 3. \tag{6.13}$$

When designing directional antennas, the half-power beamwidth (HPBW) [118] is the preferred spread parameter, and is therefore of interest for directional scenarios. The closed-form HPBW for the directional scenario modeled by the von Mises distribution is given by

$$\text{HPBW (rads)} = 2\cos^{-1}\left(1 - \frac{\ln 2}{\kappa}\right), \;\; \kappa \geq \ln\sqrt{2}. \tag{6.14}$$

As expected, the HPBW is also a function only of κ. When $\kappa < \ln\sqrt{2}$ (~ -4.6dB), the von Mises pdf becomes too broad to support an HPBW.

Figure 6.3 shows how both the HPBW and the angular spread increase as κ decreases, and illustrates the approximation of (6.13) for $\kappa > 4.8$dB. When the HPBW is smaller than 145^o, the HPBW is close to twice the angular spread. This similarity enables us to accurately approximate the angular spread in (6.12) with the HPBW in (6.14) for κ larger than 0dB. Unlike the HPBW, the angular spread remains well-defined for the full range of κ. The maximum value of $\sigma_\theta = 104^o$ corresponds to an omnidirectional scenario, but its physical interpretation requires care. The HPBW will be used in following discussion in spaced antenna design, and the results are similar to those using the angular spread.

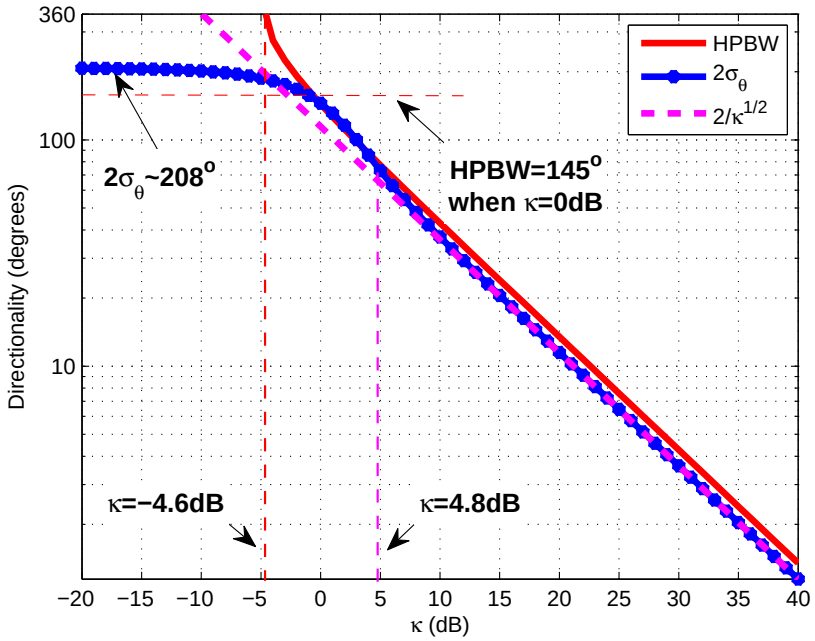

Figure 6.3: The half-power beamwidth and the angular spread (and its approximation) against κ for directional scenarios.

6.2.3 Relating Antenna spacing to the Von Mises Distribution

A modeled directional scenario in an urban area is depicted in Figure 6.4. Here, two BS antennas are separated horizontally by a distance Δz. The distance between the BS and the scatterers is assumed to be large so that the AOA of the signals received at two antennas are approximately the same, i.e. the scatterers are in the far field of the antenna array and create the incident angular power distribution.

The channel is assumed to be WSSUS, flat, and Rayleigh fading, i.e., no dominant source within the scattering distribution. The mean direction, θ_0 in Figure 6.4, is defined as the angle of the nominal center of the directional incident power relative to the vector between the two antennas (the endfire direction). Note here the antenna patterns have been included into the directional model. It is assumed that the two antenna elements have the same far-field patterns, polarization, mean direction and shape.

It has been shown that, under above assumptions, the spatial correlation function,

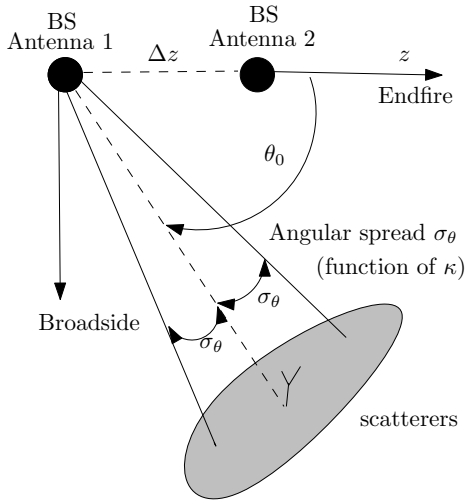

Figure 6.4: A directional scenario. The mean direction, θ_0, of the scatterers is measured from the antenna array endfire direction.

$\rho(\Delta z)$, and the angular power distribution in the u domain, $p(u)$, have the Fourier relationship given by [4, 118, 119],

$$\rho(\Delta z) \overset{F}{\Longleftrightarrow} p(u) \tag{6.15}$$

where $u = k_c \cos(\theta)$, with k_c the wavenumber at the carrier frequency. $p(u)$ is the incident angular power distribution (i.e., $p(\theta)$ in the u domain), and is also called the Doppler power profile. The distance Δz is the spacing between two points in the multipath field and corresponds to the spacing of two antennas.

If the von Mises pdf is used as the angular power distribution in a directional scenario, the Doppler power profile becomes

$$p_v(u) = \frac{\exp[\frac{\kappa}{k_c^2}(uu_0 + \sqrt{(k_c^2 - u^2)(k_c^2 - u_0^2)})]}{\pi I_0(\kappa)\sqrt{k_c^2 - u^2}} \tag{6.16}$$

where $u_0 = k_c \cos\theta_0$ is the mean direction of the directional scenario in the u domain.

The closed-form spatial correlation coefficient function follows from the Fourier transformation as

$$\rho(\Delta z) = \frac{J_0\left(\sqrt{-\kappa^2 + k_c^2 \Delta z^2 - 2j\kappa u_0 \Delta z}\right)}{I_0(\kappa)} \tag{6.17}$$

or in terms of the distance in wavelengths,

$$\rho(\Delta L) = \frac{J_0\left(\sqrt{-\kappa^2 + (2\pi\Delta L)^2 - 4j\pi\kappa\Delta L\cos(\theta_0)}\right)}{I_0(\kappa)} \tag{6.18}$$

where $\Delta L = \Delta z/\lambda$ is the antenna spacing in wavelengths. When $\kappa = 0$, the correlation function reduces to the standard result of $J_0(2\pi\Delta L)$ for the omnidirectional scenario. This correlation function is similar to the autocorrelation function given by (2.24) except for the interpretation of the correlation variable. Note that $\rho(\Delta z)$ here is the field correlation, and is, under certain conditions (which can be usually met) equivalent to the open circuit antenna voltage correlation.

Figure 6.5 illustrates the von Mises pdf at different mean directions in both θ and u domain, and the corresponding correlation coefficient function (illustrated by its power, real part, and imaginary part). The following observations are noted:

- Given non-zero κ, $p_v(\theta)$ is symmetric about the reference direction only when $\theta_0 = 0$, whereas $p_v(u)$ is symmetric only when $\theta_0 = 90^o$. When the mean direction is not broadside (i.e., when $\theta_0 \neq 90^o$), $p_v(u)$ becomes asymmetric, and the corresponding correlation coefficient function is complex, as expected from Fourier theory.

- The power correlation coefficient function decreases more slowly when $\theta_0 = 0^o$ than when $\theta_0 = 90^o$, but the real part of the correlation coefficient function decreases in an opposite manner. This shows that the real part of the correlation coefficient is not enough to describe the correlation behavior for directional scenarios, as opposed to the case of an omnidirectional scenario.

- Given the same κ, the power correlation coefficient function is the same for θ_0 and for $180^o - \theta^o$, even though their correlation coefficient functions are different.

6.2.4 0.5 Correlation Distance and HPBW

The minimum spacing of antennas can be acquired from the correlation distance that guarantees that the antenna voltages are below some correlation threshold which means "effectively uncorrelated" [4]. In this research, the power correlation coefficient of the open circuit voltages, $|\rho(\Delta L)|^2$, assigned to be 0.5, is used to calculate the minimum antenna spacing. This spacing is referred to as the 0.5 correlation distance, denoted by $d_{0.5}$.

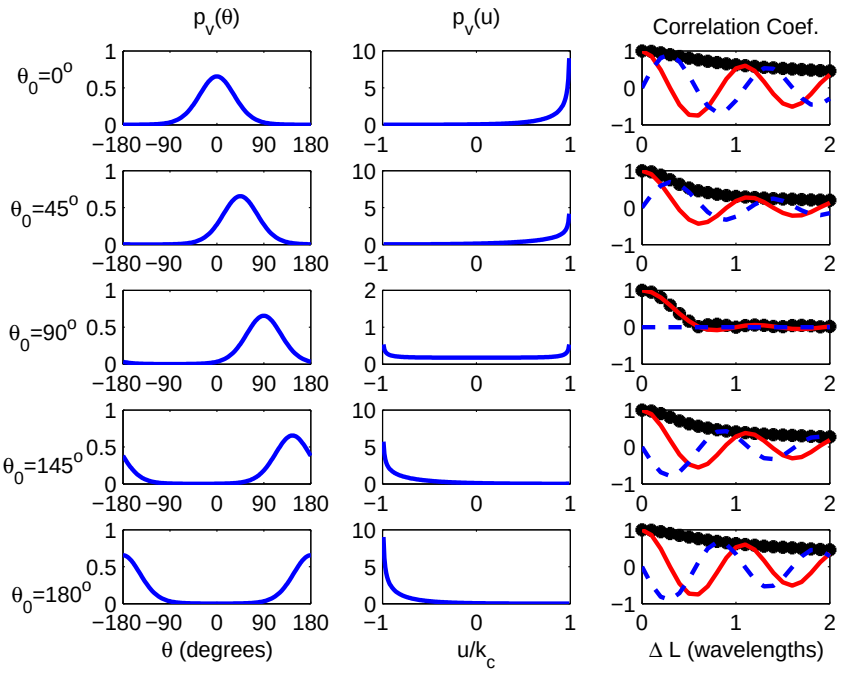

Figure 6.5: Examples of $p_v(\theta)$, $p_v(u)$, and the correlation coefficient function illustrated by its power $|\rho(\Delta L)|^2$ (stared), real part (solid), and imaginary part (dashed) for the von Mises pdf with $\kappa = 3$ and the mean directions $\theta_0 = 0^o, 45^o, 90^o, 145^o$ and 180^o.

A numerical relationship between $d_{0.5}$ and HPBW, using κ as an intermediate parameter, is illustrated in Figure 6.6. It shows:-

- The curves of θ_0 overlap those of $180^o - \theta_0$, as predicted by the power correlation coefficient function, $|\rho(\Delta L)|^2$. So only the curves with the mean directions from 0^o to 90^o are shown.

- The results are similar to those for the cosine-power distribution [118], but here, $d_{0.5}$ is well-defined for an HPBW in its full range. In particular, the small HPBWs in Figure 6.6 can continue approaching to almost 0^o if κ is increased in the calculations.

- For a fixed mean direction, $d_{0.5}$ increases as HPBW decreases. This intuitively makes sense because two signals incident from a smaller direction (i.e., a larger κ) requires a larger distance to decorrelate [3, 47]. It also follows from the uncertainty principle applied to the Fourier transform [4].

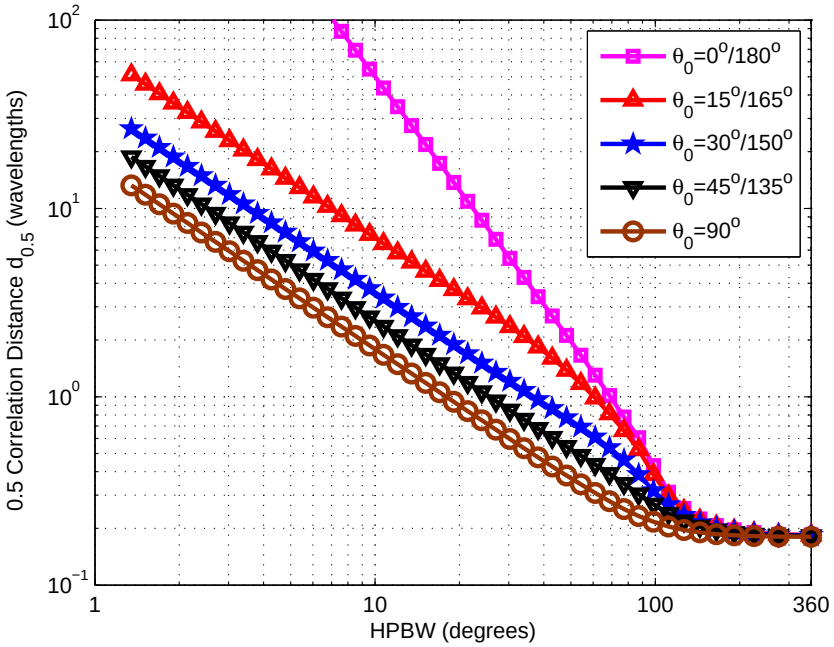

Figure 6.6: The 0.5 correlation distance in wavelengths varies with HPBW of the directional scenario. The mean directions are $\theta_0 = 0^o, 15^o, 30^o, 45^o, 90^o$.

- For a fixed HPBW, $d_{0.5}$ increases with a greater rate for the mean direction approaching 0^o (or 180^o). Mathematically, this is because the mean direction is in a cosine function while the HPBW is fixed.

- For a fixed HPBW, $\theta_0 = 0^o$ requires the maximum distance to decorrelate two signals while $\theta_0 = 90^o$ requires minimum. This can be seen from the uncertainty principle of Fourier theory; when $\theta_0 = 0^o$, the incident power $p_v(\theta)$ is symmetric about the reference direction, which corresponds to a smaller angular spread in the u domain compared with the situation where $\theta_0 = 90^o$, and an associated larger correlation distance.

- For a highly directional scenario, for example, omni incident power and small HPBWs (e.g., $\sim 10^o$), if the mean direction can be kept within about 30^o to 150^o, a spacing of 10 to 20 wavelengths is usually good enough for (effectively) uncorrelated antennas. Conversely, directional antenna spacings must be very large for antennas along the endfire directions.

- When the HPBW is larger than 120^o (corresponding to κ smaller than 1dB), $d_{0.5}$ becomes 0.18λ and hardly changes with the mean direction. So if the HPBW of the directional scenario modeled by the von Mises is larger than 120^o, the directional scenario can be treated as omnidirectional when designing the spaced antennas.

6.2.5 Practical Aspects of Antenna Spacing Design

It is emphasized that these observations and conclusions are only for uni-directional scenarios. For example, the results presented above show that omni antennas need large spacings along their direction of alignment if the distributed incident power is from only one of the alignment directions (endfire directions); but if the incident power is from both directions along the street or tunnel, etc., then the spacing can be close, as can be determined from (6.15). To fix ideas, consider a vehicle with rooftop antennas, in an urban street, where power arrives predominantly from both directions of the street. Here, the antennas require much less spacing if aligned along the street direction than across the street direction. But if the incident power is from one end of the street only, then the opposite will be the case.

The antenna spacing designed here is based on the correlation function of the antenna voltages if the mutual coupling is neglected. This means that either open circuit voltages (with open circuits, the mutual coupling is usually negligible for small antennas) is considered, or else the mutual coupling is ensured to be low by restricting to large spacing.

For selection diversity using small elements, where only one port need be terminated at a time with the others open-circuited, then the open circuit voltage correlations and the terminated circuit voltage correlations can be the same. For directional antennas, the apertures need to be consummately large, and therefore they cannot be spaced too closely in the plane of directionality. In such cases, the mutual coupling is typically small, so the basic design information presented here corresponds directly to the terminated circuit voltages and can be used as final design rules.

For diversity combination that requires simultaneous use of the antenna signals (for example, equal gain, maximum ratio, and optimum combining) or MIMO, the antennas must be (simultaneously) terminated, so the terminated circuit correlation coefficient function is required to design the antenna spacing. If terminated antennas are very closely spaced, the mutual coupling cannot be neglected. In this case, the open circuit voltage correlation function can be transformed to the terminated circuit voltage correlation function using the antenna impedance matrix and the load impedance matrix [4, 120]. Alternatively, the

embedded patterns, which include mutual coupling, can be used directly to find the terminated circuit voltage correlation function. However, the antenna impedance and embedded patterns depend on the spacing, so the design becomes iterative.

6.2.6 Summary

In this section, the von Mises distribution is used as an angular power distribution to find the basic design information for antenna spacing in directional scenarios. The minimum spacings are consistent with known ones for other directional distributions given the same threshold of 0.5. However, the formulation here has the advantage that the one pdf can model all directional scenarios without requiring approximations for different directionality. Also, owing to the well-behaved decay characteristics of the correlation function, small (much less than 0.5) correlation thresholds are well-defined and the antenna spacings can be readily found. This is important for large-N MIMO where a lower correlation coefficient is required for spaced antenna design because the capacity efficiency is sensitive to finite correlations and the associated mutual coupling losses.

Chapter 7

Conclusion and Future Work

7.1 Conclusion

The absolute phase, defined as the accumulated phase change over an observation interval, is a random variable which has not been utilized to date in mobile communications. It provides extra channel information compared with the wrapped phase, such as the Rice factor, and the angle-of-arrival and the Doppler frequency of the dominant component, and will therefore foster new techniques in mobile communications.

To be able to use the absolute phase, its statistics need to be characterized, but even the basics, such as the mean, variance, and pdf of the well-defined Rice channel are complicated. The statistics of the absolute phase are based on the channel model. The connection between the well-defined Rice channel, used in the literature for analysis, and the real-world channel, is discussed in Chapter 2. The absolute phase is defined formally, and four different formulations of the absolute phase are presented in Chapter 3, together with the suggested methods to simulate and acquire the absolute phase.

The statistics of the absolute phase given isotropic scattering are provided in Chapter 4. The mean of the absolute phase has a general, closed-form formula, but the variance of the absolute phase approximates closed forms only for several combination of K and L. The pdf of two correlated wrapped phase differences without the modulo $[-\pi, \pi)$ condition is developed for finding the pdf of the absolute phase. The pdf of the absolute phase, for large Rice factors (more than about 5dB), can be approximated by convolving the pdf of the difference of two wrapped phases with the Skellam distribution; and for small Rice factors but large observation intervals, by convolving the pdf of the difference of two

wrapped phases with the Gaussian distribution. Finding the pdfs for other general cases are open problems. Simulation results are presented to support statistical results, and some unexpected behavior is revealed, such as the pdfs of the absolute phase for small or medium Rice factor and small observation interval. Literature addressing various clicks is scattered across many decades and across different aspects of communications. Appendix B gathers and compares various clicks associated with the mobile channel, and offers new information for the mobile channel.

The absolute phase augments information about the mobile channel, and therefore allows new solutions to some applications in mobile communications. For example, the problem of estimating the Rice factor, K, has been an interesting research topic. However, existing K estimators requires magnitude or both magnitude and phase of the channel complex amplitude gain. A K estimator is developed in Chapter 5 using only the absolute phase. Since no amplitude is involved, the receiver structure can be greatly simplified. The simulation results show that this estimator performs well in a range of practical K values.

The directionality of the mobile channel does not change the envelope and phase distribution of the channel, but alters its second-order statistics, including the mean, variance and pdf of the absolute phase. In this thesis, the directional scattering for the well-defined Rice channel is modeled using the von Mises distribution, and the directionality of the scattering is considered in several research works. A generalized channel simulator is developed in Chapter 2 to simulate the channel with directional scattering using the IDFT technique. The mean of the absolute phase is derived for the channel with directional scattering in Chapter 6. The von Mises distribution is also used to model the antenna power distribution in Chapter 6, and allows a convenient design framework for the uncorrelated antenna spacing in directional scenarios.

7.2 Recommendation for Future Work

It is important to get real-world measurements for basic comparison with the models developed for the absolute phase. This measurement is very challenging, and there seem to be no channel measurement of the phase (and hence the absolute phase) readily available. Therefore, the suggested future work includes measuring the absolute phase, and comparing the statistics acquired from the measurements to those developed in this thesis.

The absolute phase in the mobile channel offers a fertile area for further research. Besides

the K estimator presented in this thesis for channel characterization, another important application of the absolute phase may include location-aware systems, such as Enhanced 911 Emergency Calling Systems, personal locator service, location billing, interactive map consultation, location-dependent e-commerce, and intelligent transportation system, etc.

The basic principle of existing techniques for mobile locating or positioning is to use two or more BSs to intercept the mobile signal. These techniques include time-of-arrival (TOA) [121], received signal strength (RSS) [122], time-difference-of-arrival (TDOA) [123], and/or angle-of-arrival (AOA) [124]. Most of the positioning systems rely on the LOS signal, and assume that NLOS signals can be detected and eliminated. The NLOS signal benefits the position estimation only when it is *a priori* information [125]. Therefore, these existing localization algorithms do not perform well in a NLOS channel.

However, if the overall phase (including the distance-dependent phase and the absolute phase, as discussed in Section 3.1.1) of the mobile channel is known, it can be used to indicate the relative distance changes between the BS and the mobile in a Rayleigh channel (i.e., no LOS signal is available). This is because the distance-dependent phase after unwrapping and the absolute phase are additive, as proved in Appendix D; the unwrapped distance-dependent phase acts as the signal that contains the distance, but the absolute phase for the Rayleigh channel acts as the noise, with a zero mean, added to the distance-dependent phase. The mean of the overall unwrapped phase can then be used to derive the relative distance change between the mobile and the BS. If the mobile and the BS are synchronized, the absolute distance between the mobile and the BS can be calculated.

If the mean of the absolute phase is available, the increasing or decreasing trends in any Rician-like channels can indicate if the mobile is moving towards or away from the dominant source. This information could be useful for some applications such as handoff or some other aspects of dynamic channel allocation.

Many other applications can be developed owing to the new channel information brought by the absolute phase. For example, if the location of the mobile can be estimated, then tracking the mobile users becomes another possible application.

Since the statistics of the absolute phase depends on the scattering distribution of the mobile channel, future work may also include analyzing the effects of directionality of the scattering on the performance of the applications related to the absolute phase.

Appendix A

Comparison of Unwrapping to an FM Receiver

The unwrapping operation produces similar results to an FM receiver consisting of a limiter, a discriminator, plus an integrator. Here the two processes are compared.

Finding the absolute phase by unwrapping to `atan2` is as follows:

- detect the 2π discontinuities by taking the difference of two consecutive phase samples;
- add/subtract 2π to the phase difference if the absolute value of the phase difference between two consecutive phase samples is larger than π;
- sum the modified phase differences over $(0, T)$ with the reference phase, $\phi_W(0)$, resulting in the continuous phase, $\phi_C(t)$;
- subtract the reference phase from the continuous phase at time T, resulting in the absolute phase, $\phi_A(T) = \phi_C(T) - \phi_W(0)$.

The first two operations are similar to the discriminator (i.e., the differentiator) in an FM receiver. The output of the discriminator is the phase derivative per sample. The third operation, summing the phase difference, acts the same as the integrator (i.e., the low-pass filter) in the FM receiver. Its output is the continuous phase. The last operation, subtracting the reference phase, $\phi_W(0)$, is analogous to the lower limit in the integrator in FM receiver, and results in the absolute phase, $\phi_A(T)$.

When the phase variation is small, which corresponds to a large magnitude of the signal, these two methods produce almost the same result, as shown in Section 3.2. However, the

dissimilarity arises when there are dramatic phase changes, i.e., when the signal is close to the origin. The phase derivative calculated by (3.5) is more sensitive to the small magnitude than by the unwrapping operation, and might result in a fake phase jump owing to finite accuracy calculation. One way to solve this problem is to detect the magnitude of the signal and accordingly force the phase variation in the continuous phase to be no larger than π. For the simulations in this thesis, the `unwrap` function to `atan2` is used.

Appendix B

Review of Click Definitions and Their Effects on the Absolute Phase

The various clicks, including the Rice click, the doublet and the false click are defined in terms of the phase derivative in an FM receiver, and are highly related to the 2π discontinuity appearing in the wrapped phase (`atan2`). Another type of click, the π jump, observed in the continuous phase, is important in mobile channels [4, 16, 29, 47]. These clicks are illustrated and discussed using a stationary well-defined Rice process.

This Rice process is denoted $h(t) = I(t) + jQ(t) = r(t)\exp[j\phi_W(t)]$, where $I(t)$ and $Q(t)$ have means of A and zero, respectively. The signal trajectory wanders around the complex plane, statistically near $I(t) = A$ and $Q(t) = 0$ but sometimes experiences the following special loci. For the figures in this appendix, $f_n = 0.001$ is used.

B.1 Rice Click

As discussed in Section 3.2.4, a Rice click appears in the phase derivative whenever the signal trajectory crosses the negative $I(t)$ axis and completes a phase change of 2π by circumnavigating the origin. An example of the Rice click was shown in Fig. 3.7. Sometimes, $I(t)$ is close to zero while the trajectory crosses the negative $I(t)$ axis, as in Fig. B.1. Compared with the Rice click in Fig. 3.7, the Rice click in Fig. B.1 has larger magnitude,

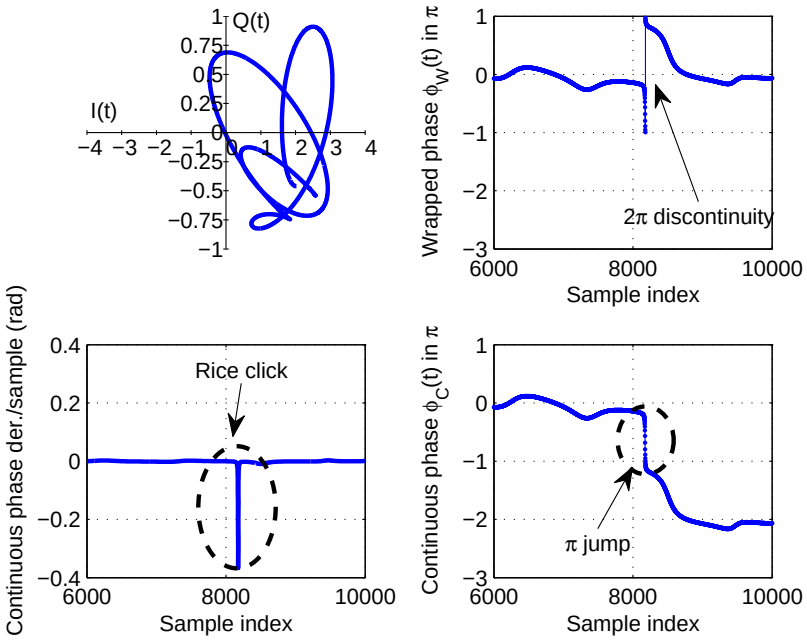

Figure B.1: Another example of Rice click in a stationary well-defined Rice process with $K = 5$dB.

but both of them correspond to one 2π discontinuity in the wrapped phase. Another view is that the Rice click is the reason why the absolute phase goes beyond $[-\pi, \pi)$.

B.2 Doublet

Sometimes, the signal trajectory is close to the origin when crossing the positive $I(t)$ axis. This event also results in a large impulse in the phase derivative and is referred to as the *doublet* in FM receivers [82], as shown in Fig. B.2. Unlike the Rice click, there is no corresponding 2π discontinuity in the wrapped phase. After the unwrapping operation, the unwrapped phase stays the same as the wrapped phase. The doublet does not affect the mean and variance of the absolute phase.

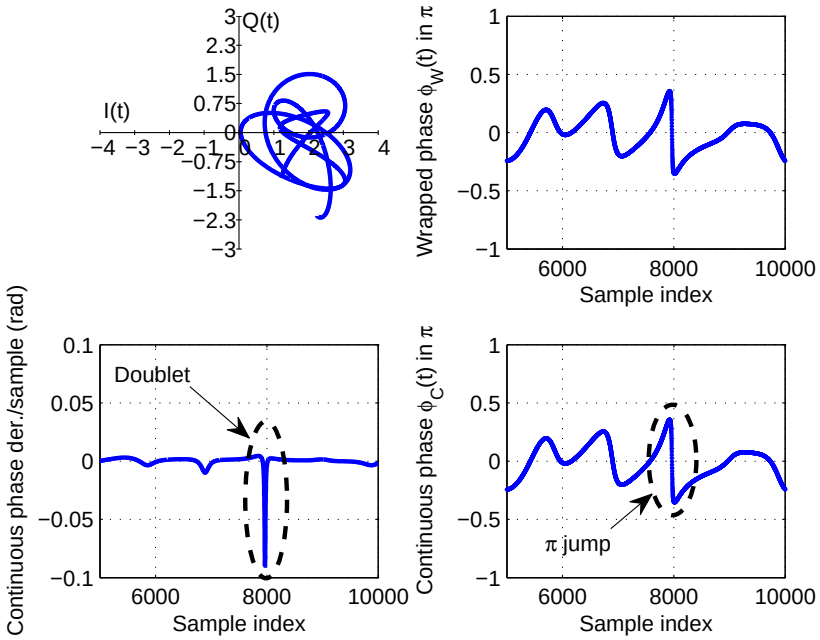

Figure B.2: An example of the doublet in a stationary well-defined Rice process with $K = 5$dB.

B.3 False Click

When the signal trajectory enters the left-half plane and crosses the negative $I(t)$ axis, it might go back to the right-half plane without circumnavigating the origin. In this case, the wrapped phase experiences two consecutive, opposite, 2π discontinuities. Instead of two impulses of an area of 2π, each 2π discontinuity results in an impulse with an area of about π in the phase derivative, as shown in Fig. B.3.

Based on the modeling given by Rice, these two impulses are miscounted as two Rice clicks in the click analysis. This is why this kind of impulse is called the *false click* in FM receivers [82, 83]. Since the false clicks appear in pairs with opposite directions, they do not contribute to the mean of the absolute phase. However, the false clicks affect the variance of the absolute phase when the Rice click analysis given by (3.7) is adopted. It has been shown that the probability of the false click decreases to infinitesimal when K is large [82, 83] and this is where the Rice click analysis becomes accurate.

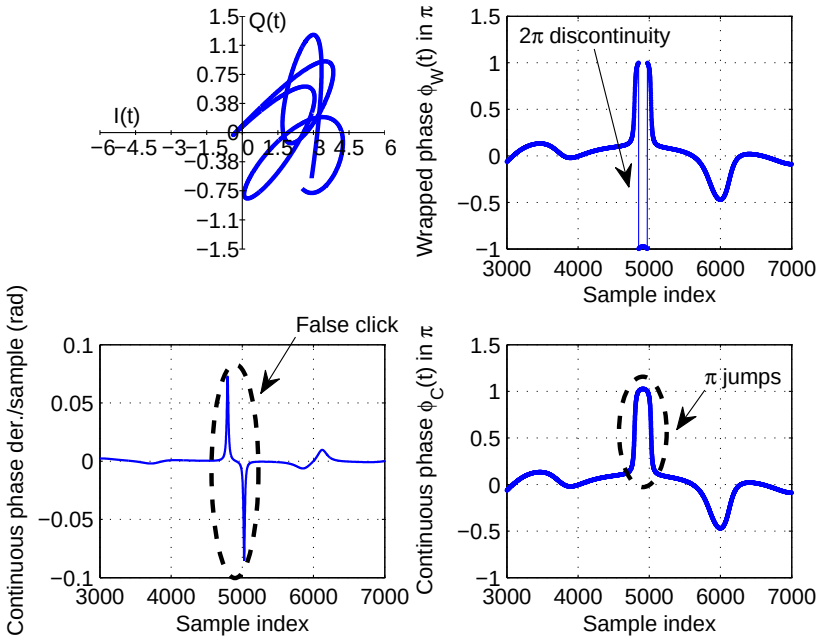

Figure B.3: Signal trajectory with phase discontinuities and false clicks in a stationary well-defined Rice process with $K = 8$dB.

B.4 π Jump

Whenever the signal trajectory passes close to the origin, there is a quick phase change of around π, which is recognized as the π *jump* in mobile communications [4, 16, 29]. The π jump, when observed without knowledge of the signal trajectory, may correspond to a Rice click, a doublet, or a false click in the phase derivative, as shown in Figs. B.1, B.2 and B.3.

The π jump turns out to be associated with a deep fade in the envelope of a mobile channel. The deeper the fade, the closer the phase jump to π. The direction of the phase jump depends on which side of the origin the signal passes.

The phase derivative is also recognized as the random FM in mobile communications [4, 47]. The π jumps, as a time function, give rise to spikes in the random FM and this is an important source of the error floor in narrowband digital communications. The π jumps also occur in the frequency domain, and these correspond to group delay spikes which causes an error floor in the BER of wideband systems.

B.5 Relation Among Various Clicks

- One Rice click in the phase derivative implies one 2π discontinuity in the wrapped phase, but a 2π discontinuity in the wrapped phase does not necessarily imply a Rice click (it could be a false click).
- The 2π discontinuity in the wrapped phase results in either an impulse with large peaks in the phase derivative if $I(t)$ is close to zero at crossing, or an impulse with small peaks if $I(t)$ is not close to zero.
- The impulse with large peaks in the phase derivative (the Rice click, the doublet, or the false click) is the result of a small signal magnitude, usually associated with a π jump in the continuous phase, but does not necessarily imply the 2π discontinuity in the wrapped phase.

When observed in the phase derivative, the Rice click, the false click, and the doublet appear as similar shapes. Therefore, in analog receivers, it remains a great challenge to discriminate the doublet and the false click from the Rice click in the noise threshold extension techniques [82]. In terms of the effects of these clicks on the statistics of the absolute phase, only the Rice click is of interest.

Appendix C

Summary of Notations for Phases

There are many names for different phases. In this thesis they are

- **Channel phase:** the phase for a mobile channel. It could be either wrapped or unwrapped depending on the context.
- **Wrapped phase:** $\phi_W(t)$, the phase defined over the period of $[-\pi, \pi)$. When used to model a mobile channel, the phase follows either the uniform or the Rice phase distribution.
- **Rice phase:** the wrapped phase following the Rice phase distribution.
- **Unwrapped phase:** the phase value after removing the 2π discontinuities from the wrapped phase, usually referred to as the output phase after the unwrapping operation. It can be any value.
- **Continuous phase:** $\phi_C(t)$, the same as the unwrapped phase, but the name is more general because the continuous phase can be obtained through many other methods (e.g., the zero-crossing or the phase derivative integration).
- **Absolute phase:** $\phi_A(T)$, the accumulated Rice phase change in $(0, T)$; It can be calculated by $\phi_C(T) - \phi_C(0)$.
- **Phase derivative:** the derivation of the continuous phase with respect to the time, also called the continuous phase derivative. In the figures from the simulation, it is represented by the (continuous) phase derivative per sample.

Appendix D

Additive Phase Effects

The phase of the mobile channel comprises a distance-dependent phase term owing to signal propagation between the mobile and the BS, and a random phase term owing to short-term fading. At any time, these two (wrapped) phase effects are additive. To obtain the continuous phase, the wrapped channel phase need to be unwrapped. In general, the unwrapping operation is nonlinear. However, this appendix proves that these two phase terms are also additive after unwrapping. In other words, the absolute phase can be separated from the unwrapped distance-dependent phase.

Refer to Fig. 3.1 in Chapter 3. At time t, the mobile has moved a distance of d relative to the BS. The distance-dependent phase is modeled as $\exp[j\omega_c d/c]$, where ω_c is the carrier angular frequency, and c is the speed of light. Rewrite the phase as following: $\omega_c d/c = 2\pi f_c vt/c = 2\pi f_D t$, where v and f_D are the velocity and the maximum Doppler frequency of the mobile, respectively.

Therefore, the channel CAG, with flat fading and distance-dependent phase, can be modeled as

$$h(t) = \exp[j2\pi f_D t] r(t) \exp[j\phi(t)] = I(t) + jQ(t) \tag{D.1}$$

where $r(t)$ and $\phi(t)$ are respectively the envelope and phase of a well-defined Rice process; $I(t)$ and $Q(t)$ are respectively the real and imaginary parts of the channel CAG. At any time, the channel phase is $\phi(t) + 2\pi f_D t$.

To find the unwrapped channel phase from time 0 to T, the phase derivative based

method, as discussed in Section 3.2.3, is used,

$$\phi_A^d(T) = \int_0^T \frac{I(t)\dot{Q}(t) - Q(t)\dot{I}(t)}{I(t)^2 + Q(t)^2} \tag{D.2}$$

where the superscript d represents the phase here includes the distance-dependent phase.

Let $r(t)\exp[j\phi(t)] = x(t) + jy(t)$, with $x(t)$ and $y(t)$ the real and imaginary part of a Rician process, respectively. Let $\exp[j2\pi f_D t] = \cos(2\pi f_D t) + j\sin(2\pi f_D t)$. Then (D.1) becomes

$$h(t) = (\cos(2\pi f_D t) + j\sin(2\pi f_D t))(x(t) + jy(t)) \tag{D.3}$$

Therefore,

$$I(t) = x(t)\cos(2\pi f_D t) - y(t)\sin(2\pi f_D t) \tag{D.4a}$$

$$Q(t) = x(t)\sin(2\pi f_D t) + y(t)\cos(2\pi f_D t). \tag{D.4b}$$

Taking derivatives of $I(t)$ and $Q(t)$ respectively,

$$\dot{I}(t) = \dot{x}(t)\cos(2\pi f_D t) - \dot{y}(t)\sin(2\pi f_D t) - 2\pi f_D x(t)\sin(2\pi f_D t) - 2\pi f_D y(t)\cos(2\pi f_D t)$$

$$\dot{Q}(t) = \dot{x}(t)\sin(2\pi f_D t) + \dot{y}(t)\cos(2\pi f_D t) + 2\pi f_D x(t)\cos(2\pi f_D t) - 2\pi f_D y(t)\sin(2\pi f_D t)$$

Consequently,

$$I(t)\dot{Q}(t) - Q(t)\dot{I}(t) = x(t)\dot{y}(t) - \dot{x}(t)y(t) + 2\pi f_D(x^2(t) + y^2(t)) \tag{D.6a}$$

$$I^2(t) + Q^2(t) = x^2(t) + y^2(t) \tag{D.6b}$$

Substituting (D.6) into (D.2), the result becomes

$$\begin{aligned} \phi_A^d(T) &= \int_0^T \left[\frac{x(t)\dot{y}(t) - \dot{x}(t)y(t)}{x^2(t) + y^2(t)} + \frac{2\pi f_D(x^2(t) + y^2(t)}{x^2(t) + y^2(t)}dt\right] \\ &= \int_0^T \frac{x(t)\dot{y}(t) - \dot{x}(t)y(t)}{x^2(t) + y^2(t)}dt + \int_0^T 2\pi f_D dt \\ &= \phi_A(T) + 2\pi f_D T \end{aligned} \tag{D.7}$$

where $\phi_A(T)$ is the absolute phase owing to short-term fading, and $2\pi f_D T$ is the accumulative phase change owing to the distance-dependent effect. This proves that these two phase effects - random and distance-dependent - are additive after unwrapping, even though the unwrapping, in general, is not a linear operation.

Another phase effect on the channel phase is the phase roll, modeled by $\exp(j\Delta\omega_o t)$, as discussed in Section 3.4.3. Here $\Delta\omega_o$ is the radial frequency difference between the transmitter and receiver oscillators. The phase roll is a function of time owing to temperature variations in the oscillators. Following similar derivation given above, the absolute phase and the unwrapped phase roll are also additive.

Bibliography

[1] G. L. Stüber, *Principles of Mobile Communication*. Norwell, MA, USA: Kluwer Academic Publishers, 1996.

[2] M. Pätzold, *Mobile Fading Channels*. Chichester, West Sussex, UK: John Wiley & Sons, Ltd, 2003.

[3] A. Molisch, *Wireless Communications*. Chichester, West Sussex, UK: John Wiley & Sons, Ltd, 2005.

[4] R. G. Vaughan and J. B. Andersen, *Channels, Propagation and Antennas for Mobile Communications*. London, UK: Institution of Electrical Engineers, 2003.

[5] H. Hashemi, "The indoor radio propagation channel," *Proc. IEEE*, vol. 81, no. 7, pp. 943–968, 1993.

[6] R. Bultitude, "Measurement, characterization and modeling of indoor 800/900 MHz radio channels for digital communications," *IEEE Commun. Mag.*, vol. 25, no. 6, pp. 5–12, 1987.

[7] D. Greenwood and L. Hanzo, "Characterisation of mobile radio channels," in *Mobile radio communications*, R. Steele, Ed. London, UK: Pentech Press Limited, 1992, pp. 163–180.

[8] P. Beckmann, *Probability in Communication Engineering*. New York, NY, USA: Harcourt, Brace & World, 1967.

[9] Y. Chen and N. C. Beaulieu, "Maximum likelihood estimation of the K factor in Ricean fading channels," *IEEE Commun. Lett.*, vol. 9, no. 12, pp. 1040–1042, 2005.

[10] C. Tepedelenlioglu, A. Abdi, and G. B. Giannakis, "The Ricean K factor: estimation and performance analysis," *IEEE Trans. Wireless Commun.*, vol. 2, no. 4, pp. 799–810, 2003.

[11] K. E. Baddour and T. J. Willink, "Improved estimation of the Ricean K-factor from I/Q fading channel samples," *IEEE Trans. Wireless Commun.*, vol. 7, no. 12, pp. 5051–5057, 2008.

[12] M. Richards, "A beginner's guide to interferometric SAR concepts and signal processing," *IEEE Aerosp. Electron. Syst. Mag.*, vol. 22, no. 9, pp. 5–30, 2007.

[13] S. R. Cloude and K. P. Papathanassiou, "Polarimetric SAR interferometry," *IEEE Trans. Geosci. Remote Sens.*, vol. 36, no. 5, pp. 1551–1565, 1998.

[14] G. G. Paulus, F. Grasbon, H. Walther, P. Villoresi, M. Nisoli, S. Stagira, E. Priori, and S. De Silvestri, "Absolute-phase phenomena in photoionization with few-cycle laser pulses," *Nature*, vol. 414, no. 6860, pp. 182–184, 2001.

[15] S. O. Rice, "Noise in FM receivers," in *Symposium on Time Series Analysis*, M. Rosenblatt, Ed. New York, USA: John Wiley & Sons, Inc., 1963, ch. 25, pp. 395–422.

[16] R. G. Vaughan, "Signals in mobile communications: A review," *IEEE Trans. Veh. Technol.*, vol. 35, no. 4, pp. 133–145, 1986.

[17] K. V. Mardia and P. E. Jupp, *Directional Statistics*. Chichester, West Sussex, UK: John Wiley & Sons, Ltd, 2000.

[18] J. Fuhl, A. F. Molisch, and E. Bonek, "Unified channel model for mobile radio systems with smart antennas," *Radar, Sonar and Navigation, IEE Proceedings*, vol. 145, no. 1, pp. 32–41, 1998.

[19] F. Stumpers, "Theory of frequency-modulation noise," *Proc. of the IRE*, vol. 36, no. 9, pp. 1081–1092, 1948.

[20] S. O. Rice, "Statistical properties of a sine wave plus random noise," *The Bell System Technical Journal*, vol. 27, pp. 109–157, 1948.

[21] H. Taub and D. L. Schilling, *Principles of Communication Systems*. New York, NY, USA: McGraw-Hill Publishing Company, 1986.

[22] N. Blachman, *Noise and Its Effect on Communication*, 2nd ed. Malabar, FL, USA: Robert E. Krieger Publishing Company, INC., 1982.

[23] N. M. Blachman, "Gaussian noise-II: Distribution of phase change of narrowbandnoise plus sinusoid," *IEEE Trans. Inf. Theory*, vol. 34, no. 6, pp. 1401–1405, 1988.

[24] D. Middleton, *An Introduction to Statistical Communication Theory*. New York, NY, USA: McGraw-Hill Publishing Company, 1960.

[25] L. L. Campbell, P. H. Wittke, and G. D. Swanson, "The distribution of the amplitude and continuous phase of a sinusoid in noise," *IEEE Trans. Inf. Theory*, vol. 34, no. 6, pp. 1388–1395, 1988.

[26] J. E. Mazo and J. Salz, "Theory of error rates for digital FM," *The Bell System Technical Journal*, vol. 45, pp. 1511–1535, 1966.

[27] R. F. Pawula, "On the theory of error rates for narrow-band digital FM," *IEEE Trans. Commun.*, vol. 29, no. 11, pp. 1634–1643, 1981.

[28] N. A. B. Svensson and C. E. W. Sundberg, "Performance evaluation of differential and discriminator detection of continuous phase modulation," *IEEE Trans. Veh. Technol.*, vol. 35, no. 3, pp. 106–117, 1986.

[29] J. B. Andersen, S. L. Lauritzen, and C. Thommesen, "Distributions of phase derivatives in mobile communications," *Microwaves, Antennas and Propagation, IEE Proceedings H*, vol. 137, no. 4, pp. 197–201, 1990.

[30] J. Ren and R. G. Vaughan, "Absolute phase in mobile channels," *Wirel. Commun. Mob. Comput., Special Issue on Emerging Wireless Technologies*, 2009.

[31] ——, "Introduction to the absolute phase in mobile channels," in *IEEE Vehicular Technology Conference (VTC10)*, 2010, submitted.

[32] ——, "A Rice factor estimator using MIMO channel phase," *IEEE Trans. Wireless Commun.*, 2010, in revision.

[33] ——, "Simulating mobile channels for directional scenarios by the inverse discrete Fourier transform," in *Proc. of IEEE Vehicular Technology Conference (VTC10)*, Taipei, Taiwan, May 2010.

[34] ——, "Spaced antenna design in directional scenarios using the von Mises distribution," in *Proc. of IEEE Vehicular Technology Conference (VTC09)*, Anchorage, Alaska, Sep. 2009.

[35] R. G. Vaughan, "Antenna evaluation for communications with diversity/MIMO," in *Printed Antennas for Wireless Communications*, R. Waterhouse, Ed. Chichester, West Sussex, UK: John Wiley & Sons, Ltd, 2007, pp. 407–445.

[36] J. Cavers, *Mobile Channel Characteristics*. Norwell, MA, USA: Kluwer Academic Publishers, 2000.

[37] T. Rappaport, *Wireless Communications: Principles and Practice*, 2nd ed. Upper Saddle River, NJ, USA: Prentice Hall PTR, 2001.

[38] M. Hata, "Empirical formula for propagation loss in land mobile radio services," *IEEE Trans. Veh. Technol.*, vol. 29, no. 3, pp. 317–325, 1980.

[39] G. E. Corazza and F. Vatalaro, "A statistical model for land mobile satellite channels and its application to nongeostationary orbit systems," *IEEE Trans. Veh. Technol.*, vol. 43, no. 3, pp. 738–742, 1994.

[40] W. Lee, *Mobile Communications Engineering: Theory and Applications*, 2nd ed. New York, NY: McGraw-Hill Inc., 1997.

[41] A. Abdi, W. C. Lau, M. S. Alouini, and M. Kaveh, "A new simple model for land mobile satellite channels: first-and second-order statistics," *IEEE Trans. Wireless Commun.*, vol. 2, no. 3, pp. 519–528, 2003.

[42] M. Gudmundson, "Correlation model for shadow fading in mobile radio systems," *Electron. Lett.*, vol. 27, no. 23, pp. 2145–2146, 1991.

[43] D. Wong and D. Cox, "An optimal local mean signal power level estimator for Rayleigh fading environments," in *Proc. of International Conference on Information, Communications and Signal Processing (ICICS97)*, 1997, pp. 1701–1704.

[44] P. Bello, "Characterization of randomly time-variant linear channels," *IEEE Trans. Commun. syst.*, vol. 11, no. 4, pp. 360–393, 1963.

[45] M. Ghavami, L. B. Michael, and R. Kohno, *Ultra-wideband Signals and Systems in Communication Engineering*, 2nd ed. Chichester, West Sussex, UK: John Wiley & Sons, Ltd, 2007.

[46] C. Tepedelenlioglu and G. B. Giannakis, "On velocity estimation and correlation properties of narrow-band mobile communication channels," *IEEE Trans. Veh. Technol.*, vol. 50, no. 4, pp. 1039–1052, Jul. 2001.

[47] W. C. Jakes, "Multipath interference," in *Microwave Mobile Communications*, W. C. Jakes, Ed. Piscataway, NJ, USA: AT&T press, 1974, reprinted by IEEE Press, 1993, pp. 11–78.

[48] P. Welch, "The use of fast Fourier transform for the estimation of power spectra: a method based on time averaging over short, modified periodograms," *IEEE Trans. Audio Electroacoust.*, vol. 15, no. 2, pp. 70–73, 1967.

[49] K. E. Baddour and N. C. Beaulieu, "Autoregressive modeling for fading channel simulation," *IEEE Trans. Wireless Commun.*, vol. 4, no. 4, pp. 1650–1662, 2005.

[50] A. Abdi, K. Wills, H. Barger, M. Alouini, and M. Kaveh, "Comparison of the level crossing rate and average fade duration of Rayleigh, Rice, and Nakagami fading models with mobile channel data," in *Proc. of IEEE 47th Vehicular Technology Conference (VTC00)*, vol. 4, no. 52, 2000, pp. 1850–1857.

[51] A. Abdi and M. Kaveh, "A space-time correlation model for multielement antenna systems in mobile fading channels," *IEEE J. Sel. Areas Commun.*, vol. 20, no. 3, pp. 550–560, Apr. 2002.

[52] J. H. Winters, "Smart antennas for wireless systems," *IEEE Trans. Wireless Commun.*, vol. 5, no. 1, pp. 23–27, 1998.

[53] W. Lee, "Effects on correlation between two mobile radio base-station antennas," *IEEE Trans. Veh. Technol.*, vol. 22, no. 4, pp. 130–140, 1973.

[54] R. G. Vaughan, "Pattern translation and rotation in uncorrelated source distributions for multiple beam antenna design," *IEEE Trans. Antennas Propag.*, vol. 46, no. 7, pp. 982–990, 1998.

[55] J. Salz and J. H. Winters, "Effect of fading correlation on adaptive arrays in digital mobile radio," *IEEE Trans. Veh. Technol.*, vol. 43, no. 4, pp. 1049–1057, 1994.

[56] F. Adachi, M. T. Feeney, A. G. Williamson, and J. D. Parsons, "Crosscorrelation between the envelopes of 900 MHz signals received at a mobile radio base station site," *IEE proceedings. Part F. Communications, radar and signal processing*, vol. 133, no. 6, pp. 506–512, 1986.

[57] M. Kalkan and R. H. Clarke, "Prediction of the space-frequency correlation function for base station diversity reception," *IEEE Trans. Veh. Technol.*, vol. 46, no. 1, pp. 176–184, 1997.

[58] N. Blaunstein, *Radio Propagation in Cellular Networks.* Norwood, MA, USA: Artech House, Inc., 1999.

[59] K. I. Pedersen, P. E. Mogensen, and B. H. Fleury, "Power azimuth spectrum in outdoor environments," *Electronics Letters*, vol. 33, no. 18, pp. 1583–1584, 1997.

[60] A. Abdi and M. Kaveh, "A versatile spatio-temporal correlation function for mobile fading channels with non-isotropic scattering," in *Proc. of the Tenth IEEE Workshop on Statistical Signal and Array Processing*, 2000, pp. 58–62.

[61] A. Abdi, J. A. Barger, and M. Kaveh, "A parametric model for the distribution of the angle of arrival and the associated correlation function and power spectrum at the mobile station," *IEEE Trans. Veh. Technol.*, vol. 51, no. 3, pp. 425–434, May 2002.

[62] M. Pätzold and B. O. Hogstad, "A space-time channel simulator for MIMO channels based on the geometrical one-ring scattering model," *Wirel. Commun. Mob. Comput.*, vol. 4, no. 7, pp. 727–737, 2004.

[63] G. J. Byers and F. Takawira, "Spatially and temporally correlated MIMO channels: modeling and capacity analysis," *IEEE Trans. Veh. Technol.*, vol. 53, no. 3, pp. 634–643, May 2004.

[64] M. Pätzold, U. Killat, and F. Laue, "An extended Suzuki model for land mobile satellite channels and its statistical properties," *IEEE Trans. Veh. Technol.*, vol. 47, no. 2, pp. 617–630, 1998.

[65] S. Fechtel, "A novel approach to modeling and efficient simulation of frequency-selective fading radio channels," *IEEE J. Sel. Areas Commun.*, vol. 11, no. 3, pp. 422–431, 1993.

[66] D. Verdin and T. C. Tozer, "Generating a fading process for the simulation of land-mobile radio communications," *Electron. Lett.*, vol. 29, no. 23, pp. 2011–2012, 1993.

[67] A. Anastasopoulos and K. M. Chugg, "An efficient method for simulation of frequency selective isotropic Rayleigh fading," in *Proc. of IEEE 47th Vehicular Technology Conference (VTC97)*, vol. 3, 1997, pp. 2084–2088.

[68] J. Smith, "A computer generated multipath fading simulation for mobile radio," *IEEE Trans. Veh. Technol.*, vol. 24, no. 3, pp. 39–40, 1975.

[69] D. J. Young and N. C. Beaulieu, "The generation of correlated Rayleigh random variates by inverse discrete Fourier transform," *IEEE Trans. Commun.*, vol. 48, no. 7, pp. 1114–1127, 2000.

[70] C. Patel, G. L. Stüber, and T. G. Pratt, "Comparative analysis of statistical models for the simulation of Rayleigh faded cellular channels," *IEEE Trans. Commun.*, vol. 53, no. 6, pp. 1017–1026, 2005.

[71] S. Fard, A. Alimohammad, B. Cockburn, and C. Schlegel, "A single FPGA filter-based multipath fading emulator," in *Proc. of IEEE Global Communications Conference (GLOBECOM2009)*, 2009.

[72] C.-D. Iskander, "A MATLAB-based object-oriented approach to multipath fading channel simulation," White Paper, MathWorks, Natick, MA. [Online]. Available: http://www.mathworks.com/matlabcentral/fileexchange/18869

[73] G. Azemi, E. Zandi, and L. Mohammadi, "Simulation of multipath fading channels with non-isotropic scattering," in *1st International Conference on Signal Processing and Communication Systems (ICSPCS07)*, 2007.

[74] E. Zandi and G. Azemi, "Simulation of multipath-fading channel with non-isotropic scattering using filtered Gaussian noise method," in *Iranian Conference on Electrical Engineering (ICEE09)*, Tehran, Iran, May 2009.

[75] J. Tribolet, "A new phase unwrapping algorithm," *IEEE Trans. Acoust., Speech, Signal Process.*, vol. 25, no. 2, pp. 170–177, 1977.

[76] D. Bone, "Fourier fringe analysis- the two-dimensional phase unwrapping problem," *Applied Optics*, vol. 30, no. 25, pp. 3627–3632, 1991.

[77] M. Jenkinson, "Fast, automated, N-dimensional phase-unwrapping algorithm," *Magnetic Resonance in Medicine*, vol. 49, no. 1, pp. 193–197, 2003.

[78] W. Xu, I. Cumming, D. MacDonald, and A. Ltd, "A region-growing algorithm for InSAR phase unwrapping," *IEEE Trans. Geosci. Remote Sens.*, vol. 37, no. 1, pp. 124–134, 1999.

[79] N. M. Blachman, "FM reception and the zeros of narrow-band Gaussian noise," *IEEE Trans. Inf. Theory*, vol. 10, no. 3, pp. 235–241, 1964.

[80] T. Tjhung, C. Ng, K. Yeo, and P. Wittke, "Error performance analysis for narrow-band duobinary FM with discriminator detection," *IEEE Trans. Commun.*, vol. 33, no. 5, pp. 399–408, 1985.

[81] D. Yavuz, "FM click shapes," *IEEE Trans. Commun.*, vol. 19, no. 6, pp. 1271–1273, 1971.

[82] I. Bar-David and S. Shamai, "On the Rice model of noise in FM receivers," *IEEE Trans. Inf. Theory*, vol. 34, no. 6, pp. 1406–1419, 1988.

[83] D. Yavuz and D. Hess, "False clicks in FM detection," *IEEE Trans. Commun.*, vol. 18, no. 6, pp. 751–756, 1970.

[84] A. Papoulis and S. Pillai, *Probability, Random Variables, and Stochastic Processes*, 4th ed. New York, NY, USA: McGraw-Hill Publishing Company, 2002.

[85] J. Proakis, *Digital Communications*, 4th ed. New York, NY,USA: McGraw-Hill Higher Education, 2001.

[86] M. Lecours, M. Tetu, A. Chefaoui, J. Ahern, and A. Michaud, "Phase measurements and characterization of mobile radio channels," *IEEE Trans. Veh. Technol.*, vol. 45, no. 1, pp. 105–113, 1996.

[87] J. K. Cavers, "An analysis of pilot symbol assisted modulation for Rayleigh fading channels," *IEEE Trans. Veh. Technol.*, vol. 40, no. 4, pp. 686–693, 1991.

[88] P. Ho and J. Kim, "Pilot symbol-assisted detection of CPM schemes operating in fast fading channels," *IEEE Trans. Commun.*, vol. 44, no. 3, pp. 337–347, 1996.

[89] G. Xu, H. Liu, L. Tong, and T. Kailath, "A least-squares approach to blind channel identification," *IEEE Trans. Signal Process.*, vol. 43, pp. 2982–2993, 1995.

[90] B. Muquet, M. De Courville, and P. Duhamel, "Subspace-based blind and semi-blind channel estimation for OFDM systems," *IEEE Trans. Signal Process.*, vol. 50, no. 7, pp. 1699–1712, 2002.

[91] S. R. J. Axelsson, "Analysis of the quantizing error of a zero-counting frequency estimator," *IEEE Trans. Inf. Theory*, vol. 22, no. 5, pp. 596–599, 1976.

[92] H. Meyr, "Nonlinear analysis of correlative tracking systems using renewal process theory," *IEEE Trans. Commun.*, vol. 23, no. 2, pp. 192–203, 1975.

[93] R. F. Pawula, S. O. Rice, and J. H. Roberts, "Distribution of the phase angle between two vectors perturbed by Gaussian noise," *IEEE Trans. Commun.*, vol. 30, no. 8, pp. 1828–1841, 1982.

[94] R. F. Pawula, "Distribution of the phase angle between two vectors perturbed by Gaussian noise II," *IEEE Trans. Veh. Technol.*, vol. 50, no. 2, pp. 576–583, 2001.

[95] D. Yavuz and D. Hess, "FM noise and clicks," *IEEE Trans. Commun.*, vol. 17, no. 6, pp. 648–653, 1969.

[96] W. Lindsey and M. Simon, *Telecommunication Systems Engineering.* Mineola, NY, USA: Dover Publications, Inc., 1991.

[97] "http://en.wikipedia.org/wiki/Skellam_distribution."

[98] D. Karlis and I. Ntzoufras, "Analysis of sports data by using bivariate Poisson models," *The Statistician*, vol. 52, no. 3, pp. 381–393, 2003.

[99] D. Karlis and E. Xekalaki, "A simulation comparison of several procedures for testing the Poisson assumption," *The Statistician, Journal of the Royal Statistical Society-Series D*, vol. 49, no. 3, pp. 355–382, 2000.

[100] W. Mendenhall and T. Sincich, *Statistics for Engineering and the Sciences.* Upper Saddle River, NJ, USA: Prentice-Hall, Inc., 2007.

[101] V. Erceg, P. Soma, D. Baum, and S. Catreux, "Multiple-input multiple-output fixed wireless radio channel measurements and modeling using dual-polarized antennas at 2.5 GHz," *IEEE Trans. Wireless Commun.*, vol. 3, no. 6, pp. 2288–2298, 2004.

[102] G. G. Messier and J. A. Hartwell, "An empirical model for nonstationary Ricean fading," *IEEE Trans. Veh. Technol.*, vol. 58, no. 1, pp. 14–20, 2009.

[103] C. Loo, "A statistical model for a land mobile satellite link," *IEEE Trans. Veh. Technol.*, vol. 34, no. 3, pp. 122–127, 1985.

[104] F. Vatalaro, "Generalised Rice-lognormal channel model for wireless communications," *Electron. Lett.*, vol. 31, pp. 1899–1900, 1995.

[105] S. H. Hwang, K. J. Kim, J. Y. Ahn, and K. C. Whang, "A channel model for non-geostationary orbiting satellite system," in *Proc. of IEEE 47th Vehicular Technology Conference (VTC97)*, 1997, pp. 41–45.

[106] A. Naimi and G. Azemi, "K-factor estimation in shadowed Ricean mobile communication channels," *Wirel. Commun. Mob. Comput.*, 2009.

[107] K. K. Talukdar and W. Lawing, "Estimation of the parameters of the Rice distribution," *J. Acoust. Soc. Amer.*, vol. 89, pp. 1193–1197, 1991.

[108] L. J. Greenstein, D. G. Michelson, and V. Erceg, "Moment-method estimation of the Ricean K-factor," *IEEE Commun. Lett.*, vol. 3, no. 6, pp. 175–176, 1999.

[109] C. Tepedelenlioglu, A. Abdi, and G. B. Giannakis, "The Ricean K factor: estimation and performance analysis," *IEEE Trans. Wireless Commun.*, vol. 2, no. 4, pp. 799–810, 2003.

[110] T. L. Marzetta, "EM algorithm for estimating the parameters of a multivariate complex Rician density for polarimetric SAR," in *Proc. of International Conference on Acoustics, Speech, and Signal Processing(ICASSP-95)*, vol. 5, 1995, pp. 3651–3654.

[111] G. Azemi, B. Senadji, and B. Boashash, "Estimating the Ricean K-factor for mobile communication applications," in *Proc. of Seventh International Symposium on Signal Processing and Its Applications*, vol. 2, 2003, pp. 311–314.

[112] A. Abdi, C. Tepedelenlioglu, M. Kaveh, and G. Giannakis, "On the estimation of the K parameter for the Rice fading distribution," *IEEE Commun. Lett.*, vol. 5, no. 3, pp. 92–94, 2001.

[113] Y. Chen and N. C. Beaulieu, "Maximum likelihood estimation of the K factor in Ricean fading channels," *IEEE Commun. Lett.*, vol. 9, no. 12, pp. 1040–1042, 2005.

[114] Y. Chen and N. Beaulieu, "Estimation of Ricean K parameter and local average SNR from noisy correlated channel samples," *IEEE Trans. Wireless Commun.*, vol. 6, no. 2, pp. 640–648, 2007.

[115] G. Azemi, B. Senadji, and B. Boashash, "Ricean K-factor estimation in mobile communication systems," *IEEE Commun. Lett.*, vol. 8, no. 10, pp. 617–619, 2004.

[116] W. H. Greene, *Econometric Analysis*, 5th ed. Upper Saddle River, NJ: Prentice Hall, 2003.

[117] A. G. Zajic and G. L. Stüber, "Space-time correlated mobile-to-mobile channels: modelling and simulation," *IEEE Trans. Veh. Technol.*, vol. 57, no. 2, pp. 715–726, 2008.

[118] R. G. Vaughan, "Spaced directive antennas for mobile communications by the Fourier transform method," *IEEE Trans. Antennas Propag.*, vol. 48, no. 7, pp. 1025–1032, 2000.

[119] P. A. Bello, "Characterization of randomly time-variant linear channels," *IEEE Trans. Commun.*, vol. 11, no. 4, pp. 360–393, 1963.

[120] R. G. Vaughan and J. B. Andersen, "Antenna diversity in mobile communications," *IEEE Trans. Veh. Technol.*, vol. 36, no. 4, pp. 149–172, 1987.

[121] M. A. Pallas and G. Jourdain, "Active high resolution time delay estimation for large BT signals," *IEEE Trans. Signal Process.*, vol. 39, no. 4, pp. 781–788, 1991.

[122] K. W. Cheung, H. C. So, W. Ma, and Y. T. Chan, "Received signal strength based mobile positioning via constrained weighted least squares," in *Proc. of IEEE International Conference on Acoustics, Speech, and Signal Processing (ICASSP03)*, vol. 5, 2003, pp. 137–140.

[123] S. Belanger, "Multisensor TDOA estimation in a multipath propagation environment using the EM algorithm," in *Proc. of 29th Asilomar Conference on Signals, Systems and Computers*, vol. 2, 1995, pp. 1096–1100.

[124] J. Caffery, *Wireless Location in CDMA Cellular Radio Systems.* Norwell, Mass, USA: Kluwer Academic Publisher, 2000.

[125] Y. Qi, H. Kobayashi, and H. Suda, "On time-of-arrival positioning in a multipath environment," *IEEE Trans. Veh. Technol.*, vol. 55, no. 5, p. 1516, 2006.